FUNCTIONAL TRANSFORMATIONS OF VISUAL INPUT BY AUDITORY THALAMUS AND CORTEX: AN EXPERIMENTALLY INDUCED VISUAL PATHWAY IN FERRETS

by

ANNA WANG ROE

B.A. Harvard/Radcliffe Colleges
(1984)

Submitted to the Department of Brain and Cognitive Sciences
in Partial Fulfillment of the Requirements for the Degree of

DOCTOR OF PHILOSOPHY

at the

MASSACHUSETTS INSTITUTE OF TECHNOLOGY

June 1991

Signature of Author_____
Department of Brain and Cognitive Sciences
May 8, 1991

Certified by_____
Mriganka Sur
Professor, Department of Brain and Cognitive Sciences
Thesis Supervisor

Accepted by_____
Emilio Bizzi, Chairman
Departmental Graduate Committee
Department of Brain and Cognitive Sciences

FUNCTIONAL TRANSFORMATIONS OF VISUAL INPUT BY AUDITORY THALAMUS AND CORTEX: AN EXPERIMENTALLY INDUCED VISUAL PATHWAY IN FERRETS

by

ANNA WANG ROE

Submitted to the Department of Brain and Cognitive Sciences on May 8, 1991
in partial fulfillment of the requirements for the Degree of
Doctor of Philosophy in Neuroscience

ABSTRACT

Anatomical studies of the mammalian sensory pathways suggest that sensory pathways of different modalities share many common aspects of organization; at the same time, there are many distinguishing features. What functional significance do these similarities and differences have? I have examined this issue by rerouting the sensory input of one modality, namely visual input, into the pathway of another modality, namely the auditory thalamus and cortex, and subsequently examining how the auditory pathway processes visual information. Specifically, by making specific brain lesions during development in the ferret, an aberrant retinal projection to the auditory thalamus can be established, thereby providing visual input to auditory thalamus (MGN) and auditory cortex (A1). I have studied the functional organization of this novel visual pathway in "rewired" ferrets and compared it with that of the normal visual pathway.

Retinal Source: Identification of the retinal source of this pathway is crucial to interpretation of subsequent thalamic and cortical transformations. I find anatomical, physiological, and developmental evidence suggesting that this pathway arises from retinal ganglion cells of the W cell class. Retinal ganglion cells projecting to the MGN have small soma sizes. These inputs to the MGN produce visual cells in the MGN with large receptive fields, sluggish responsiveness to visual stimulation, and long latencies of response to electrical stimulation of the optic chiasm. Furthermore, subpopulations of retinal W cells can be induced to reroute to the MGN following specific combinations of neonatal lesions.

Topography: In contrast to sensory maps in the normal auditory thalamus and cortex which contain a single topographic axis (that representing sound frequency), a two-dimensional visuotopic map is established in auditory thalamus and in auditory cortex of these rewired ferrets. Azimuthal representations map onto the axis in MGN and in A1 that normally

represents frequency. Elevations map orthogonal to this axis within isofrequency domains. Thus, the orientations of these maps within the target zone bears a predictable relationship with the normal organization of frequency and isofrequency representation in these zones; this suggests that the orientation of mapping from one sensory structure to another is likely to be guided by the target structure. The finding that a topographic elevational representation is established along the isofrequency axis, an axis which is not normally topographic, suggests that generation of topography within the isofrequency axis may be input-dependent.

Receptive Field Properties: Consistent with a retinal W cell source of input, visual cells in primary auditory cortex exhibit large receptive field sizes, poor visual responsiveness, and long latencies to optic chiasm stimulation. Receptive field properties which were related to intracortical circuitry revealed striking resemblances to those of normal visual cortical cells. These similarities include the presence of orientation and direction selectivity, and simple and complex receptive field organizations. These similarities suggest that certain intracortical circuitries may be common to all sensory cortices. Differences between sensory areas may be due to sensory-specific input patterns. This work suggests that there are indeed fundamental aspects of thalamic and cortical sensory processing that are independent of input modality.

Thesis Supervisor: Dr. Mriganka Sur
Title: Professor of Brain and Cognitive Sciences

Acknowledgements

I am indebted to the following people for their support during my graduate years:

Mriganka Sur My mentor who has walked me through from making my first electrodes to my first manuscripts, who has given me crucial training and guidance in my development as a scientist, and who has respected and supported the role of women in science.

Peter H. Schiller My thesis committee member, a scientist for whom I have a great deal of respect, who has taken the time to discuss experiments, science, and the scientific process with me, and given me much guidance throughout my graduate years.

Gerald E. Schneider My thesis committee member, a pioneer in developmental and behavioral neuroscience, without whom any of this work would have been possible.

Michael M. Merzenich My thesis committee member, whose extensive work in the somatosensory and auditory systems has strongly influenced my views on cortical function and organization.

Preston E. Garraghty My friend, semi-mentor, and colleague for developing my intellectual curiosity and enthusiasm for experimental work. "Get to work!"

Jong-On Hahm My friend and colleague for going through the best of times and worst of times with me.

Young Ha Kwon My friend and colleague for all those late night sessions, from brilliance to bs.

Manny Esguerra My friend and colleague for many years of shared experiences.

Sarah L. Pallas My friend and colleague for showing me that women can make it in science.

Terry Sullivan My friend who has suffered many years cutting, reacting, and mounting brain sections, followed by heavy drinking at the Muddy.

KiYun Roe My husband for making life rich, fun, and loving.

Hanju Roe My son for smiling at me everyday.

Norman Wereley My friend who is like family.

Yeh-chien and Yu-yin L. Wang My parents who have always taught me that I could do anything and that whatever I do I should do well.

My deepest thanks to Mriganka Sur, Sarah Pallas, Preston Garraghty, Jong-On Hahm, Young Ha Kwon, and Manny Esguerra for contributing their time and effort in the experiments that made this thesis possible. Thanks also to Terry Sullivan and Martha MacAvoy for excellent technical assistance, and KiYun Roe for writing programs to aid in data analysis. This work was supported by grants from the National Institutes of Health, the McKnight Foundation, and the Whitaker Health Science Foundation.

Table of Contents

Abstract 2

Acknowledgements 4

Introduction 6

Chapter 1 Retinal Ganglion Cell Population
Experimentally Induced Visual Projections to the Auditory Thalamus in Ferrets: Evidence for a W Cell Pathway 11

Chapter 2 Topography
A. Experimentally Induced Establishment of Visual Topography in Auditory Thalamus 68
B. Experimentally Induced Establishment of Visual Topography in Auditory Cortex 102

Chapter 3 Cortical Receptive Fields
Visual Projections Routed to the Auditory Pathway in Ferrets: Receptive Fields of Visual Neurons in Primary Auditory Cortex 131

Summary Discussion 195

Introduction

Sensory systems subserving different modalities in the mammalian central nervous system share many common aspects of organization. Sensory input, collected by specialized sensory receptors at the periphery, is transmitted (via multiple synapses) to a thalamic relay nucleus and subsequently to a primary sensory cortical area. Within a modality, several fairly independent channels run in parallel and subsequently create topographically organized representations of the sensorium in each of the thalamic and cortical waystations. Furthermore, intrinsic circuitry in thalamus and cortex as well as extrinsic connectivity between thalamic and cortical areas share many common features across sensory modalities. These organizational similarities suggest that common functional processing strategies exist across sensory systems and that perhaps similar stereotypical transformations are performed on sensory inputs regardless of modality. That sensory systems process input in similar fashions may be suggested by anatomical studies; however, *functional* assessment of this hypothesis is more difficult. This difficulty becomes apparent when, for example, one attempts to identify the auditory functional correlate of visual orientation selectivity.

One possible approach to this problem is to replace the input to a particular sensory system with that of another. I present a hypothetical situation in which auditory input to the auditory system is replaced by visual input (Fig. 1B, hatched input), thereby establishing a novel visual pathway through auditory structures. If visual response properties in this novel pathway remain similar to those found in the normal visual pathway (Fig. 1C, hatched output), it is parsimonious to suggest that inputs are likely to be processed similarly in the auditory and visual systems. This finding would imply that sensory pathways perform similar functional transformations on their inputs. If, however, novel visual response properties emerge (Fig. 1D, black output), then it is likely that there are aspects of auditory processing not found in the normal visual system. Each sensory modality, then, would process its input in a unique fashion.

This hypothetical pathway has been realized to some extent in an experimentally produced aberrant pathway from the retina to the auditory system in ferrets (Sur et al. 1988). In response to specific neonatal lesions (see Fig. 2; cf. Schneider, 1973; Frost, 1982), retinal fibers innervate the auditory thalamus (specifically, the medial geniculate nucleus, MGN), a thalamic nucleus that normally does not receive visual input. Thus in these "rewired" ferrets, visual input is routed through the MGN to primary auditory cortex (A1). I have now examined the functional properties of this novel pathway and compared them to functional properties of the normal visual pathway. In Chapter 1, I examine the identity of retinal ganglion cells giving rise to this pathway and the properties they confer to visual cells in the MGN. In Chapter 2, I examine the resulting visual topography in the MGN and in A1. In Chapter 3, I describe the visual receptive field properties of single cells in A1 of these animals. The interpretation of these data with respect to possible afferent-induced changes in target structures and with respect to implications for normal sensory processing will be discussed.

References

Frost DO (1982) Anomalous visual connections to somatosensory and auditory systems following brain lesions in early life. Dev Brain Res 3:627-635.

Schneider GE (1973) Early lesions of superior colliculus: factors affecting the formation of abnormal retinal projections. Brain Behav Evol 8:73-109.

Sur M, Garraghty PE, Roe AW (1988) Experimentally induced projections into auditory thalamus and cortex. Science 242:1437-1441.

Figure Legends

Fig. 1. Do sensory systems perform stereotypical transformations on their sensory input? For example, are visual thalamic and cortical structures (hatched circle) similar in function to those of the auditory system (grey circle)? A) Sensory input (square) in the normal visual (hatched) and auditory (grey) systems is processed by a central sensory structure (circle) to produce a characteristic output (rectangle). B) In a hypothetical experiment, auditory input to the auditory processor is replaced by visual input. How will the input be transformed? C) If the auditory processor (grey circle) is similar to visual processor (hatched circle), then the output will resemble normal visual output. D) If the auditory processor is different from the visual processor, then the output will not resemble normal visual output (black rectangle).

Fig. 2. Surgical paradigm which produces retinal innervation of auditory thalamus in the ferret (Sur et al. 1988; cf. Schneider, 1973; Frost, 1982). Normal targets of the retina are removed or reduced: the superior colliculus (SC) is ablated directly and the lateral geniculate nucleus (LGN) degenerates following large visual cortical ablations. In addition, alternative target space in the medial geniculate nucleus (MGN) is provided by interrupting ascending auditory inputs from the inferior colliculus (IC). These manipulations, performed on the neonatal ferret, result in rerouting of some retinal afferents to the MGN. A novel visual pathway is thus established from the retina to the MGN to primary auditory cortex.

Fig. 1

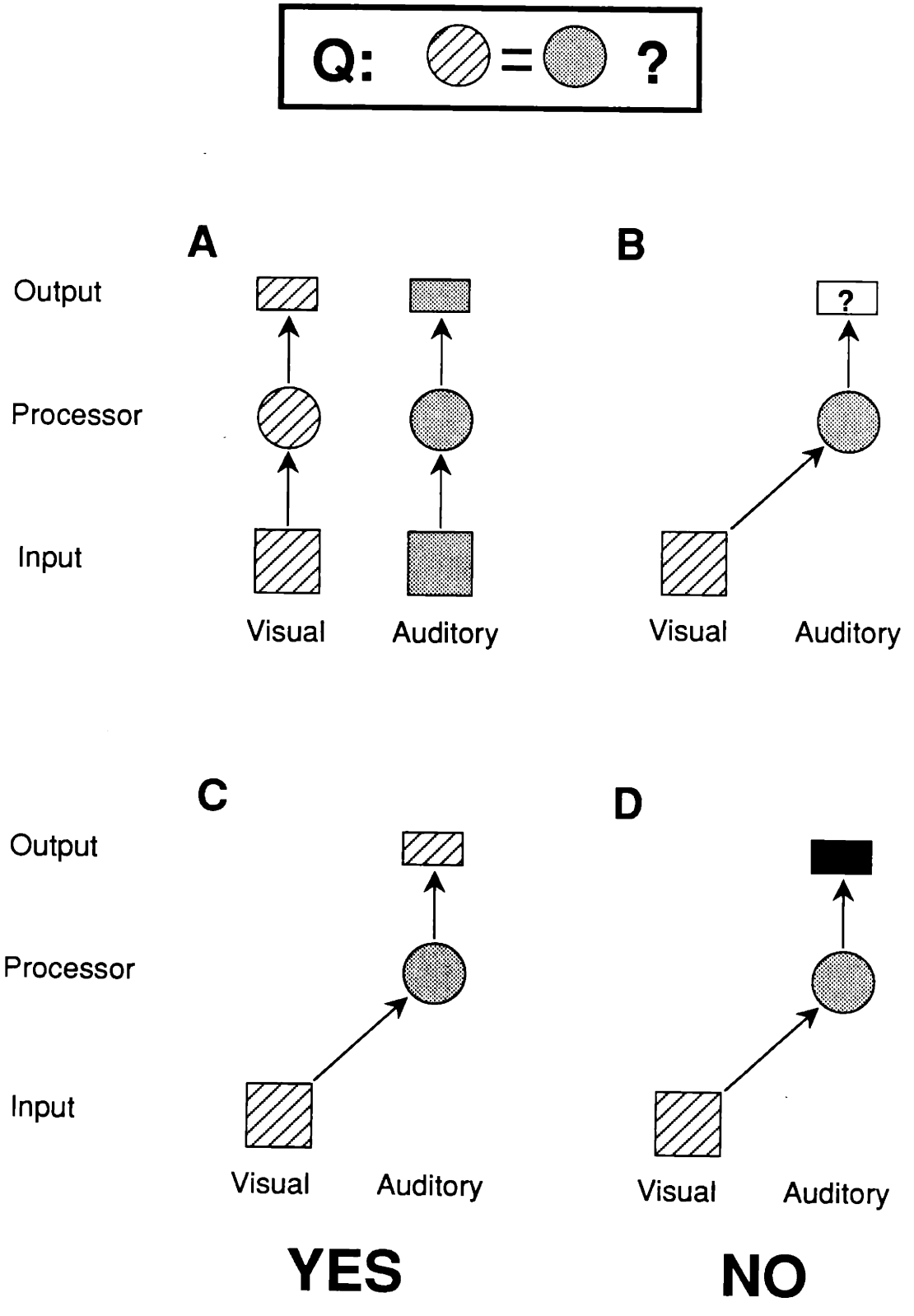
Q: = ?
A
Output
Processor
Input
Visual
Auditory
B
?
Visual
Auditory
C
Output
Processor
Input
Visual
Auditory
YES
D
Visual
Auditory
NO

Fig. 2

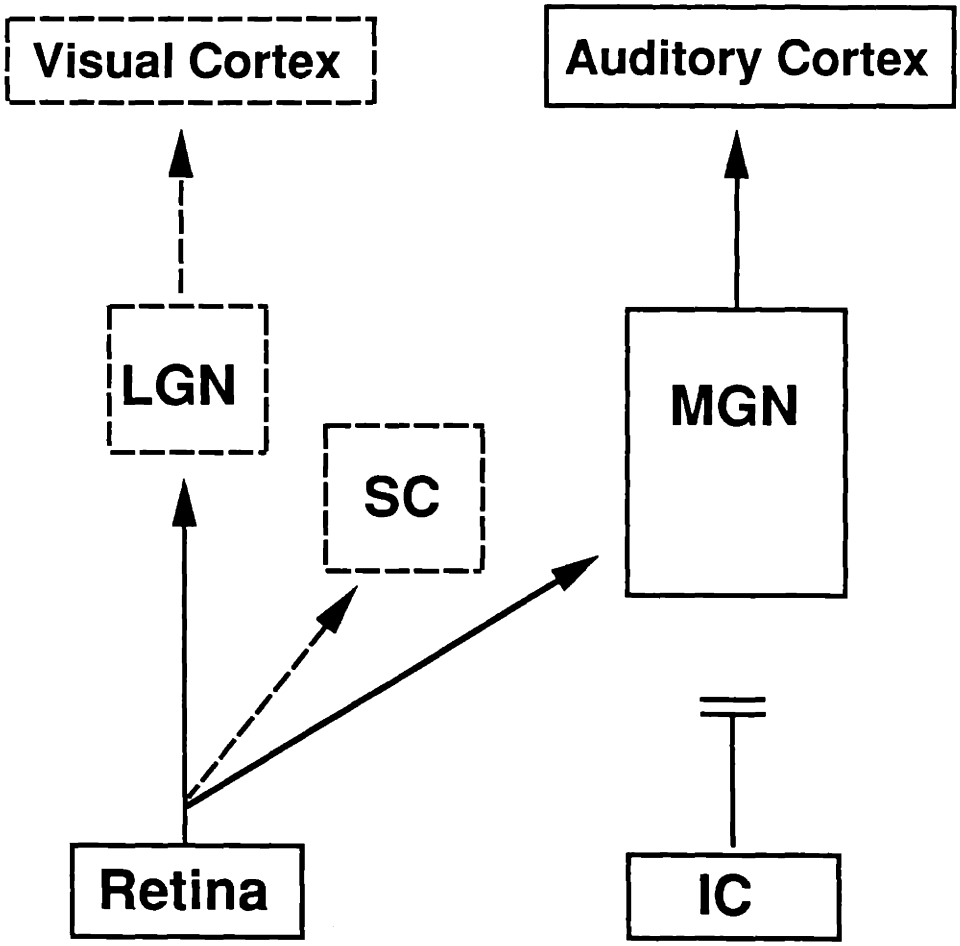

Chapter 1

Experimentally Induced Visual Projections to the Auditory Thalamus in Ferrets: Evidence for a W Cell Pathway

Abstract

We have previously reported that following specific neonatal brain lesions in ferrets, a retinal projection is induced into the auditory thalamus (the medial geniculate nucleus, MGN). This establishes a novel visual pathway through auditory thalamus and primary auditory cortex (Sur et al., 1988). To be able to interpret the visual transformations occurring in the thalamus and cortex in these "rewired" ferrets, it is important to identify which retinal cell class(es) come to project to the MGN.

Typical of the carnivore retina, the normal ferret retina contains three classes of ganglion cell (X, Y, and W), each with distinct morphologies and physiologies (Henderson, 1985; Vitek et al., 1985; Roe et al., 1989). In this paper, we use three approaches--physiological, anatomical, and developmental--to establish that in these rewired ferrets the projection to the MGN arises from retinal W cells. We find that: 1) physiological response properties of postsynaptic visual cells in the MGN are W-like, 2) retinal ganglion cells back-filled from the MGN are small in size and 3) subpopulations of these W cells can be preferentially rerouted to the MGN in response to different surgical manipulations at birth. These findings not only provide a basis on which to interpret functional properties of this visual pathway, but also provides important information about the the developmental capabilities of specific retinal ganglion cell classes and the regulation of their projections by target structures in the brain during development.

Introduction

In ferrets, specific neonatal lesions result in the redirection of some retinal ganglion cells into non-visual thalamic targets--specifically, the medial geniculate nucleus (MGN), the auditory thalamic relay nucleus (Sur et al., 1988). This "rewiring" of retinal input produces a novel visual pathway through the MGN and into primary auditory cortex (Sur et al., 1988). Such a preparation provides a unique approach to studying the relative contributions of afferent and target to the generation of thalamic and cortical visual receptive field properties. Crucial to this approach is the identification of the specific types of retinal input to this pathway.

In the normal ferret retina, similar to the cat retina, there are three retinal ganglion cell classes--X, Y, and W--each of which can be distinguished on both physiological and morphological grounds. The X and Y cell classes are each rather homogeneous in structure and function: X cells have medium-sized somata, small receptive field sizes, exhibit linear spatial and temporal summation, and project primarily to the lateral geniculate nucleus (LGN); Y cells are large in size, have large receptive fields, respond non-linearly to spatial and temporal summation, and project primarily to both the LGN and the superior colliculus (SC). In contrast, W cells are much more heterogeneous as a class. They have small to medium sized somata, diverse physiological characteristics (often poor spatial and temporal sensitivities, slow axonal conduction velocities, sluggish responsiveness, and large receptive field sizes), and diverse patterns of retinofugal projections (including the C laminae of the LGN and the superficial grey of the SC). Indeed, the term "W cells" may encompass several distinct subclasses of retinal ganglion cells. A third potentially useful criterion for differentiating retinal ganglion cell classes is their normal patterns and modes of development and their responses to abnormal sensory inputs during development. X and Y axons are known to develop in quite distinct manners in the normal LGN and following alterations of normal visual input during development (for review see Sur et al., 1988). While not much is

known about the developmental capabilities of retinal W cells, it is possible that W cells (small cells) are among the last to be born in the retina (Walsh et al., 1983), and that these cells may be the most likely to project to novel targets if their normal targets are lesioned. Based on these three criteria--physiological, anatomical, and developmental characterization--we investigate which retinal ganglion cell class(es) give rise to the experimentally induced visual pathway in "rewired" ferrets.

Methods

Three methodological approaches were taken in this study: physiological, developmental, and anatomical. 1) Physiological characterization of retinal input to MGN was done primarily by characterizing visual response properties in the MGN and comparing these responses with responses of cells in the normal LGN. 2) The capacity of retinal ganglion cell classes to innervate the MGN was examined by attempting different combinations of neonatal brain lesions which potentially could selectively redirect subpopulations of retinal ganglion cells. 3) The soma sizes of retinal ganglion cells projecting to specific thalamic and midbrain targets were measured following tracer injections into the target nuclei. Taken together, these experiments allowed us to address the issue of what retinal cell class(es) provide the aberrant projection to the MGN in rewired ferrets.

Neonatal Surgery to Produce Retinal Innervation of MGN

To induce retinal innervation of non-visual thalamic structures, it is necessary to remove normal retinal targets and to make alternative target space available (Schneider, 1973). We removed or greatly reduced the two major retinal targets (the lateral geniculate nucleus, LGN, and the superior colliculus, SC) and deafferented the auditory thalamus, the medial geniculate nucleus (MGN). These lesions performed at a sufficiently early stage of development resulted in induction of developing retinofugal afferents to terminate in the MGN (Sur et al., 1988).

Procedures are similar to those described previously (Pallas et al., 1990). Briefly, timed pregnant pigmented ferret jills were bred in our colony or purchased from a commercial supplier (Marshall Farms). Within 24 hours of parturition, ferret kits were removed and anesthetized by deep hypothermia. All surgery was performed under sterile conditions. A 1 cm midline incision was made in the scalp and the skull exposed. After removing a small piece of overlying skull, the SC was ablated by heat cautery. To induce massive retrograde

degeneration of the LGN, large regions of visual cortex (including Areas 17, 18, and often 19) were lesioned by cauterizing through the skull. Fibers running in the brachium of the inferior colliculus were transected at mid-SC level, thereby denervating the MGN and providing alternative target space for retinal axon terminals. All lesions were made unilaterally (note: bilateral lesions resulted in significantly reduced survival rates). On completion of surgery, the skin was sutured and the kit revived under a heat lamp. A single dose of antibiotics (0.01 cc amoxycillin, 100 mg/ml) was given subcutaneously and antibacterial ointment was applied to the wound. The kit was then returned to the mother for rearing.

Visual Physiology in Adult Ferrets

Surgical Preparation

Normal and neonatally-lesioned adult ferrets were prepared for visual physiology using procedures similar to those described previously (Roe et al., 1988). Normal ferrets were pigmented Sable ferrets obtained from Marshall Farms. All experimental ferrets used for physiological recordings had received lesions of the visual cortex, superior colliculus, and brachium of the inferior colliculus at birth as described above. Animals were anesthetized, paralyzed, and respirated. Following induction of anesthesia with ketamine hydrochloride (30 mg/kg) and xylazine (2 mg/kg), a cannula (24g) for anesthetic and paralytic delivery was implanted in either the femoral or the jugular vein, and an endotracheotomy was performed. Animals were then placed in a stereotaxic apparatus, paralyzed with a bolus of gallamine triethiodide, and artificially respired (rate 30-40/min, volume 25-30cc) with a 70/30 mixture of nitrous oxide/oxygen. Ferrets received a constant intravenous infusion of a 5% dextrose solution containing ketamine hydrochloride (10 mg/kg/hr) for anesthesia and gallamine triethiodide (3.6 mg/hr/kg) for muscular paralysis. End-tidal CO_2 was maintained at 4.0%, heart rate monitored, and body temperature maintained at 38°C with a heating pad.

Supplemental halothane (1%) was supplied during all surgical procedures. The skull and dura over cortex above lateral thalamus were removed. Stimulating electrodes were lowered into the optic chiasm and cemented in place. Drops of atropine sulfate and phenylephrine hydrochloride were applied to the eyes to dilate the pupils. Eyes were fitted with zero power contact lens and focussed on a tangent screen 114 cm in front of the animal. Optic disks were plotted by reflection onto the tangent screen and used to specify the locations of visual receptive fields.

Recording and Data Collection

We used parylene insulated tungsten microelectrodes (2-3 megohm impedances) to record extracellularly from thalamic cells of14 lesioned ferrets and 4 normal ferrets (see also Esguerra et al., 1986). Initial recording penetrations were made on the basis of stereotaxic coordinates for the LGN in normal ferrets (Zahs and Stryker, 1985, see results). Upon reaching thalamus, unit activity was assessed every 50-100 μm in each penetration for 1) response to electrical stimulation of the optic chiasm and 2) response to visual stimulation. In two lesioned animals and one normal animal, broad-band auditory stimuli (clicks or white noise) were delivered through earphones. Visually responsive units were plotted and characterised on the tangent screen with a hand-held projection lamp. In addition to receptive field location and size, a number of other response characteristics were also examined. These included ocular dominance, linearity of spatial summation, orientation, direction, and velocity selectivities, on and off preferences, presence or absence of inhibitory surrounds, and strength of response. Electrolytic lesions (5μA for 5 sec) or tracer injections (see below) were made in selected penetrations.

For quantitative determination of orientation and direction preferences, moving bar stimuli, either projected with an optic bench or generated on a Tektronix monitor driven by a stimulus generator ("Picasso"), were swept at different orientations over the receptive field. Spike responses of the cell under study were isolated with a pulse-shape discriminator

(Ealing). For each stimulus, 20 cycles were collected and summed by the Unkelscope Program run on an IBM PC 286 computer and post-stimulus time (PST) histograms generated on-line. Spike responses were also stored on tape and PST histograms analyzed off-line.

Histology

Following the completion of data collection, the animal was sacrificed with an intravenous or intraperitoneal overdose of pentobarbital (65 mg/kg) and perfused through the heart with saline followed by fixative (1% paraformaldehyde, 2% glutaraldehyde) and 10% and 20% sucrose solutions. The brain was then removed from the cranium and stored in 30% sucrose overnight. After brain sulcal patterns were recorded photographically, frozen sections were cut at 50 μm and were Nissl-stained. Lesions and recording tracks were located and reconstructed.

Selective Redirection of Retinal Ganglion Cell Subpopulations

Surgery

We reasoned that considerable insight could be gained into the nature and source of retinal inputs to the MGN by examining their response to changes in target availability. By using various combinations of each of three neonatal lesions, we thus varied the amount and type of available target space for developing retinal afferents, and subsequently examined the resulting retinal innervation in the MGN. Lesions which reduced normal retinal target zones included: 1) ablation of visual cortex (VCX) resulting in massive retrograde degeneration of the lateral geniculate nucleus and 2) direct ablation of the superior colliculus (SC). The third lesion, transection of the brachium of the inferior colliculus (BC), denervated the MGN and increased retinal target space, albeit in an aberrant zone. We performed the following 7 combinations of lesions (see neonatal surgery) in neonatal ferrets and examined the resulting retino-MGN projection at adulthood:

1) VCX + SC + BC

2) VCX + BC

3) SC + BC

4) VCX + SC

5) VCX

6) SC

7) BC

Eye Injections, Histology, and Autoradiography

After these operated ferrets were raised to adulthood, 20 µl of 20% HRP and 1% WGA-HRP (wheat germ agglutinin-conjugated horseradish peroxidase) was injected with a Hamilton syringe into the eye contralateral to the operated hemisphere. Following a 3-5 day survival, the animal was given an overdose of pentobarbitol and perfused through the heart with fixative (1% paraformaldehyde/2% glutaraldehyde) and 10% and 20% sucrose in phosphate buffers, and subsequently stored in 30% sucrose in phosphate buffer overnight. The brain was then sectioned and reacted with TMB histochemistry (Mesulam, 1978). Following mounting, clearing, and coverslipping, the sections were then examined for HRP reaction product.

In two animals, a second tracer, ^{35}S-methionine, was additionally injected into the eye ipsilateral to the lesioned hemisphere. In these cases, several series of the thalamic sections were dipped in NTB-2 (Kodak) photographic emulsion, dried, and stored in the dark. Periodically (between 2 weeks and 2 months), series of exposed sections were photographically developed, cleared, coverslipped. The series with the maximal retinal terminal label compared to the background was chosen for analysis.

Data Analysis

Thalamic label was mapped and quantified. In each animal that had received an eye injection, the LGN, MGN, and regions of retinal label were drawn by camera lucida at a magnification of 58X. The areas of the LGN, the MGN, and the zones of labelled retinofugal axons in each section were measured with a SummaSketch digitizing pad run by SigmaScan software on an IBM PC 286. The volume of each zone was then determined by multiplying the area of the zone by the inter-section distance. The size of retinal projection to the MGN was then calculated as a percentage of the MGN volume in each animal.

Retinal Cells Filled Retrogradely in Rewired and Normal Ferrets

Thalamic HRP Injections

In 7 rewired ferrets and 4 normal ferrets, injections of tracers were made in thalamus. Placement of tracer injections were made either under stereotaxic guidance or in combination with physiological recordings (see above). For large thalamic injections, up to 1 µl of 20% HRP was injected with a Hamilton syringe. For more restricted injections, 10% HRP was iontophoresed through a glass micropipette (impedance 10-30 Megohms) for 15-30 minutes (0.6 - 1.0 µA at 0.5s on, 0.5s off). This produced HRP deposits 0.25-1.00 mm in diameter.

Depending on the type of experiment being conducted, transport time ranged from 12 hrs to 3-4 days. Animals were then given an overdose of pentobarbitol (65mg/kg) and perfused through the heart with saline followed by fixative (1% paraformaldehyde and 2% glutaraldehyde in 0.1M phosphate buffer), and then 10% and 20% sucrose solutions. Brains and retinae were removed and stored overnight. In brains in which HRP injections had been made, alternate brain sections (cut at 100 µm) were processed for HRP visualization with diamino benzidine intensified with cobalt chloride. HRP back-filled retinae were reacted with O'dianisidine (DeOlmos, 1977) and flat-mounted.

Data Analysis

Location and extent of each thalamic injection was determined and soma sizes of back-filled retinal ganglion cells measured. To compare retinal ganglion soma size populations from different retinae, in all but 2 cases, measurements were taken from each retina contralateral to the injected hemisphere at a region superior to area centralis corresponding approximately to the 1500 cells/mm^2 isodensity contour of Henderson (1985). In two cases in which retinal ganglion cells were back-filled from the superior colliculus, only the retina nasal to the optic disk was labelled; in these cases, measurements were taken from the 1500 cells/mm2 isodensity contour approximately midway between the optic disk and the nasal retinal border. At these locations in each retina, back-filled retinal ganglion somatas were drawn with a camera lucida attachment at a final magnification of x670; all back-filled cells within each single field of view were drawn and as many adjacent fields of view were drawn as required to reach a number of at least 100 cells per retina. Soma size areas were subsequently measured with a SummaSketch digitizing pad run by SigmaScan software on an IBM PC 286 . Distributions, means, and variances were calculated and appropriate statistical tests (Mann-Whitney U) used for comparison of soma size measurements.

Results

We present physiological, developmental, and anatomical evidence suggesting that the retinal projection to the MGN arises from retinal W cells. Our dat include: 1) physiological characterization of the postsynaptic visual cells in the MGN, 2) selective redirection of retinal ganglion cell subpopulations, and 3) soma size measurements of retinal ganglion cells projecting to the MGN.

I. Physiological Properties of Visual Cells in the MGN

To identify the functional class(es) of retinal ganglion cell giving rise to the aberrant retino-MGN projection, one would ideally record from retinal ganglion cells back-fired from the MGN and characterize the features of these cells. Given the substantial technical difficulty of such an experiment, however, an alternative approach is to record from retinal afferent fibers projecting to the MGN or from MGN cells post-synaptic to the retinal afferent terminations. Given the similarity in response characteristics of retinal and geniculate X and Y cells (for review, see Sherman and Spear, 1982), we find it reasonable to expect that the visual response characteristics of MGN cells will be indicative of their presynaptic retinal input. The validity of this interpretation will be further examined in the discussion.

We examined the responses of thalamic cells in lesioned ferrets to three types of stimulation: electrical stimulation of the optic chiasm, visual stimulation, and auditory stimulation. The placements of our initial penetrations in each experiment were based on stereotaxic coordinates of the normal LGN. In rewired ferrets the LGN tended to be shifted rostrally and medially with respect to the normal LGN position. Along the depth of each penetration, thalamic recordings were usually preceded by characteristic hippocampal activity (highly active cells with large amplitude spikes) followed by silence as the electrode advanced through the lateral ventricle. In any penetration in which both LGN and MGN cells were

recorded, the transition between LGN and MGN was quite evident, often marked by an immediate decrease in background activity and briskness of response to visual stimulation, and sudden shift in visual topography (see Chapter 2). We report on units histologically determined to be in all three major divisions of the MGN--the ventral (MGv), medial (MGm), and dorsal (MGd) divisions (Morest, 1965).

Out of a total of 238 units recorded in the MGN, almost all (95%) were electrically driven from the chiasm and approximately half (55%) were visually driven (see Table 1). Auditory responsiveness was observed in 7 out of 27 units tested.

Responses to electrical stimulation: Latency of Spike Responses

Two hundred and twenty-six MGN units were driven by electrical stimulation of the optic chiasm (Table 1, Fig. 1A). Cellular responses were usually bimodal (negative-positive) and sometimes trimodal (negative-positive-negative) in waveform. Jitter in latencies for any single unit usually fell within a 1.0 ms range and synaptic failure was elicited at high rates of stimulation (10-100 shocks/s). For each unit, the mode of the latencies elicited by multiple chiasm shocks was taken as the cell's spike latency to optic chiasm stimulation. Recording from retinal afferents (recognized by monophasic spike responses that exhibit no synaptic failure even at high stimulation rates and no jitter in latency), while common in the LGN (Roe et al., 1989), was rare in the MGN. This is likely to be due to the small size of the afferent axons (Pallas et al., 1990) as well as the relative sparseness of the projection (see below). Almost all units (94%) driven visually were responsive to electrical stimulation of the optic chiasm.

Latencies of MGN cells were longer that those of X or Y cells in the normal LGN. Normal LGN X cell latencies ranged from 1.1-2.5 msec ($n = 48$, $x = 1.9$), while those of LGN Y cells ranged from 1.2-2.1 ($n = 22$, $x = 1.6$). Consistent with observations from cats (e.g. Hoffman, 1973; Berson, 1987), the latencies of normal LGN W cells (range 2.1-3.7

msec, n=13, x=2.8) were longer than most X and Y cell latencies; 2 W cells were not responsive to chiasm shocks (Fig. 1B).

Latencies of MGN cells (n=226) spanned quite a large range (1.5 - 35.0 msec, mean = 5.6 msec), the majority of which (80%) fell between 2.0 and 7.0 msec (Fig. 1A). The latencies of the visually responsive subpopulation (n = 123, x = 4.8 msec) exhibited a very similar distribution (Fig. 1A). These latencies are significantly longer than those of LGN X ($p < .0001$) or Y ($p < .0001$) cells. 85% of the MGN latencies are longer than any recorded for LGN X and Y cells. Another 13% of the MGN latencies (those falling in the 2 msec range) overlap with the lower range of LGN W cell latencies and the upper range of LGN X cell latencies; there is virtually no overlap between MGN latencies and LGN Y cell latencies.

The overlap in the latency distribution with LGN W cell latencies is considerable: 61% of the MGN latencies fall into the 2.0-4.0 msec range. A second small peak in the MGN latency distribution occurs at 7.0-8.0 msec, perhaps indicating the presence of a second, more slowly conducting population reaching the MGN. In the normal cat retina, two subpopulations of W cells have slow and very slow axonal conduction velocities, respectively (Hoffman, 1973; Cleland and Levick, 1974a; Berson, 1987; Stanford, 1987). The large range of these latencies recorded in the MGN (up to > 16.0 msec) may also be indicative of W cell input heterogeneity, as is characteristic of the normal retinal W cell population (e.g. Cleland and Levick, 1974b).

To address the possibility that, in the rewired ferrets, retinal axons of all cell classes may have longer optic chiasm latencies, we recorded latencies to optic chiasm stimulation of LGN cells in rewired ferrets (Fig. 1C). There was a prominant reduction (from 62% to 22%) in the percentage of X cells recorded in rewired ferret LGN (Sur et al., 1987; cf. Tong et al). However, the latency distributions of Y (range 1.1-2.7 msec, n=61, x=1.8), X (range 1.2-3.0, n=24, x=1.8), and W (range 1.8-5.8 msec, n=23, x=3.1) cells were not significantly different from their normal LGN counterparts (Y, $p > .13$; X, $p > .18$; W, $p > .30$). These

data indicate that, at least for retinal afferents projecting to the LGN, conduction latencies are not affected in some non-specific fashion by the neonatal lesions.

Responses to visual stimulation: Response Characteristics and Receptive Field Organization

Response characteristics. Response characteristics of visual MGN cells were reminiscent of those previously described for retinal and LGN W cells (Cleland et al., 1971; Sur and Sherman, 1982), both in terms of response quality and in terms of diversity. In general, responsiveness of cells in the MGN to visual stimulation was poor in comparison to those of LGN cells in normal ferrets. Whereas normal LGN X and Y cells respond briskly and consistently to flashing or moving bars and spots, these same visual stimuli produced much weaker, more labile, "sluggish" responses in visual MGN cells. Such sluggishness of response was also found in some W cells recorded in the LGN. We rated the responsiveness of visual MGN cells in three experiments. Each visual unit recorded was given a responsivity rating ranging from 1-4, with 1 indicating low responsivity and 4 a responsivity comparable to those of normal LGN X and Y cells. This responsivity index reflected both strength and consistency of response. Of 46 visual cells rated in this manner (35% of all visual cells recorded), over half were given a rating of 1 and none were rated as 4 (Fig. 2). In contrast, normal X and Y LGN cells would be rated 4 (Roe, Esguerra, personal experience). A further reflection of poor responsiveness is the significant proportion of units (42%) that were driven by chiasm stimulation but were visually unresponsive (cf. Wilson et al, 1976). Thus, reliable determine of visual receptive field properties in the MGN required increased experimental effort and time-consuming repetitive visual stimulations.

MGN cells are a diverse lot. Some MGN cells exhibited a moderate level of spontaneous activity which was modulated by visual stimuli (Fig. 3A, B, 4A). In contrast, a few cells exhibited virtually no background activity and responded to visual stimuli with only a few spikes or even a single spike. Most MGN cells responded to either onset (n=30) or offset (n=23) of light stimuli and a few (n=6) responded to both stimulus onset and offset.

(In comparison, the few on/off cells recorded in LGN were of the W cell class; all X and Y cells were either on-center or off-center.) MGN cells preferred slowly flashing spots in their receptive field, and often "fatigued" with prolonged stimulus presentation. For some cells, only if the frequency of stimulation was extremely low (e.g. less than 0.5 hz) could responses be consistently elicited. 10 out of 131 cells responded only to very strong stimuli, such as full field flashes. All units were monocularly driven, with a predominant contralateral bias (contralateral, n=69; ipsilateral, n=4).

Similar to LGN cells, visually driven MGN cells were not orientation selective. MGN cells exhibited similar responses to bars flashed at different orientations within their receptive fields and to bars swept at different orientations across their receptive fields. We quantified orientation tuning for a small population of MGN cells (n=10). We defined an orientation tuning index as: 1 - (Orthogonal Response/Peak Response) (cf. Felleman and Van Essen, 1987). A cell whose response in the best orientation is twice the level of that in the orthogonal orientation would have an orientation selectivity index of 0.5; one whose best response is 1.5 times that in the orthogonal orientation would have an index of 0.33. Therefore, we consider those units with indices below 0.3 to be unoriented, those with indices from 0.3-0.5 to be broadly oriented, and those with indices above 0.5 to be sharply oriented. All MGN cells had orientation indices below 0.3 (range 0.0-0.29, mean = 0.11). Fig. 4A illustrates an MGN cell from our sample with the highest orientation tuning index (0.29). Fig. 4B displays the distribution of all orientation tuning indices obtained. This distribution contrasts sharply with the orientation tuning indices obtained for visual cells in primary auditory cortex of rewired ferrets (see Chapter 3).

Some MGN cells preferred moving stimuli more than flashing stimuli. Slowly moving (<5°/s) stimuli were most effective in eliciting responses from most cells. A few cells responded well to large rapidly moving, or to rapidly jiggling, bars or spots. Directional selectivity was also seen. Figure 5A illustrates an MGN cell excited by a bar of light sweeping in one direction but inhibited by the bar sweeping in the opposite direction. We

quantified direction selectivity using a directionality index defined as: 1- (Non-preferred /Preferred Response). The directionality indices of 21 MGN cells which were quantitatively studied for this purpose ranged from 0.02 - 0.50 (mean = 0.18). Of these, 17 MGN cells were non-directional (index < 0.3), 4 were moderately directional (index 0.3 - 0.5), and none highly directional (index > 0.5) (Fig. 5B).

Receptive Field Size. Receptive fields were circular or elongated and exhibited either weak or absent inhibitory surrounds (not unlike normal LGN cells, cf. Esguerra et al., 1986; Roe et al., 1989). Receptive field sizes of MGN cells were, in general, quite large. Of the 105 MGN cells whose receptive field locations were determined, 38% (n=40) were sufficiently responsive to allow confident characterization of receptive field size. Receptive field sizes (defined as the average diameter of the long and the short axis of the receptive field) of MGN cells ranged from 1° to over 16° in diameter and were significantly larger (Mann Whitney-U, $p < .0001$) than those of normal LGN cells (Fig. 6A). These differences in receptive field size are not eccentricity-related: when eccentricity-matched (eccentricity < 30°) LGN and MGN cell populations are compared, receptive field sizes of MGN cells are still larger (Mann Whitney-U, $p < .0001$). While neither X, Y, or W cells in the normal LGN exhibited receptive field sizes as large as some seen in the MGN, some LGN W cells (Fig. 6C) did have large receptive fields with diffuse borders (n=2) or otherwise difficult to plot receptive fields (n=3) (cf. Cleland and Levick, 1974ab; Sur and Sherman, 1982). Such receptive fields were similar to those seen for some cells in the MGN (n=10, Fig. 6A).

Responses to auditory stimulation

Auditory responsiveness of MGN cells (n=27) was examined in two experiments. Responses to broad-band auditory stimuli such as clicks and white noise were obtained in some (n=4) MGN cells. The physiological characteristics of auditory responses were not examined in further detail. A few (n=3) MGN cells exhibited both visual and auditory responsiveness. In these cells, the response to stimulation of one modality dominated that of

the other modality. While very few such cells were observed, the convergence of auditory and visual inputs onto single cells remains an intriguing developmental issue.

II. Selective Redirection of Ganglion Cell Subpopulations

We have studied whether different subpopulations of retinal ganglion cells project to the MGN in ferrets by examining the retinal projections resulting from various combinations of the visual cortical (VCX), superior colliculus (SC), and brachium of the inferior colliculus (BC) lesions. There are different subpopulations of W cells in the retina. Making different combinations of lesions might vary the size of the retino-MGN projection based on removal of the normal targets of each subpopulation.

In normal ferrets, the LGN and the SC are the major retinal target zones. The laminar pattern of innervation seen in the LGN (Fig. 7A) is typical of the carnivore LGN: the A and C laminae receive contralateral input and the A1 and C1 laminae receive ipsilateral input. The MGN receives no retinal input (Fig. 7A). In ferrets which received a full complement of visual cortical, superior colliculus, and brachium of inferior colliculus lesions (VCX+SC+BC) at birth, a significant projection to the MGN is established. In these animals, retinal afferents terminate in almost all divisions of the MGN, including the dorsal, ventral, and medial divisions as defined by Morest (1965) (Fig. 7B, Fig. 8). The caudalmost portion of the MGN, which in normal animals does not project to primary auditory cortex, never receives retinal input. Unlike the retino-LGN projection, retinal afferents to the MGN terminate in a patchy fashion (Fig. 7B, Fig. 8). Often fibers are seen streaming into the MGN from the ventral optic tract at the base of the LGN or from the dorsocaudal border of the MGN.

Ferrets that had received less than the full complement of lesions at birth also demonstrated aberrant induction of retinal terminations; however, the size of the projection is significantly smaller. Ferrets that had only the superior colliculus and brachium lesions

(SC+BC, n=3) also received retinal input to the ventral, dorsal, and medial divisions of the MGN; however, the extent of these projections to the MGN were much smaller in comparison (Fig. 7C). Ferrets that received only visual cortical and brachium lesions (VCX+BC, n=3) at birth exhibited the least extensive retino-MGN projections (Fig. 7D).

To quantify these impressions, we mapped the regions of retinal termination (both heavy and light) in the MGN and calculated the extent of retinal termination in the MGN as a percent of total MGN volume in each animal. In the example shown in Fig. 8 (a VCX+SC+BC case), the volume of retinal termination in the MGN is 0.47 mm^3, the total MGN volume is 1.70 mm^3, and the resulting innervated MGN volume is 28%. Fig. 9 illustrates the result of such calculations for ferrets which had undergone different lesion combinations as neonates. The heaviest retinal innervation is seen in the VCX+SC+BC animals in which 28% and 17% of the MGN contained retinal label. In three SC+BC lesioned animals, 8%, 6%, and 2%, respectively, of the MGN contained retinal label. Only 0.5%, 1.2%, and 1.2% of the MGN volumes in the three VCX+BC animals, respectively, contained label. No innervation of the MGN was seen in ferrets that did not receive brachium transection (VCX, n=1; SC, n=2; VCX+SC, n=1). Neither did the BC lesion alone (n=1) induce MGN innervation. Thus, it appears that the VCX lesion and the SC lesion when done in conjunction with the brachium transection is the most effective for induction of retinal afferents into the MGN.

We make three observations about these findings: 1) Denervation of the MGN is a *necessary, but not sufficient* condition for retinal afferent induction. 2) When done in conjunction with the brachium transection, either the visual cortical or superior colliculus lesion alone is *sufficient* for induction of some afferents. 3) The inductive effect of VCX+SC+BC lesions is much larger than the sum of VCX+BC and SC+BC lesions. This third observation would imply that in the ferret retina there is a large population of W cells with axons bifurcating to innervate both the LGN and the SC. The interpretation of these

results and their bearing on the retinal cell classes that project to the MGN will be examined in the discussion.

III. Retinal Ganglion Cell Soma Sizes

Retinal Ganglion Cell Morphologies

Retinal ganglion cells were labelled following injections of HRP into retinal target nuclei. Retinal ganglion cell morphologies in normal ferrets were similar to those described previously in ferret retina (Henderson, 1985; Vitek et al., 1985). The retinal morphological cell types seen following thalamic injections in lesioned ferrets were qualitatively indistinguishable from normal (Fig. 10). In retinae of both normal and lesioned ferrets, cells with α-like morphologies were most easily distinguished by their large, angular somatas and often extensively-filled dendritic processes. Cells of the β cell class (fewer in rewired ferret retinae, see below) were often identified by their round, medium-sized somata and typically a single prominent proximal dendrite. Other morphological cell types were rarely distinguished due to the limited dendritic labelling of small and medium-sized cells.

Retinal Ganglion Soma Sizes

Large thalamic injections of HRP (which also labelled optic tract fibers running toward SC) in normal (n=1) and lesioned (n=2) ferrets resulted in extensive labelling of both the contralateral retina and the temporal crescent of the ipsilateral retina, as has been described in detail previously (Morgan et al., 1987). Retinal ganglion cells were well-labelled and soma sizes readily measured. For the purposes of discussion, we have divided the soma size distribution into small, medium, and large size ranges. We base the large soma size range on the percentage of α cells (approximately 5%) reported in the ferret retina (Vitek et al., 1985). Our small soma size range was based on the small cells labelled from injections in the SC

[cells projecting to the SC are primarily small (presumably W) or large (presumably Y) in size--this paper, Wingate et al.,1990; cf. Leventhal et al., 1985]. The medium size range (presumably X) is simply the intermediate range between the small and the large. These cell size divisions are only to be meant as guides; the interpretation of our data is not critically dependent on the exact placement of these divisions.

In both normal and lesioned ferret retinae, soma size measurements ranged from less than 50 um^2 to more than 400 um^2 (Fig. 11A). In the normal ferret (white bars), 48%, 46%, and 6% of the back-filled retinal ganglion cells fell into the small, medium, and large categories, respectively. Soma sizes back-filled from the VCX+SC+BC (black bars) and the SC+BC (grey bars) thalamic injections were significantly smaller than normal (VCX+SC+BC, Mann Whitney-U, $p < .025$; SC+BC, Mann Whitney-U, $p < .0001$). In the lesioned ferrets, there is a marked reduction in the number of medium-sized retinal ganglion cells (from 46% to 28% in VCX+SC+BC; from 46% to 11% in SC+BC). This is consistent with the significant retinal X-cell loss (Tong and Spear, 1982; cf. Sur et al., 1987) as well as medium-sized W cell loss (Rowe, 1990) found in cats with neonatal visual cortical ablations. There is also a significantly greater increase in the proportion of small-sized cells in the SC+BC lesion (87%) than in the VCX+SC+BC lesion (69%) (Mann Whitney-U, $p < .0001$).

To address more specifically which retinal ganglion cell populations comprise these distributions, restricted injections were made into retinal target zones of normal and lesioned animals. In normal animals, restricted injections into the LGN (n=1) resulted in labelling of small (74%), medium (19%), and large (7%) soma sizes (Fig. 11B, white bars). Similar to retinal projections to the SC in the cat, SC-projecting cells in the ferret (n=1) were primarily small (87%) or large (4%) in size (Fig. 11B, hatched bars). A small injection restricted to the most superficial layer of the SC superficial grey (n=1) labelled only cells in the extremely small (<100 um^2) cell size range (Fig. 11B, grey bars). Comparing the small cells that project to the LGN and to the superficial SC, these results are consistent with those in the cat in which

W cells projecting to the SC are smaller in size than those projecting to the C laminae of the LGN (Leventhal et al., 1985; Stanford, 1987).

In lesioned ferrets, restricted injections into the LGN revealed somewhat different retinal soma size distributions. An injection centered in the A lamina and impinging on the C lamina (Fig. 12A) labelled small (43%, mostly 100-200 um^2) and medium (57%) sized cells (Fig. 11C, grey bars). (We attribute the lack of large cells labelled from this injection to variation in a low frequency encounter rate of large size cells.) In another lesioned ferret, an injection almost entirely restricted to the C lamina (with some encroachment into the optic tract, Fig. 12B) labels many more small cells (68%) as well as some large (6%) cells (Fig. 11C, black bars). These results from these two LGN injections suggest that in lesioned ferrets the C laminae retain both retinal Y and larger-sized W input. Labelling of medium-sized cells from these injections may represent surviving β cells (Sur et al., 1987; see also above). In a third lesioned ferret, a restricted injection was made in the LP/Po complex (Fig. 12C). The soma size distribution resulting from this injection is shifted towards medium sized cells (57%, Fig. 11C, hatched bars). The enhanced projection to LP/Po previously described in lesioned ferrets (Pallas et al., 1990) is thus likely to be comprised of larger W or remaining X retinal ganglion cells.

In contrast, retinal ganglion cells projecting to the MGN of lesioned ferrets are primarily small in size (Fig. 11D). In one VCX+SC+BC lesioned ferret, a restricted injection was made into the MGN; however, a small amount of label did spread dorsally into the LGN from the injection site (Fig. 12D). Despite this, the retinal soma size distribution resulting from this injection is clearly shifted towards smaller soma sizes (Fig. 11D, black bars). Almost 80% fall in the small cell range, approximately 30% of which are <100 um^2 and 70% of which are >100 um^2. Similarly, an injection into the MGN (which impinged slightly on the optic tract, Fig. 12E) of a VCX+BC lesioned ferret produced a soma size distribution consisting of almost 80% small cells, 60% of which were > 100 um^2 in size (Fig. 11D, grey bars). Interestingly, this distribution is not significantly different from that obtained following

the large thalamic VCX+SC+BC injection (Fig. 11A, black bars; Mann Whitney-U, $p > .3$); it is, however, shifted significantly towards larger cells than the distribution resulting from the SC+BC thalamic injection (Fig. 11A, grey bars; MW-U, $p < .002$).

In summary, in VCX+SC+BC lesioned ferrets, there is an increased proportion of small-sized retinal ganglion cells in the retina. Retinal ganglion cells projecting to the MGN of lesioned ferrets (VCX+SC+BC, SC+BC, and VCX+BC) are primarily small in size. These small cells overlap in size with those of W cells projecting to the superficial layer of the superior colliculus (primarily <100 um^2) as well as those projecting to the C laminae of the LGN (primarily >100 um^2). We also find evidence that in VCX+BC lesioned animals a greater percentage of the MGN-projecting population is of the larger size W cells (Fig. 11D, grey bars), while in SC+BC lesioned animals there is a greater proportion of smaller size W cells (compare SC+BC thalamic injection with VCX+SC+BC thalamic injection, Fig. 11A, grey and black bars, respectively; also compare SC+BC thalamic injection with VCX+BC MGN injection, Fig. 11D, grey bars). These findings are consistent with the hypothesis that the W cell populations that are directly deprived of their normal targets are more likely to innervate alternative target zones.

Discussion

We have presented physiological, developmental, and anatomical evidence that the retinal ganglion cell population(s) projecting to the MGN in the lesioned ferrets belong to the W cell class. We discuss the anatomical evidence first below.

Retinal Ganglion Cells Projecting to MGN: Comparison with normal retinal W cells

Retinal Ganglion Cell Morphologies

Each physiological class of ganglion cell in the carnivore retina possesses distinct morphologies (Stone and Clarke, 1980; Fukuda et al., 1984; Stanford and Sherman, 1984; Stanford, 1987a,b), retinal distributions (Stone, 1978; Wassle and Illing, 1982; Leventhal, 1982) and central projection patterns (Kelly and Gilbert, 1975; Leventhal et al., 1985). Similar to the cat, the ferret retina contains ganglion cells with large alpha-type somata (Y cells, 5%), medium-size beta-type somata (X cells, 25%), and other small and medium size somata (W cells, 70%) (Henderson, 1985; Vitek et al., 1985; Wingate et al., 1990). There is good evidence that Y cells project primarily to the A, A1, and magnocellular C laminae of the LGN and the deeper part of the superficial superior colliculus. X cells project primarily to the A laminae of the LGN.

Our current understanding of the projection patterns of retinal W cells is schematized in Fig. 13A. Medium-sized W cells, which compose a significant proportion (30%) of the medium-sized retinal ganglion cell population (Stanford 1987a), project primarily to the parvocellular C laminae of the LGN and the MIN (Rowe and Dreher, 1982; Leventhal et al., 1985). Small-sized W cells project to the upper superficial SC, the ventral LGN, and the pretectum (Hoffman and Schoppmann, 1975; Guillery and Oberdorfer, 1977; Spear et al., 1977; Wassle and Illing, 1980). Some of these small cells (20%, Leventhal et al., 1985; 43%, Illing and Wassle, 1981) bifurcate to both the LGN and the SC (see Illing, 1980 and

Wingate, 1990 for direct demonstration of bifurcating γ cells). One study demonstrates (indirectly) dramatic loss of medium-sized W cells following neonatal visual cortical ablations in cats (Rowe, 1990); this could suggest that many cells that project to the C laminae of the LGN do not bifurcate.

In this study, neonatal ablation of superior colliculus deprives the SC-projecting (small-sized) W cell population of its normal target (Fig. 13B). Similarly, neonatal ablation of the visual cortex most strongly affects the C laminae-projecting (medium-sized) W cells (Fig. 13C). Thus, we find that small cells labelled in VCX+BC cases are somewhat larger in general than those labelled in SC+BC cases. When both lesions are done in conjunction, not only are these two W cell populations affected, but also the W cells which bifurcate to both the SC and the LGN. The resulting aberrant projection to the MGN is correspondingly larger (Fig. 13D).

We also consider other possible explanations of our findings. While we cannot entirely discount the possibility that a small number of the medium-sized cells labelled are X cells, we have no compelling indications that X cells contribute significantly to the MGN projection (see below). Still better dendritic filling techniques than that resulting from HRP back-fills would be required to exclude this possibility (Gitelman, in progress). The substantially increased projection in the doubly lesioned VCX+SC+BC cases may also result from enlarged W cell terminal arbors in the MGN. However, labelling of single arbors arising from the optic tract and terminating in the MGN suggest otherwise (Pallas et al., 1989). It is also possible that due to visual cortical removal an increased number of superior-colliculus projecting W cells are rescued. This might be achieved via elimination of dendritic competition in the retina during the period of cell death (cf. Linden and Serfaty, 1985). However, retinal ganglion cell densities in the VCX+SC+BC and the SC+BC case are not significantly different (data not shown).

MGN Physiology

Y, X, and W retinal ganglion cells exhibit very distinct physiological characteristics. Y cells exhibit non-linear spatial summation, respond phasically, have large receptive fields, and axons with fast conduction velocities, while X cells exhibit linear spatial summation, respond tonically, have small receptive fields, and axons with moderate conduction velocities (Esguerra et al., 1986; Roe et al., 1989; see Sherman, 1985 for review of cat X, Y, W cell classes). In cats, W-type ganglion cells are actually a heterogeneous class composed of at least several subclasses (e.g. Stanford 1987a). W cells have poor, inconsistent (sluggish) responses to visual stimuli; either tonic (medium-sized cells) or phasic (small sized cells) responsiveness; large receptive field sizes, some with center-surround organization and others with diffuse receptive fields; poor and either linear or nonlinear spatial summation; and thin, poorly-myelinated, slowly-conducting axons. Contrast preferences of W cells include on, off, on/off, contrast-suppressed, and color-coded types. Direction-selective W cells have also been described (Cleland and Levick, 1974ab; Wilson et al., 1976; Rodieck, 1979; Sur and Sherman, 1982; Rodieck and Brening, 1983; Fukuda et al., 1984; Stanford, 1987a).

Physiological response properties of visual cells in the MGN suggest strongly that visual input arises from retinal W cells. These cells have 1) long conduction latencies indicating input from finely myelinated, slowly conducting retinofugal axons, 2) poor sluggish responsiveness, 3) large receptive field sizes some of which exhibited diffuse borders, 4) heterogeneity in stimulus preferences, and 5) the presence of some directionally selective cells.

Inferring presynaptic source from postsynaptic responses. With our electrodes, retino-MGN axons were not encountered, presumably because of their small axon diameter. Even in normal ferrets, W retinogeniculate axons are rarely encountered, while X and Y retinogeniculate axons are commonly encountered in the optic tract or in the LGN (Roe et al., 1989). Thus, our physiological determination of the nature of presynaptic retinal input is based on the characterizations of postsynaptic visual cells in the MGN.

Post-synaptic thalamic cells are likely to have response properties similar to those of their input cells. LGN cells receive input from retinal ganglion cells of a single physiological class and thus exhibit response properties very similar to those of their afferent retinal ganglion cells (X and Y cells: Cleland et al. 1971, Hochstein and Shapley, 1976; Lehmkuhle et al., 1980; So and Shapley 1981; W cells: Wilson et al., 1976; Sur and Sherman 1982). These shared characteristics include nearly every major physiological feature described for retinal ganglion cells, such as center-surround organization of the receptive field, linearity of spatial and temporal summation, tonicity of center response, receptive field size, strength of surround suppression, response to large, fast-moving targets, and axon conduction velocity.

The fact that these three W, X, and Y channels exist fairly independently in parallel in the adult suggests that during development retinal afferents must recognize some cue(s) that enable them to establish channel-specific connections. Conversely, convergence of input from multiple retinal cell classes onto single MGN cells is also unlikely. This suggests that each visual target cell in the MGN may receive input from a single class of retinal ganglion cell and thus exhibit receptive field properties very similar to its retinal source. In support of this notion, in the normal ascending auditory projection, each subdivision of the MGN receives input from specific subdivisions of the inferior colliculus (Kudo and Niimi, 1978; Anderson et al., 1980). Thus, the segregation of retinal cell class connectivity with thalamic targets appears to be quite a robust phenomenon and is unlikely to disintegrate following these neonatal lesions in ferrets.

It is also possible that X or Y inputs to the MGN participate in abnormal thalamic connectivities and thereby produce W-like responses in MGN cells. We find this possibility unlikely for several reasons. First, thalamic nuclei across sensory modalities share similar intrathalamic circuitries. For example, characteristic triadic arrangements of sensory input, projection cell, and local inhibitory input has been described in the LGN (Guillery, 1969; Wilson et al., 1984; Mize et al., 1986), MGN (Morest, 1975; Majorossey and Kiss,1976), as well as the VB (Penny et al., 1983; Spreafico et al., 1983). Thalamic neurons in LGN,

MGN, and VB have common and characteristic cellular physiological responses (e.g. relay vs. burst mode) which are influenced by the presence or absence of specific extrathalamic influences (McCormick and Prince, 1988; Deschenes and Hu, 1990; Salt and Eaton, 1990; Steriade and Llinas, 1988; Esguerra et al., 1991). Evidence also suggests that the intra-MGN circuitry in these lesioned ferrets is similar to that of the normal MGN (Campbell and Frost, 1988). Second, Y cell input to the MGN is incompatible with the long conduction velocities of MGN cells and small soma sizes back-filled from the MGN. We have, furthermore, demonstrated that long conduction velocity is not due to a general, non-specific effect on conduction latencies in lesioned ferrets (Fig. 1C). Third, the overlap between X cell and W cell latencies and soma sizes raises the possibility that X cells contribute to the retino-MGN projection; however, this is also unlikely based on the extensive X cell loss following visual cortical ablation, the large, often diffuse receptive fields, and other visual responses recorded in the MGN.

Retinal W Cell Plasticity: Developmental Implications

Under what conditions do retinal W cells sprout to innervate a novel target such as the MGN? Our experiments suggest that there are necessary and sufficient conditions for such sprouting to take place. We discuss below the implications of these data for underlying mechanisms.

Target Availability

We have demonstrated that two minimal conditions are necessary to achieve rerouting (sprouting) of a projecting cell population: 1) severe deprivation of normal target zones and 2) availability of alternative target space. More specifically, removal/reduction of the SC or the LGN results in selective induction of the SC-projecting or the LGN-projecting W cell

populations, respectively. Lesions reducing terminal space in both SC and LGN additionally appears to induce sprouting of W cells with axons bifurcating to both SC and LGN; partial deprivation (i.e. lesion of either collateral) is not sufficient to cause extensive rerouting of this population.

There is evidence that the availability of alternative target space is crucial for a retinal ganglion cell's survival. Extensive removal of normal target zones without making available alternative target space leads to extensive cell death of affected retinal ganglion cells. Thus, neonatal ablation of visual cortex leads to extensive X cell death in both retina and LGN of cats (Murphy and Kalil, 1979; Tong and Spear, 1982; Payne et al., 1984); medium-sized retinal W cells are also lost (Rowe, 1990). Y cells survive such insults, presumably because they are maintained by other sustaining collaterals. We note that the smaller projection to MGN established following VCX+BC lesions than following SC+BC lesions may be due to the fact that a remnant portion of the LGN remains following neonatal visual cortical lesions (due to projections from the LGN to nonablated visual cortical areas) while tectal lesions remove the superficial SC entirely.

These observations may reflect the principle of "conservation of arbor" (Schneider, 1973; Jhaveri et al., 1990). That is, reduction of a cell's arbor size is accompanied by compensatory sprouting elsewhere in the arbor, either in a pre-existing collateral or at any point along an axon's trajectory where there is available terminal space (e.g. in LP/Po or even in a non-visual structure such as the MGN). This principle is strengthened by the fact that establishment of the retino-MGN projection in lesioned ferrets is due to reactive sprouting, and not to maintainence of pre-existing exuberant connections (cf. Frost, 1982, 1984, 1986): we have never seen any retinal projection to the MGN in neonatal ferrets (Hahm, 1991). Furthermore, the course of the optic tract in lesioned ferrets is much more expanded than normal (Pallas et al., 1989), extending over the surface of the MGN instead of remaining restricted over the LGN surface. This expanded optic tract is not seen in normal neonatal ferrets (Hahm, 1991).

Timing

Why do retinal W cells (and not X or Y cells) innervate the MGN? One possibility is that at the time of lesions W cells are the most able to reroute their axons. To obtain successful rerouting of retinal ganglion cell projections, lesions must be done at an early stage of retinofugal development: no retinal innervation of the MGN results from lesions done past P1 (unpublished observations). In the cat, medium sized retinal ganglion cells are generated from E21-E31, large cells from E25-E31, and small cells from E21-E36 (Walsh et al., 1983). Ferret retinal ganglion cells are generated during approximately the same period (Greiner and Weidman, 1981). At birth (E41), retinal afferents have invaded the LGN (Linden et al., 1981) and the SC (Roe, unpublished observations), but have not yet segregated into eye specific zones. Thus, small cells are among the last to be generated in the retina and are likely to be at an earlier developmental stage at the time of the brain lesions in neonatal ferrets. Thus, those cells generated last may not have yet exceeded their critical period for reactive sprouting at the time of lesioning and may be most able to innervate alternative target space (cf. Perry and Cowey, 1982). On this view, lesions done earlier might enable X or Y retinal cells to project to the MGN as well.

Intrinsic Developmental Programs

An alternative explanation for the selective induction of W cell fibers into the MGN is that W cells are intrinsically different in their developmental program than X or Y cells. W cells could have a greater capacity to innervate alternative structures or, put another way, simply be less selective in target selection than X or Y cells. In anecdotal support of this, W cells innervate multiple thalamic and midbrain nuclei, whereas Y cells, and even more so X cells, target fewer structures.

Although there are no studies on the development of W cell terminations, there is substantial evidence that X and Y cells differ in their developmental programs. Normally, X cell arbors undergo a period of exuberance followed by pruning, have very direct trajectories,

and are small in size; Y cell arbors expand monotonically, have varied trajectories, and are large in size (Sur et al., 1984; Sur et al., 1987; Roe et al., 1989). X and Y cells respond very differently to alterations in visual input: X cells typically are much less affected by such changes whereas Y cells display severe reductions in size and abnormalities in termination patterns (see Sur, 1988 for review). Whether the timing of lesions or intrinsic differences in developmental programs is the key factor in W cells innervating the MGN in rewired ferrets could be tested directly by performing the lesions at an earlier (prenatal) stage of development.

References

Anderson RA, Roth GL, Aitkin LM, Merzenich MM (1980) The efferent projections of the central nucleus and the pericentral nucleus of the inferior colliculus in the cat. J Comp Neurol 194:649-662.

Berson DM (1987) Retinal W-cell input to the upper superficial gray layer of the cat's superior colliculus: a conduction-velocity analysis. J Neurophysiol 58:1035-1051.

Callahan EC, Tong L, Spear PD (1984) Critical period for the marked loss of retinal X-cells following visual cortex damage in cats. Brain Res 323:302-306.

Campbell G, Frost DO (1988) Synaptic organization of anomalous retinal projections to the somatosensory and auditory thalamus: target-controlled morphogenesis of axon terminals and synaptic glomeruli. J Comp Neurol 272:383-408.

Cleland BG, Dubin MW, Levick WR (1971) Sustained and transient neurones in the cat's retina and lateral geniculate nucleus. J Physiol Lond 217:473-496.

Cleland BG, Levick WR (1974a) Brisk and sluggish concentrically organized ganglion cells in the cat's retina. J Physiol Lond 240:421-456.

Cleland BG, Levick WR (1974b) Properties of rarely encountered types of ganglion cells in the cat's retina and an overall classification. J Physiol Lond 240:457-492.

DeOlmos JS (1977) An improved HRP method for the study of central nervous connections. Exp Brain Res 29:541-551.

Deschenes M, Hu B (1990) Electrophysiology and pharmacology of the corticothalamic input to lateral thalamic nuclei: an intracellular study in the cat. Eur J Neurosci 2:140-152.

Esguerra M, Garraghty PE, Russo GS, Sur M. (1986) Lateral geniculate nucleus in normal and monocularly deprived ferrets: X- and Y- cells and cell body size. Soc Neurosci Abstr 12:10.

Esguerra M, Kwon YH, Sur M (1991) Retinogeniculate EPSPs recorded intracelluarly in the ferret lateral geniculate nucleus *in vitro*: role of NMDA receptors, *submitted.*

Friedlander MJ (1982) Structure of physiologically classified neurones in the kitten dorsal lateral geniculate nucleus. Nature 300:180-183.

Frost DO (1982) Anomalous visual connections to somatosensory and auditory systems following brain lesions in early life. Dev Brain Res 3:627-635.

Frost DO (1984) Axonal growth and target selection during development: retinal projections to the ventrobasal complex and other "nonvisual" structures in neonatal Syrian hamsters. J Comp Neurol 230:576-592.

Frost DO (1986) Development of anomalous retinal projections to nonvisual thalamic nuclei in Syrian hamsters: a quantitative study. J Comp Neurol 252:95-105.

Fukuda Y, Hsiao CF, Watanabe M, Ito H (1984) Morphological correlates of physiologically identified Y-, X-, and W-cells in cat retina. J Neurophysiol 52:999-1013.

Garraghty PE (1985) Mixed cells in the cat lateral geniculate nucleus: functional convergence or error in development? Brain Behav Evol 26:58-64.

Greiner JV,Weidman TA (1981) Histogenesis of the ferret retina. Exptl Eye Res 33:315-332.

Guillery RW (1969) The organization of synaptic interconnections in the laminae of the dorsal lateral geniculate nucleus of the cat. Z Zellforsch 96:1-38.

Guillery RW, Oberdorfer MD (1977) A study of fine and coarse retino-fugal axons terminating in the geniculate C laminae and in the medial interlaminar nucleus of the mink.

Henderson Z. (1985) Distribution of ganglion cells in the retina of adult pigmented ferret. Brain Res. 358:221-228.

Hochstein S, Shapley RM (1976) Quantitative analysis of retinal ganglion cell classifications. J Physiol 262:237-264.

Hoffman K-P (1973) Conduction velocity in pathways from retina to superior colliculus in the cat: a correlation with receptive field properties. J Neurophysiol 36:409-424.

Hoffman K-P, Schoppmann A (1975) Retinal input to direction selective cells in the nucleus tractus opticus of the cat. Brain Res 99:359-366.

Illing R-B (1980) Axonal bifurcation of cat retinal ganglion cells as demonstrated by retrograde double labelling with fluorescent dyes. Neurosci Lett 19:125-130.

Illing R-B, Wassle H (1981) The retinal projection to the thalamus in the cat: a quantitative investigation and a comparison with the retinotectal pathway. J Comp Neurol 202:265-285.

Jhaveri S, Schneider GE, and Erzurumlu RS (1990) Axonal plasticity in the context of development.

Kelly JP, Gilbert CD (1975) The projections of different morphological types of ganglion cells in the cat retina. J Comp Neurol 163:65-80.

Kudo M, Niimi K (1978) Ascending projections of the inferior colliculus onto the medial geniculate body in the cat studied by anterograde and retrograde tracing techniques. Brain Res 155:113-117.

Lehmkuhle S, Kratz KE, Mange SC, Sherman SM (1980) Spatial and temporal sensitivity of X- and Y-cells in the dorsal lateral geniculate nucleus of the cat. J Neurophysiol 43:520-541.

Leventhal AG (1982) Morphology and distribution of retinal ganglion cells projecting to different layers of the dorsal lateral geniculate nucleus in normal and siamese cats. J Neurosci 2:1024-1042.

Leventhal AG, Rodieck RW, Dreher B (1985) Central projections of cat retinal ganglion cells. J Comp Neurol 237:216-226.

Linden DC, Guillery RW, Cucchiaro J (1981) The dorsal lateral geniculate nucleus of the normal ferret and its postnatal development. J Comp Neurol 203:189-211.

Linden R, Serfaty CA (1985) Evidence for differential effects of terminal and dendritic competition upon developmental neuronal death in the retina. Neurosci 15:853-868.

Majorossey K, Kiss A (1976) Specific patterns of neuron arrangement and of synaptic articulation in the medial geniculate body. Exp Brain Res 26:1-17.

McCormick DA, Prince DA (1988) Noradrenergic modulation of firing pattern in guinea pig and cat thalamic neurons, *in vitro*. J Neurophysiol 59:978-996.

Mesulam M.-M. (1978) Tetramethyl benzidine for horseradish peroxidase neurohistochemistry: a non-carcinogenic blue reaction product with superior sensitivity for visualizing neural afferents and efferents. J Histochem Cytochem 26:106-117.

Mize RR, Spencer RF, Horner LH (1986) Quantitative comparison of retinal synapses in the dorsal and ventral (parvicellular) C laminae of the cat dorsal lateral geniculate nucleus. J Comp Neurol 248:57-73.

Morest K (1965) The laminar structure of the medial geniculate body of the cat. J Anat Lond 99:143-160.

Morest K (1975) Synaptic relationships of Golgi Type II cells in the medial geniculate body of the cat. J Comp Neurol 162:157-194.

Morgan JE, Henderson Z, Thompson ID (1987) Retinal decussation patterns in pigmented and albino ferrets. Neurosci 20:519-535.

Murphy EH, Kalil RE (1979) Functional organization of lateral geniculate cells following removal of visual cortex in the newborn kitten. Science 206:713-716.

Pallas SL, Hahm JO, Sur M (1989) Retinal axon arbors in a novel target: morphology of ganglion cell axons induced to arborize in the medial geniculate nucleus of ferrets. Soc Neurosci Abstr 15:495.

Pallas SL, Roe AW, Sur M (1990) Visual projections induced into the auditory pathway of ferrets. I. Novel inputs to primary auditory cortex (A1) from the LP/pulvinar complex and the topography of the MGN-A1 projection. J Comp Neurol 298:50-68.

Payne BR, Pearson HE, Cornwell P (1984) Transneuronal degeneration of beta retinal ganglion cells in the cat. Proc Roy Soc Lond 222:15-32.

Penny GR, Fitzpatrick D, Schmechel DE, Diamond IT (1983) Glutamic acid decarboxylzase-immunoreactive neurons and horseradish peroxidase-labeled projection neurons in the ventral posterior nucleus of the cat and *Galago senegalensis*. J Neurosci 3:1868-1887.

Perry VH, Cowey A (1982) A sensitive period for ganglion cell degeneration and the formation of aberrant retino-fugal connections following tectal lesions in rats. Neurosci. 7:583-594.

Price DJ, Morgan JE (1987) Spatial properties of neurones in the lateral geniculate nucleus of the pigmented ferret. Exp Brain Res 68:28-36.

Rodieck RW (1979) Visual pathways. Ann Rev Neurosci 2:193-225.

Rodieck RW, Brening RK (1983) Retinal ganglion cells: properties, types, genera, pathway, and trans-species comparisons. Brain Behav Evol 23:121-164.

Roe AW, Garraghty PE, Sur M (1987) Retinotectal W-cell plasticity: experimentally induced retinal projections to auditory thalamus in ferrets. Soc Neurosci Abstr 13:1023.

Roe AW, Garraghty PE, Sur M (1989) The terminal arbors of single on-center and off-center X and Y retinogeniculate axons within the ferret's lateral geniculate nucleus. J Comp Neurol 288:208-242.

Rowe MH, Dreher B (1982) Retinal W-cell projections to the medial interlaminar nucleus in the cat: implications for ganglion cell classification. J Comp Neurol 204:117-133.

Rowe MH (1990) Evidence for degeneration of retinal W cells following early visual cortical removal in cats. Brain Behav Evol 35:253-267.

Salt TE, Eaton SA (1990) Postsynaptic potentials evoked in ventrobasal thalamus neurones by natural sensory stimuli. Neurosci Lett 114:295-299.

Schneider GE (1973) Early lesions of superior colliculus: factors affecting the formation of abnormal retinal projections. Brain Behav Evol 8:73-109.

Sherman SM (1985) Functional organization of the W-, X-, and Y-cell pathways in the cat: a review and hypothesis. Prog Psychobiol Physiol Psych, 2:233-314.

So Y-T, Shapley R (1981) Spatial tuning of cells in and around lateral geniculate nucleus of the cat: X and Y relay cells and perigeniculate interneurons. J Neurophysiol 45:107-120.

Spear PD, Smith DC, Williams LL (1977) Visual receptive field properties of single neurons in cat's ventral lateral geniculate nucleus. J Neurophysiol 40:390-409.

Spreafico R, Schmechel DE, Ellis LC, Rustioni A (1983) Cortical relay neurons and interneurons in the n. ventralis posterolateralis of cats: a horseradish peroxidase, electron microscopic, Golgi and immunocytochemical study. Neurosci 9:491-509.

Stanford LR (1987a) W-cells in the cat retina: correlated morphological and physiological evidence for two distinct classes. J Neurophysiol 57:218-244.

Stanford LR (1987b) X-cells in the cat retina: relationships between the morphology and physiology of a class of cat retinal ganglion cells. J Neurophysiol 58:940-964.

Stanford LR, Sherman SM (1984) Structure/function relationships of retinal ganglion cells in the cat. Brain Res 297:381-386.

Steriade M, Llinas RR (1988) The functional states of the thalamus and the associated neuronal interplay. Physiol Rev 68:649-742.

Stone J (1978) The number and distribution of ganglion cells in the cat's retina. J Comp Neurol 180:753-772.

Stone J, Clarke R (1980) Correlation between soma size and dendritic morphology in cat retinal ganglion cells: evidence of further variation in the γ-cell class. J Comp Neurol 192:211-217.

Sur M (1988) Development and plasticity of retinal X and Y axon terminations in the cat's lateral geniculate nucleus. Brain Behav Evol 31:243-251.

Sur M, Esguerra M, Garraghty PE, Kritzer MF, Sherman SM (1987) Morphology of physiologically identified retinogeniculate X- and Y-axons in the cat. J Neurophysiol 58:1-32.

Sur M, Roe AW, Garraghty PE (1987) Evidence for early specificity of the retinogeniculate X cell pathway. Soc Neurosci Abstr 13:590.

Sur M, Sherman SM (1982) Linear and nonlinear W-cells in C-laminae of the cat's lateral geniculate nucleus. J Neurophysiol 47:869-884.

Sur M, Weller RE, Sherman SM (1984) Development of X- and Y-cell retinogeniculate terminations in kittens. Nature 310:246-249.

Tong L, Spear PD (1982) Loss of retinal X-cells in cats with neonatal or adult visual cortex damage. Science 217:72-75.

Vitek DJ, Schall JD, Leventhal AG (1985) Morphology, central projections, and dendritic field orientation of retinal ganglion cells in the ferret. J Comp Neurol 241:1-11.

Walsh C, Polley EH, Hickey TL, Guillery RW (1983) Generation of cat retinal ganglion cells in relation to central pathways. Nature 302:611-614.

Wassle H, Illing RB (1980) The retinal projection to the superior colliculus in the cat: a quantitative study with HRP. J Comp Neurol 190:333-356.

Weber AJ, Kalil RE, Stanford LR (1989) Morphology of single, physiologically identified retinogeniculate Y-cell axons in the cat following damage to visual cortex at birth. J Comp Neurol 282:446-455.

Williams RW, Chalupa LM (1982) Prenatal development of retinocollicular projections in the cat: an anterograde tracer transport study. J Neurosci 2:604-622.

Wilson PD, Rowe MH, Stone J (1976) Properties of relay cells in cat's lateral geniculate nucleus: a comparison of W-cells with X- and Y-cells. J Neurophysiol 39:1193-1209.

Wilson JR, Friedlander MJ, Sherman WM (1984) Fine structural morphology of identified X- and Y-cells in the cat's lateral geniculate nucleus. Proc R Soc Lond B 221:411-436.

Wingate RJT, Fitzgibbon T, Webb EI, Thompson ID (1990) Lucifer yellow, fluorescent retrograde tracers and fractal analysis characterize ferret retinal ganglion cells. Soc Neurosci Abstr 16:1216.

Figure Legends

Fig. 1. Latencies to electrical stimulation of the optic chiasm of A) MGN cells in rewired ferrets B) LGN cells of normal ferrets and C) LGN cells in rewired ferrets. A) Latencies of all MGN cells recorded (light bars, n=226, x=5.6, range 1.5-35.0 msec) are not significantly different (MW-U $p > .25$) from those of visually driven MGN cells (dark bars, n=123, x=4.8, range 1.5-18.6). B) Latencies of normal LGN X (light bars, n=48, x=1.9), Y (dark bars, n=22, x=1.6), and W (grey bars, n=13, x=2.8) cells. C) Latencies from LGN of rewired ferrets for LGN X (light bars, n=24, x=1.80), Y (dark bars, n=61, x=1.76), and W (grey bars, n=23, x=3.15) cells.

Fig. 2. Responsivity ratings for visual MGN cells (n=46) from three rewired ferrets. 1 indicates low responsivity and 4 responsivity comparable to that of normal X and Y LGN cells.

Fig. 3. On and Off cells in the MGN. A) On-center cell responding to grating (0.25 cyc/deg) drifting at 2 hz. (Sum of 20 cycles). This cell responds to light increment in each cycle and is silent upon light decrement. B) The activity level of this off-center cell is slightly depressed by a light bar passing over its receptive field. Bar size 1.8°x11.3° moving at 8.7°/s. Sum of 30 cycles.

Fig. 4. MGN cells are not selective for orientation. A) Post-stimulus time histograms illustrating the response of an MGN cell to a moving vertically oriented bar of light (left) and to a moving horizontally oriented bar of light (right). This cell had the highest orientation index (0.29) of the ten MGN cells studied in this fashion. Its directionality index is 0.24. (Bar 2°x25° moving at 15°/s. Sum of 20 cycles.) B)

Distribution of orientation indices of MGN cells (n=10, x=0.11, range 0.0 - 0.29). See text.

Fig. 5. Directional selectivity of MGN cells. A) Post-stimulus time histogram illustrating a directionally selective MGN cell. Directionality index 0.5. (Stimulus is 2°x8° bar moving at 6°s. Sum of 20 cycles). B) Directionality indices of MGN cells (n=21, range 0.02-0.50, x=0.18). See text.

Fig. 6. Receptive field sizes (in degrees, calculated as the average diameter of the long and the short axis of the receptive field) of A) MGN (dark bars, n=40, x=13.1°) and LGN (light bars, n=121, x=3.2°) cells, B) MGN (n=16, x=11.5°) and LGN (n=80, x=2.5) cells with eccentricities less than 30°, and C) normal LGN cells shown by class (same data as in A: X, n=71, x=2.6; Y, n=40, x=4.0; W, n=13, x=3.9).

Fig. 7. Photomicrograph of the LGN and MGN following injection of HRP-WGA in contralateral eye. A) Normal adult ferret: laminae A and C are well delineated. MGN is devoid of label. B) Adult ferret that received neonatal lesions of visual cortex, superior colliculus, and brachium of inferior colliculus (VCX+SC+BC). Remnant LGN, retaining retinal afferents, is shrunken in size and displays abnormal lamination pattern. In contrast to the normal MGN, MGN in lesioned ferrets receive substantial amount of retinal input. C) Adult ferret that received only SC and BC lesions at birth: LGN is normal in size and lamination. MGN also contains retinal terminal label, but to a lesser degree than in VCX+SC+BC animals. D) Adult ferret that received only VCX+BC lesions at birth: LGN is shrunken in size. MGN contains much less retinal innervation than in VCX+SC+BC animals (small zone of retinal termination indicated by white arrowhead). Scale bar: 500 μm applies to A-D.

Fig. 8. Reconstruction of retinal terminal label in sagittal sections of the MGN in a neonatally lesioned (VCX+SC+BC) ferret. Dense hatching indicates regions of heavy terminal label; more widely spaced hatching indicates regions of light label. Rostral is to left and dorsal is up. Section numbers (each section 50 um thick) run from lateral (60) to medial (80). Subdivisions of MGN are indicated: ventral (MGv), dorsal (MGd), and medial (MGm) divisions.

Fig. 9. Size of retino-MGN projection expressed as a percent of MGN volume for each of the animals that received VCX+SC+BC lesions (n=2), SC+BC lesions (n=3), or VCX+BC lesions (n=3) at birth. Animals which received VCX+SC+BC lesions have the most enhanced projection to MGN.

Fig. 10. Photomicrograph of retinal ganglion cells back-filled from thalamus of a neonatally lesioned (VCX+SC+BC) ferret. Cells with α morphologies are easily distinguishable. Cells are primarily small and large in size.

Fig. 11. Soma size distributions of retinal ganglion cells back-filled from thalamic injections of HRP. A) Total retinal ganglion soma size distribution (following large thalamic injections) in normal (white bars, x=190 um^2), VCX+SC+BC lesioned (black bars, x=173 um^2), and SC+BC lesioned (grey bars, x=141 um^2) ferrets. B) Soma size distributions of retinal ganglion cells projecting to LGN (white bars, x=178 um^2), SC (hatched bars, x=146 um^2), and upper superficial SC (grey bars, x=67 um^2) in normal ferrets. C) Soma size distributions of retinal ganglion cells projecting primarily to the A laminae of the LGN (grey bars, x=222 um^2), the C laminae of the LGN (black bars, x=162 um^2), and the LP/Po complex (hatched bars, x=218 um^2) in VCX+SC+BC lesioned ferrets. D) Soma size distributions of retinal ganglion cells projecting

primarily to the MGN of VCX+SC+BC (black bars, x=165 um^2) and of VCX+BC (grey bars, x=162 um^2) lesioned ferrets.

Fig. 12. Restricted HRP injection sites in VCX+SC+BC (A-D) and in VCX+BC (E) lesioned ferrets producing retinal back-fills presented in Fig. 11C, D. Sections shown in photomicrographs shown on left with explanatory drawings on right (injection site indicated by hatched lines. A) An injection centered in the A lamina and impinging on the C lamina of the LGN (see Fig. 11C, grey bars). B) An injection restricted to the LGN C lamina (see Fig. 11C, black bars). C) An injection into LP/Po complex (see Fig. 11C, hatched bars). D) An injection into MGN (see Fig. 11D, black bars). There is some spread of label into LGN above. E) An injection into MGN with some encroachment into the optic tract (see Fig. 11D, grey bars). Scale bar: 500 μm applies to A-E. ET: electrode track. OT: optic tract. BC: blood clot.

Fig. 13. Schematic diagram of retinal W cells and their central projection patterns in normal and neonatally lesioned ferrets. A) In normal ferrets, medium-sized W cells (W_m) project primarily to the LGN C laminae. Some small-sized W cells (W_s) project to upper superficial SC; others project to both LGN C laminae and SC via an axonal bifurcation. The medial geniculate nucleus (MGN) receives afferent input from the inferior colliculus (IC). B) In SC+BC ferrets, non-bifurcating small-sized W cells reroute to the MGN. [Solid lines indicate projections. Dotted lines indicate projections which are lost.] C) In VCX+BC ferrets, medium-sized W cells reroute to the MGN. D) In VCX+SC+BC ferrets, all W cell populations depicted reroute to the MGN, thus resulting in a more extensive projection than in either SC+BC or the VCX+BC cases.

Table 1. Number of Units Recorded in MGN

	MGN	
Total	238	(%)
Electrically Driven	226	(95)
Visually Driven	131	(55)
Visually and Electrically Driven	123	(52)
Receptive Field Location Determined	105	(44)
Responsivity Rated	46	(19)
Receptive Field Size Determined	40	(17)
Ocular Dominance Determined	73	(31)
Quantitatively Characterized for		
Orientation	10	(9)
Direction	21	(4)
Driven by Auditory Stimuli	4	(15[a])
Driven by Auditory and Visual Stimuli	3	(11[a])

[a]Calculated from a total of 27 units tested with auditory stimulation in two experiments.

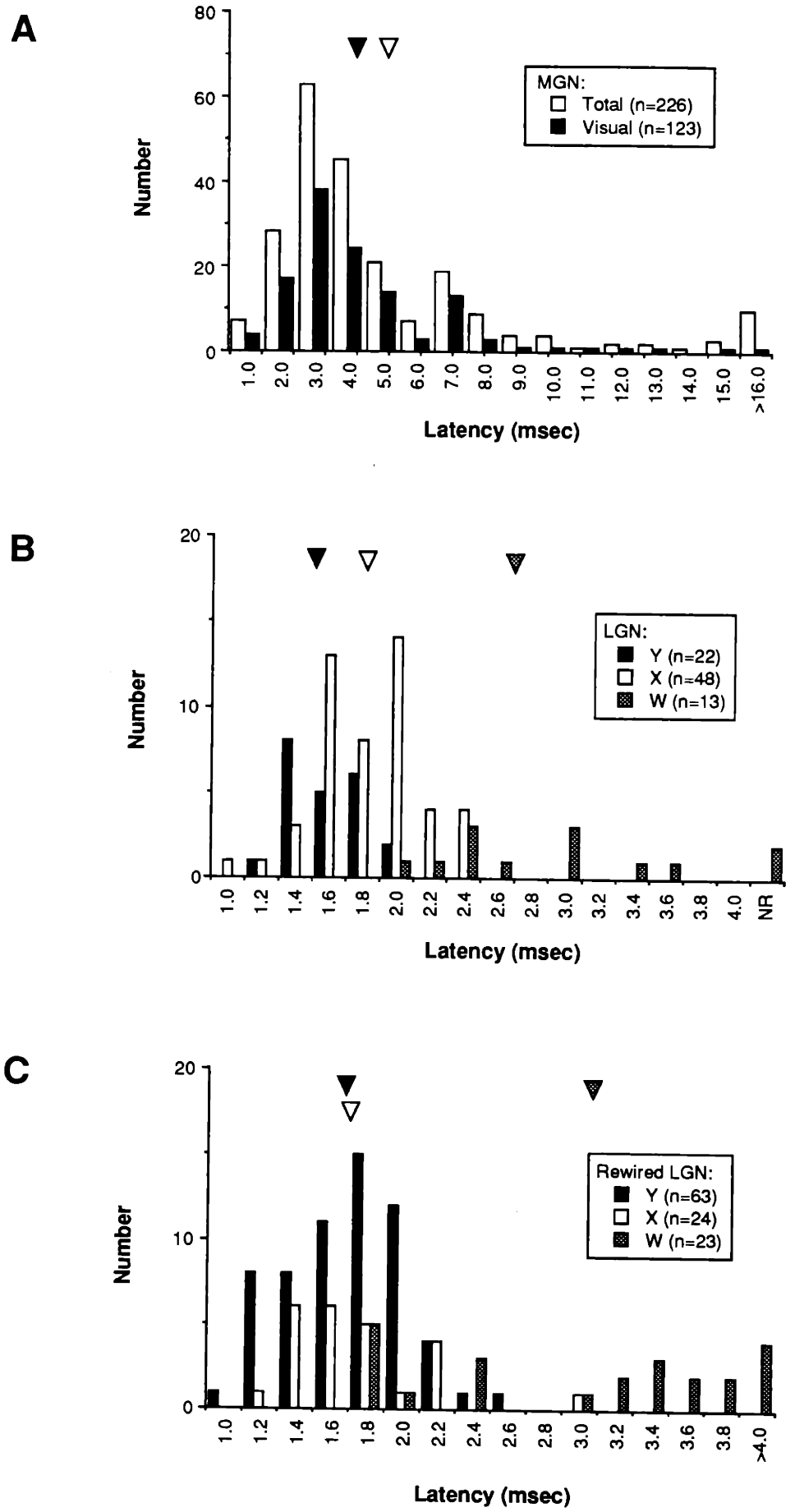
A
80
60
40
20
0
Number
MGN:
Total (n=226)
Visual (n=123)
1.0
2.0
3.0
4.0
5.0
6.0
7.0
8.0
9.0
10.0
11.0
12.0
13.0
14.0
15.0
>16.0
Latency (msec)
B
20
10
0
Number
LGN:
Y (n=22)
X (n=48)
W (n=13)
1.0
1.2
1.4
1.6
1.8
2.0
2.2
2.4
2.6
2.8
3.0
3.2
3.4
3.6
3.8
4.0
NR
Latency (msec)
C
20
10
0
Number
Rewired LGN:
Y (n=63)
X (n=24)
W (n=23)
1.0
1.2
1.4
1.6
1.8
2.0
2.2
2.4
2.6
2.8
3.0
3.2
3.4
3.6
3.8
>4.0
Latency (msec)

Fig. 2

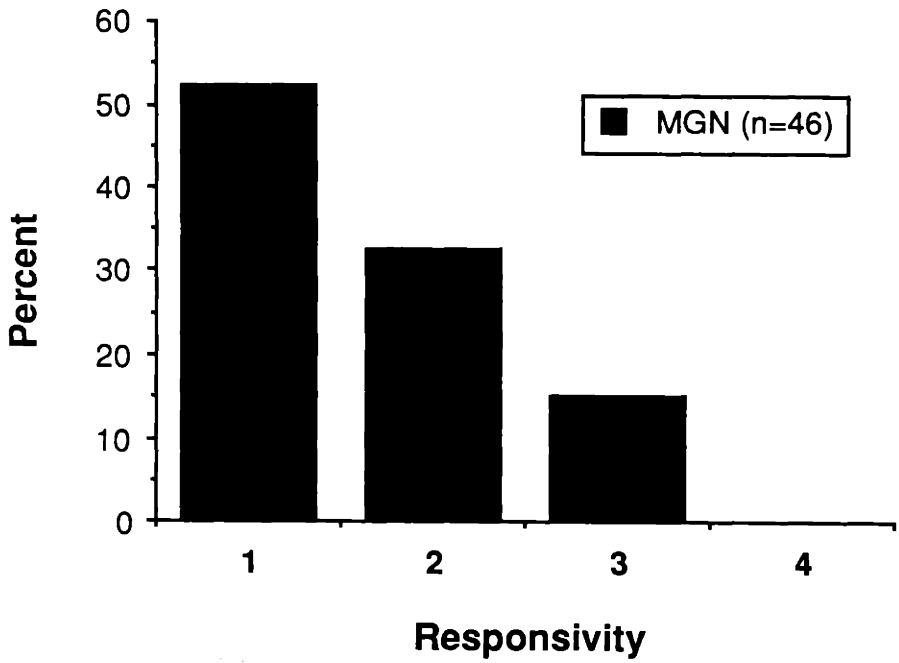

Fig. 3

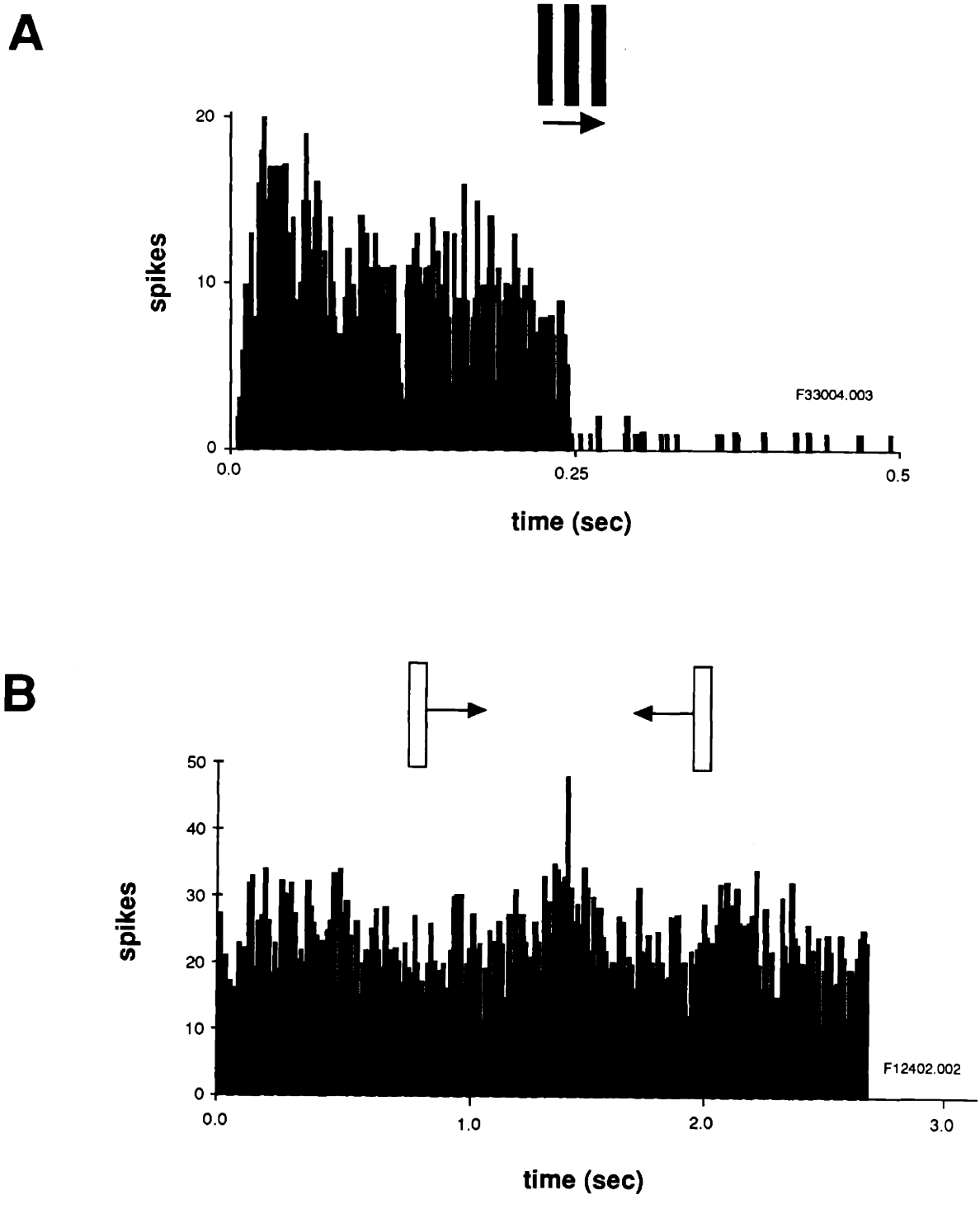
A
20
10
0
spikes
F33004.003
0.0
0.25
0.5
time (sec)
B
50
40
30
20
10
0
spikes
F12402.002
0.0
1.0
2.0
3.0
time (sec)

Fig. 4

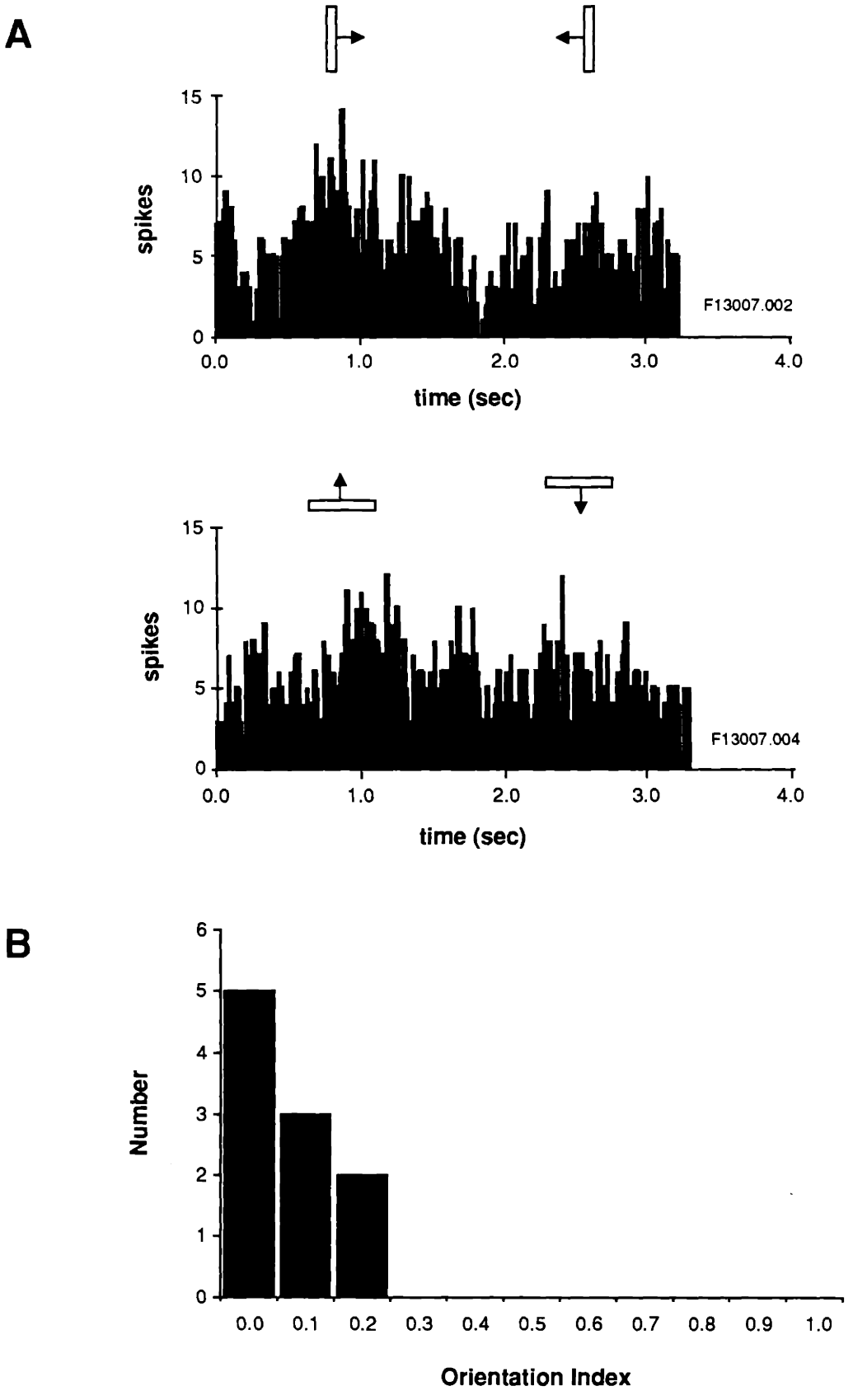
A
spikes
15
10
5
0
0.0
1.0
2.0
3.0
4.0
time (sec)
F13007.002
spikes
15
10
5
0
0.0
1.0
2.0
3.0
4.0
time (sec)
F13007.004
B
Number
6
5
4
3
2
1
0
0.0
0.1
0.2
0.3
0.4
0.5
0.6
0.7
0.8
0.9
1.0
Orientation Index

Fig. 5

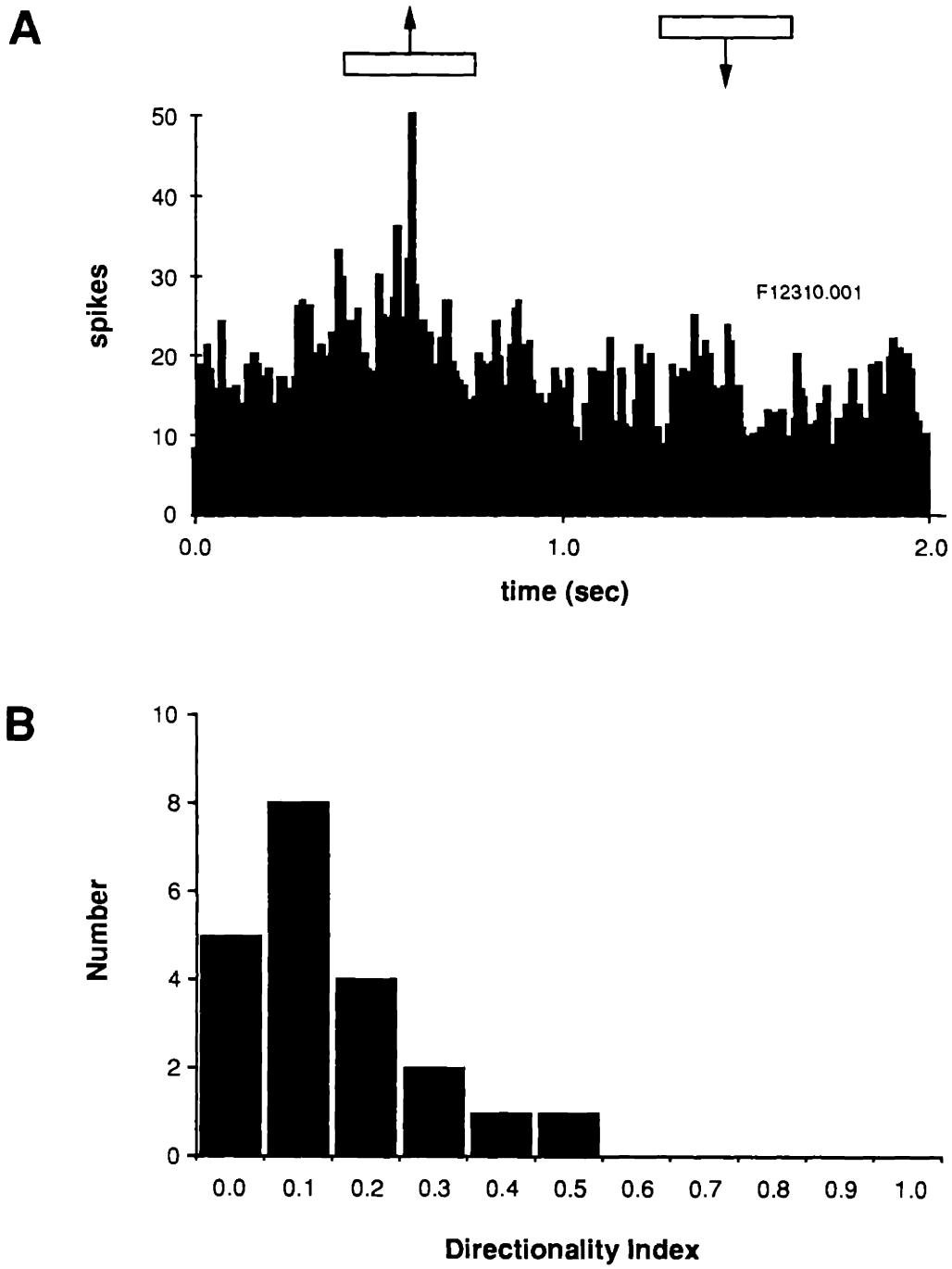
A
50
40
30
20
10
0
spikes
F12310.001
0.0
1.0
2.0
time (sec)
B
10
8
6
4
2
0
Number
0.0
0.1
0.2
0.3
0.4
0.5
0.6
0.7
0.8
0.9
1.0
Directionality Index

Fig. 6

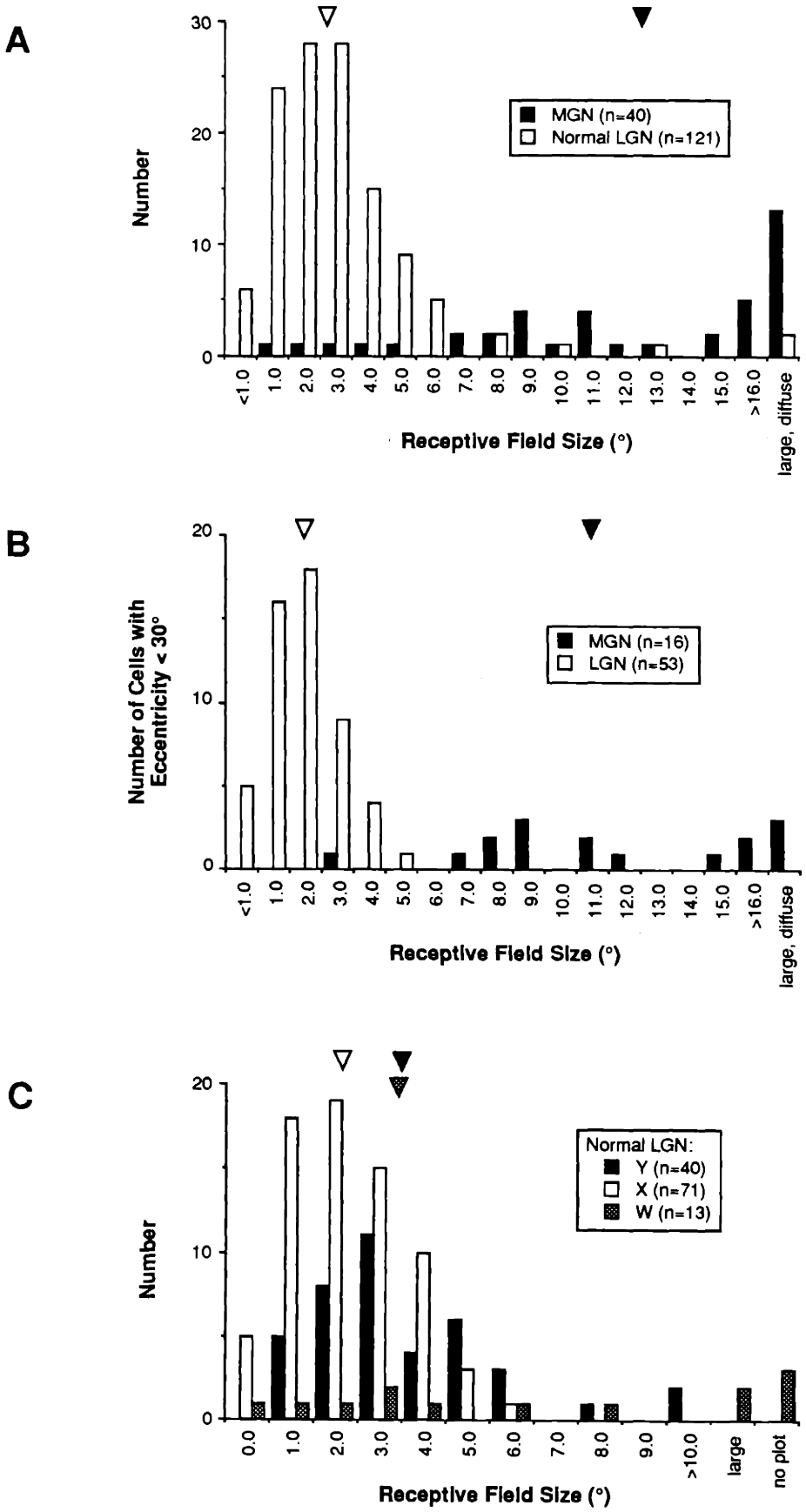
A
Number
MGN (n=40)
Normal LGN (n=121)
Receptive Field Size (°)
B
Number of Cells with Eccentricity < 30°
MGN (n=16)
LGN (n=53)
Receptive Field Size (°)
C
Number
Normal LGN:
Y (n=40)
X (n=71)
W (n=13)
Receptive Field Size (°)

Fig 7

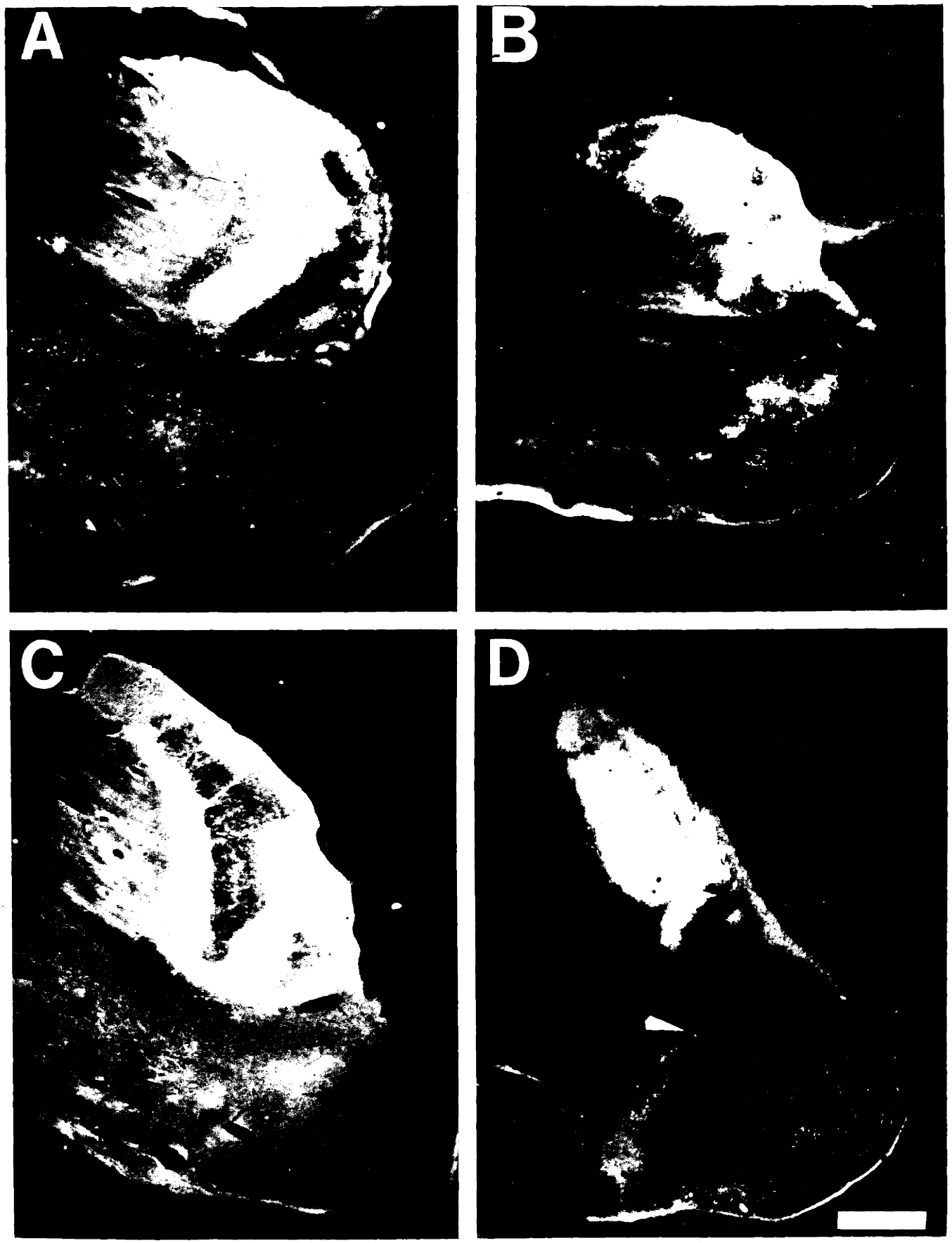

Fig. 8

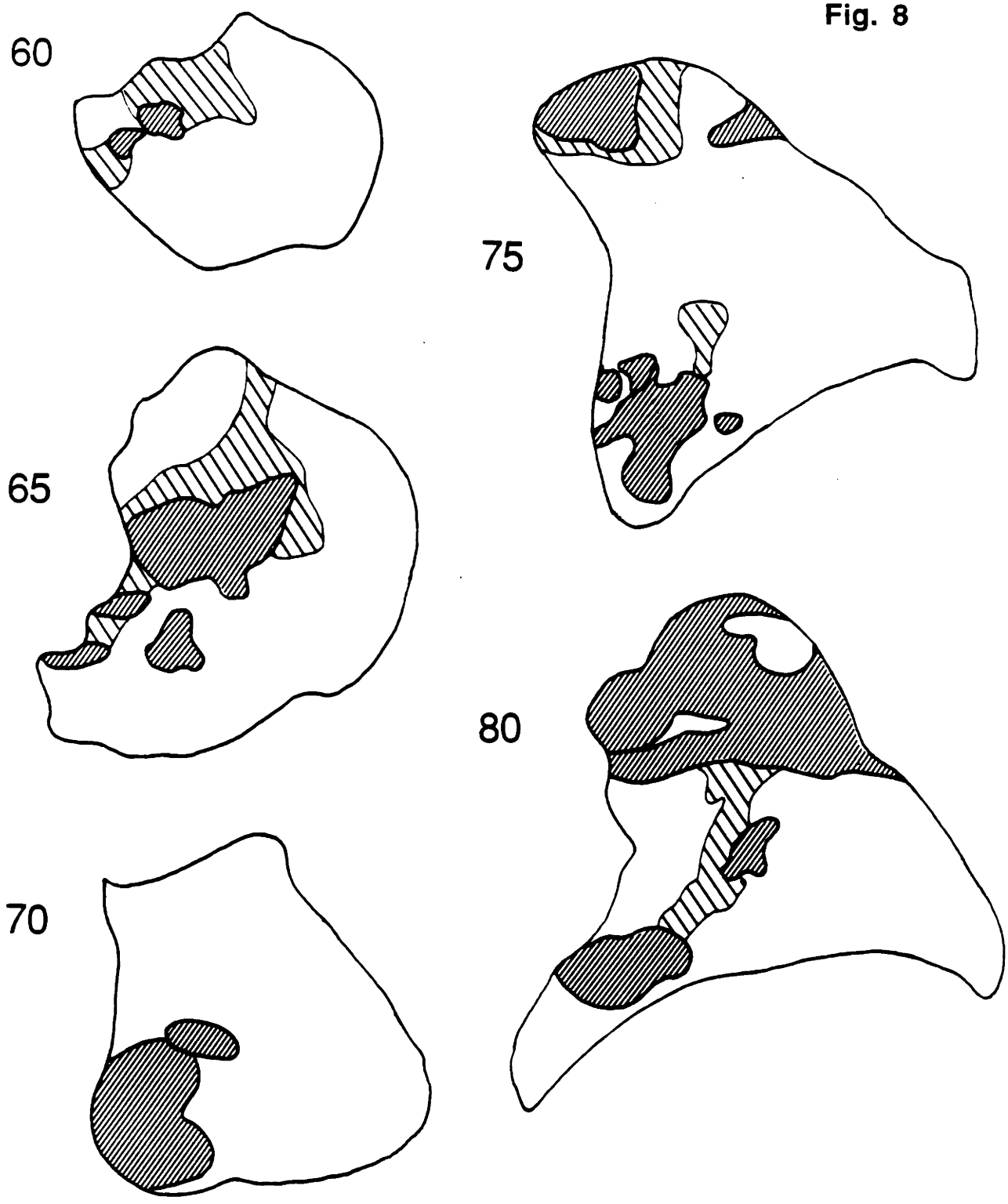

Fig. 9

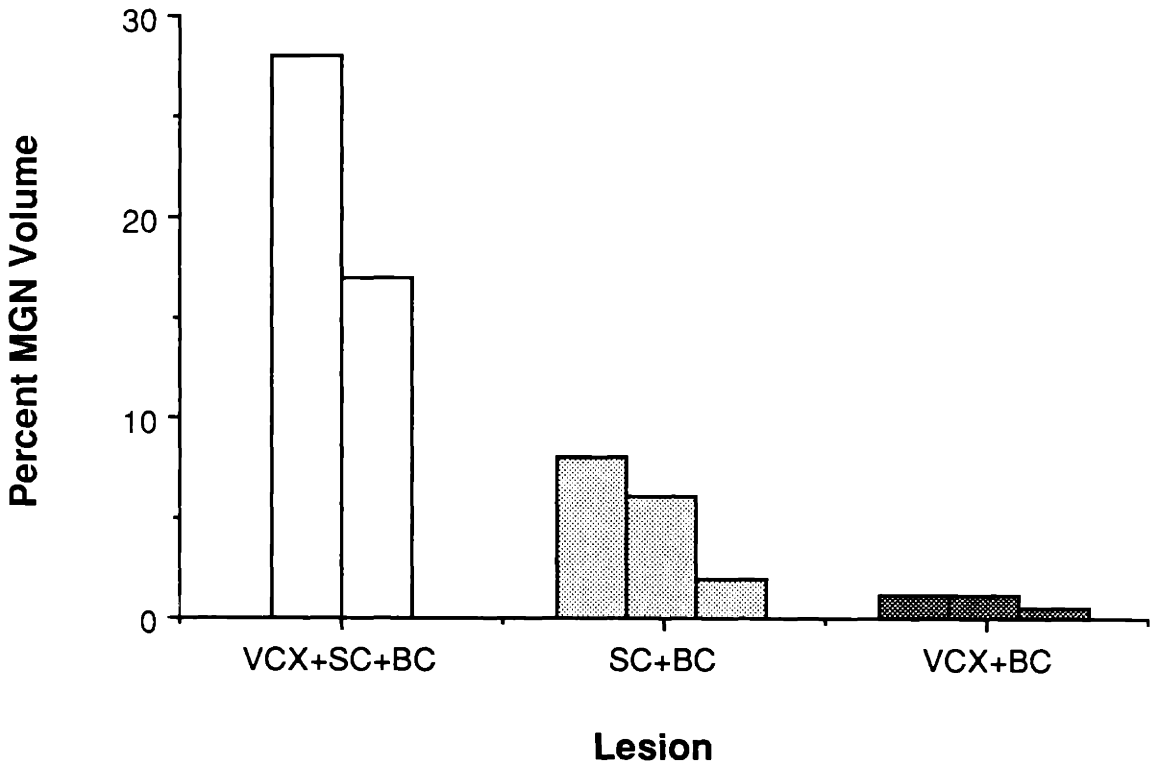

Fig 10

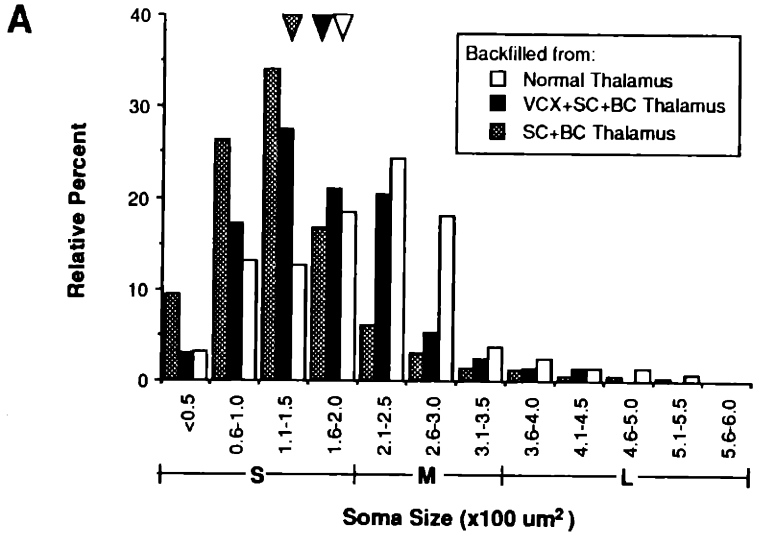
A
Relative Percent
Backfilled from:
Normal Thalamus
VCX+SC+BC Thalamus
SC+BC Thalamus
<0.5
0.6-1.0
1.1-1.5
1.6-2.0
2.1-2.5
2.6-3.0
3.1-3.5
3.6-4.0
4.1-4.5
4.6-5.0
5.1-5.5
5.6-6.0
S
M
L
Soma Size (x100 um²)

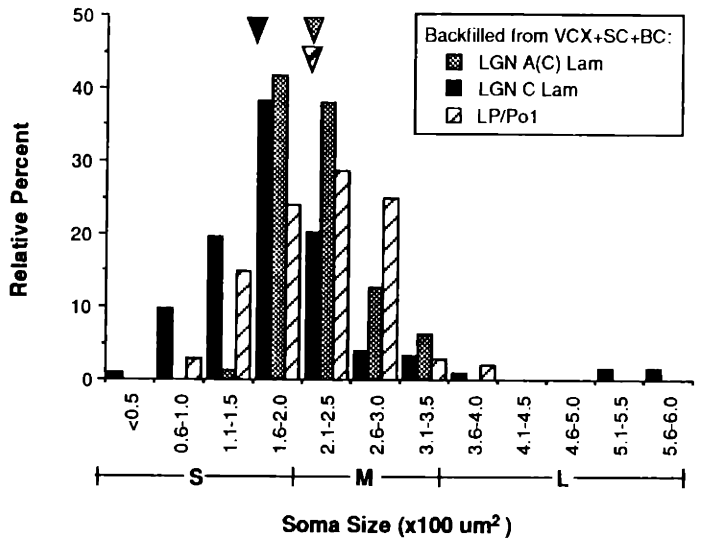
C
Relative Percent
Backfilled from VCX+SC+BC:
LGN A(C) Lam
LGN C Lam
LP/Po1
<0.5
0.6-1.0
1.1-1.5
1.6-2.0
2.1-2.5
2.6-3.0
3.1-3.5
3.6-4.0
4.1-4.5
4.6-5.0
5.1-5.5
5.6-6.0
S
M
L
Soma Size (x100 um²)

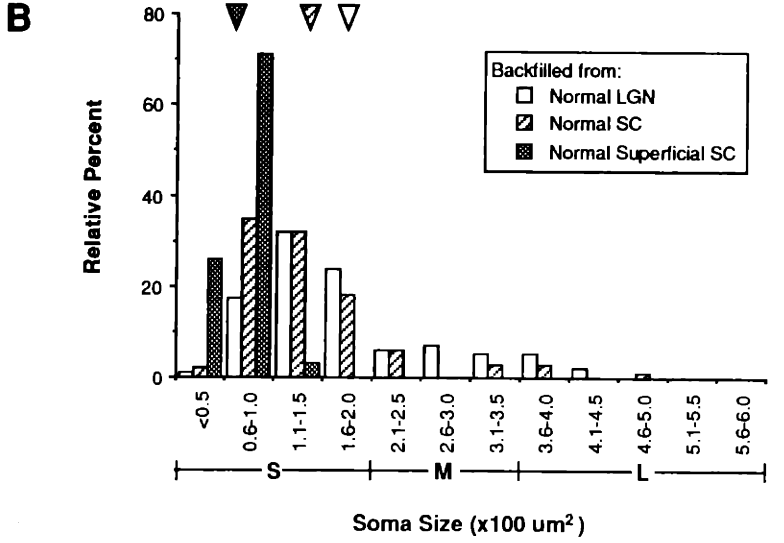
B
Relative Percent
Backfilled from:
Normal LGN
Normal SC
Normal Superficial SC
<0.5
0.6-1.0
1.1-1.5
1.6-2.0
2.1-2.5
2.6-3.0
3.1-3.5
3.6-4.0
4.1-4.5
4.6-5.0
5.1-5.5
5.6-6.0
S
M
L
Soma Size (x100 um²)

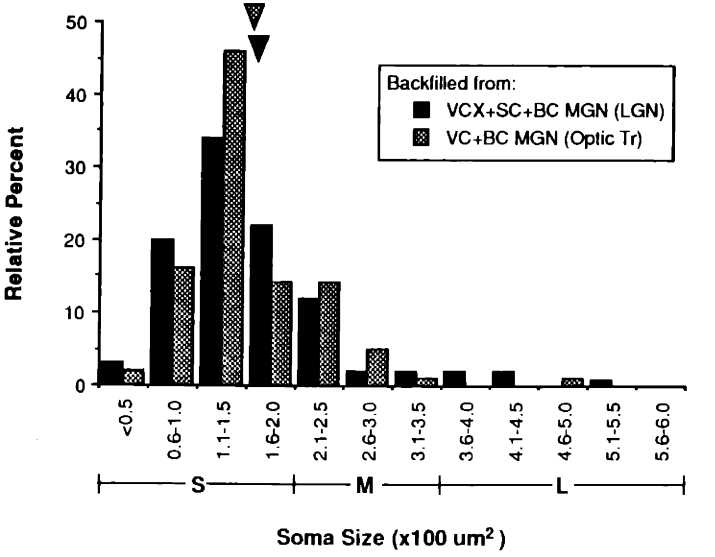
D
Relative Percent
Backfilled from:
VCX+SC+BC MGN (LGN)
VC+BC MGN (Optic Tr)
<0.5
0.6-1.0
1.1-1.5
1.6-2.0
2.1-2.5
2.6-3.0
3.1-3.5
3.6-4.0
4.1-4.5
4.6-5.0
5.1-5.5
5.6-6.0
S
M
L
Soma Size (x100 um²)

Fig. 11

Fig 12

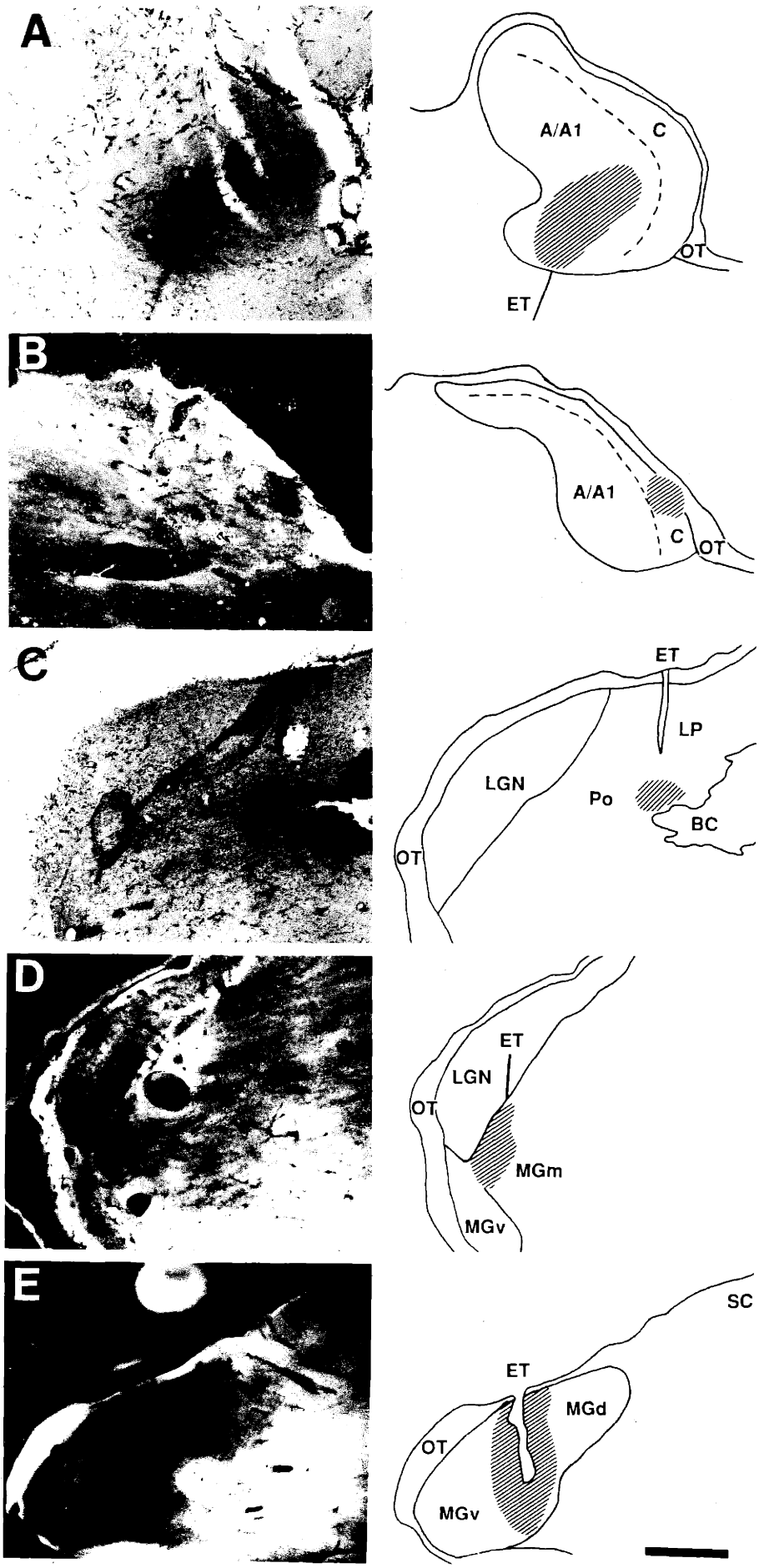
A
A/A1
C
OT
ET
B
A/A1
C
OT
C
ET
LP
LGN
Po
BC
OT
D
ET
LGN
OT
MGm
MGv
E
SC
ET
MGd
OT
MGv

Fig. 13

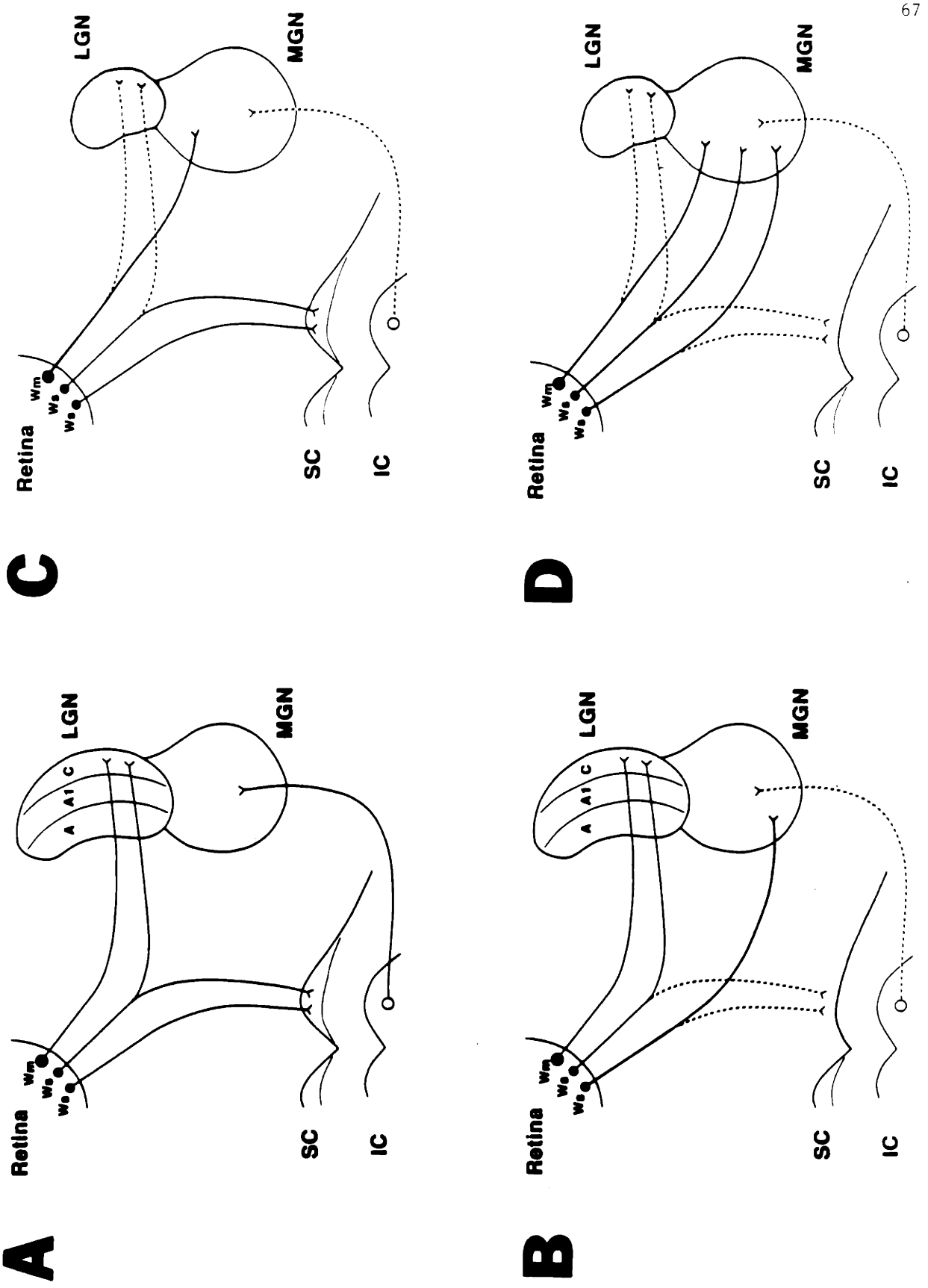

Chapter 2

Part I: Thalamic Topography

Experimentally Induced Establishment of Visual Topography in Auditory Thalamus

Abstract

We have previously reported (Sur et al., 1988) that following specific neonatal brain lesions in ferrets, a retinal projection is induced into the auditory thalamus (specifically, the medial geniculate nucleus, MGN). Single cells in the MGN are visually responsive and have receptive field properties similar to those of their retinal W cell inputs (Chapter 1). We now investigate whether this projection confers onto the MGN a retinotopic representation of the visual world.

We find that topographically organized retinal maps can be established in the MGN. While these maps are less ordered than the visual maps in the normal lateral geniculate nucleus (LGN), we find that azimuthal representations map onto the axis in the MGN that normally represents sound frequency. Elevations map orthogonal to this axis within isofrequency domains. Thus, retinal inputs can map in a coherent and visuotopically representative fashion onto a non-visual thalamic structure. Furthermore, the overall orientation and polarity of the retinal mapping is likely to be guided by the target structure, the MGN.

Introduction

In the present set of experiments, we have examined the issue of topographic mapping from one sensory structure to another by experimentally creating a potential dimensional mismatch between input and target structure. More specifically, we have investigated how a two-dimensional representation of the visual world (as seen by the retina) maps onto a sensory structure that normally receives its input from a one-dimensional sensory epithelium, the cochlea. Following specific neonatal lesions in the developing ferret brain, retinal afferents are induced to innervate the auditory thalamus, the medial geniculate nucleus (MGN) (Sur et al., 1988). In this paper, we examine whether a topographic visual map is established in the MGN of these lesioned ferrets. We examine what the characteristics of the map are, and what the map indicates regarding the relative roles of afferents and targets in generating central maps of sensory structures in the brain.

In the normal retinogeniculate projection, the retina maps onto the lateral geniculate nucleus (LGN) in a point-to-point fashion, such that a single locus on the retina will be represented by a isorepresentational column (typically termed "line of projection") that spans all layers (A, A1, and C laminae) of the LGN (Fig. 1A, shaded bar). Within each of the A, A1, and C laminar planes an entire visual field is represented (axes depicted by heavy and light arrows). In contrast, in the normal auditory pathway, the cochlea is indirectly mapped onto the MGN in a point-to-plane fashion. First suggested from anatomical data by Morest (1965) and later confirmed physiologically (Imig and Morel, 1985), each frequency on the cochlea is mapped onto an isorepresentational lamellar plane in the ventral or principle division of the MGN, the MGv (Fig. 1B, shaded plane). These isofrequency lamellae are organized in mediolateral fashion with low frequency representations located laterally and high frequencies medially (heavy arrow). Thus, whereas the visual field is represented *within* laminar planes in the LGN, the frequency field is represented *across* lamellar planes in the MGN.

Two possible topographic mappings from the retina to the MGN (more specifically, the MGv) are depicted in Fig. 1C and 1D. If the retina were to map onto the MGN in a manner similar to that in the normal LGN, one might expect that points of isorepresentation would run orthogonal to lamellar planes (Fig. 1C). Each lamella would then contain a complete two-dimensional representation of the visual world (orthogonal axes depicted by heavy and light arrows). On the other hand, a mapping more similar to that found in the auditory system would predict that points of isorepresentation would lie within a lamella in some orientation (Fig. 1D, one possible orientation depicted by shaded contour). One axis of the visual field representation would map across lamellar planes (heavy arrow) and the orthogonal visual axis would then map within lamellae orthogonal to the line of projection (light arrow). Evidence for the former scheme would suggest that sensory afferents determine the resulting orientation of sensory maps within a target nucleus, whereas the latter scheme would suggest that establishment of topographic orientation is target-directed.

Methods

Neonatal Surgery

Induction of retinal afferents to non-visual thalamic structures requires both removal of normal retinal targets and availability of alternative target space (Schneider, 1973). Our procedures are similar to those described previously (Pallas et al., 1990). Briefly, neonatal ferret kits were anesthetized by hypothermia and underwent three unilateral lesions: 1) superior colliculus was ablated, 2) visual cortex (including Areas 17, 18, and often 19) was lesioned, thus leading to severe retrograde degeneration of the LGN, and 3) the brachium of the inferior colliculus was transected, thereby denervating the MGN and providing alternative target space for retinal terminals. Kits were then revived and returned to the mother for rearing.

Visual Physiology in Adult Ferrets

Neonatally-lesioned ferrets reared to adulthood were prepared for visual physiology using procedures similar to those described previously (Roe et al., 1989). Animals were anesthetized, paralyzed, and respirated. Ferrets received a constant intravenous infusion of a 5% dextrose solution containing ketamine hydrochloride (10 mg/kg/hr) for anesthesia and gallamine hydrochloride (3.6 mg/hr/kg) for muscular paralysis. End-tidal CO_2 was maintained at 4.0%, heart rate monitored, and body temperature maintained at 38°C with a heating pad. Supplemental halothane (1%) was supplied during all surgical procedures. The skull and dura overlying lateral thalamus were removed. Stimulating electrodes were lowered into the optic chiasm and cemented in place. Pupils were dilated with atropine sulfate drops and eyes were fitted with zero power contact lens. Optic disks were plotted by reflection onto the tangent screen.

We recorded extracellularly from thalamic cells of 11 lesioned ferrets. In most cases we used parylene insulated tungsten microelectrodes (2-3 megaohm impedances); in 2 cases

we recorded with micropipettes filled with 10% HRP in 0.05 M KCl-Tris. We examined visual topography in the MGN by making grids of vertical or angled (45° from vertical in coronal plane) electrode penetrations spaced 250-500 um apart over the regions of lateral and posterior thalamus (around A-1.0 L6.0). Due to their relatively shrunken size, the LGN and MGN in rewired ferrets were usually shifted rostrally and medially compared to normal. In our search procedure, we first located the LGN and then mapped thalamic regions lateral, posterior, and deep to the LGN. When crossing the border from LGN to MGN, there usually was a marked reduction in background activity, visual responsiveness, and encounter rate of visual units accompanied by increase in response latencies to optic chiasm shock, increase in receptive field sizes, and often an abrupt change in visual topography (for more detail on response characteristics, see chapter 1). In each penetration, unit activity was assessed every 50-100 μm for 1) response to electrical stimulation of the optic chiasm and 2) response to visual stimulation. Visually responsive units were plotted and characterised on the tangent screen with a hand-held projection lamp. Receptive field location and size of each visual unit were recorded. In selected penetrations in each experiment, electrolytic lesions (5μA for 5 sec or 10μA for 10 sec) or iontophoretic injections of tracer label (10% HRP) were made to aid in histological reconstruction of electrode tracks. HRP (10%) was iontophoresed either through the recording pipette or with an HRP-filled pipette placed at the same coordinate and depth of the recording metal electrode.

Histology and Data Analysis

Following the completion of data collection, the animal was sacrificed with an intravenous or intraperitoneal overdose of pentobarbital (65 mg/kg) and perfused through the heart with saline followed by fixative and 10% and 20% sucrose solutions. The brain was then blocked in the coronal plane, removed from the cranium, and stored in 30% sucrose overnight. After brain sulcal patterns were recorded photographically, 50 um frozen sections

were cut, mounted onto slides, and Nissl-stained. In brains in which HRP injections were made, alternate sections were processed for HRP visualization with DAB-cobalt chloride.

In each case, thalamic sections (every 200-400 um) through the MGN were drawn by *camera lucida*. Using electrolytic lesions, HRP label, and electrode tracks as guides, recording tracks were marked on these drawings. As there are no published studies on organization of the ferret MGN, we have relied upon studies and atlases (Berman and Jones, 1982) of the cat MGN to make determinations of subnuclear boundaries. Our criteria have included cell size, cell packing density, cellular orientation, amount and orientation of white matter content (seen best under dark field illumination), as well as thalamic labelling following injections of tracer label in auditory cortex (Pallas et al., 1990). Under these conditions we felt comfortable delineating the ventral (MGv), medial (MGm), dorsal (MGd), and caudodorsal (MGc) divisions of the MGN. Boundaries were most clearly seen in coronal sections. For each recording penetration, positions of recording sites within MGv, MGm, MGd, and MGc were then determined by depth of recording, lesion sites, and records of visual responses along each penetration.

Results

Extent of Visual Field Representation in the MGN

Sixty-three penetrations were made through the MGN of 11 rewired ferrets; out of these, 43 encountered at least one visual cell in the MGN. No visual responses were recorded in 5 penetrations through the caudal-most regions of the MGN (the caudodorsal nucleus, MGc). This is consistent with the absence of retinal terminal label in the caudal-most portion of the MGN following an injection of tracer in the contralateral eye (see Chapter 1).

Receptive field locations were determined for 105 out of 131 visual units recorded in the MGN. The remaining 26 responded either only to very strong stimuli such as full field flashes or were too weakly or inconsistently responsive to permit confident receptive field localization. Of the 105 recording sites, 63 were located in the MGv, 29 in the MGm, and 13 in the MGd.

The receptive field locations of all visual units recorded are shown in Fig. 2. In MGv (filled circles), the receptive fields recorded span all regions of the ferret's visual field. Azimuths ranged from -6° to +72° and elevations ranged from -63° to +31°. The relatively poor representation of upper visual fields parallels that found in the normal ferret LGN and visual cortex (Law et al., 1988; Zahs and Stryker, 1985; Roe et al., 1989). While our MGm sample is smaller (open squares), receptive fields recorded in the MGm exhibit a similar range of eccentricities (azimuths range from -7° to +73°; elevations range from -59° to +7°). The small sample of visual units recorded in the MGd (open triangles) spans a similar range of azimuths (ranging from -10° to 67°) and a more limited range of elevations (from -29° to15°).

Due to the sparseness and patchiness of the retino-MGN projection as well as due to the poor responsiveness of W-driven MGN cells (see Chapter 1), searching for and characterizing visual units reliably was very time consuming in these experiments. We searched the visual field for a receptive field only if a unit responded to electrical stimulation of the optic chiasm with a consistent latency or if it exhibited visual responsiveness at the eye.

Location of receptive fields required repeated searches of the visual field, searches which in many cases necessitated slow moving or flashing spots as effective stimuli. Furthermore, responses were usually not robust and fatigued easily. For all these reasons, in most of the penetrations (n=33) only one or two visual units were recorded. We have first concentrated our analysis on penetrations in which multiple (3 or more) visual units were recorded. In each case, we drew every third or every fourth section through the MGN and, with the aid of electrode tracks and electrolytic lesions, reconstructed each electrode penetration through the MGN. To conceptualize the map, we have illustrated electrode penetrations from different animals on a single representative MGN; corresponding sections from separate cases were then matched. Such reconstruction is crucial to deciphering topography in a 3-dimensional volume with discrete subnuclei.

Visual Topography in the MGv

A rough three-dimensional topography in the MGv is indicated by penetrations through the MGv in which 3 or more visual units were recorded (n=8, Fig. 3). Figure 3A illustrates the progression of the receptive field locations with increasing depth in each of these penetrations (each penetration labelled by letters A-G). Figure 3B illustrates the positions of the electrode tracks (straight lines) in the MGv as well as the the locations of recording sites along these tracks (dots). Visual units which are located rostral in the MGv tend to have receptive fields with higher elevations and those more caudally located represent lower elevations: in a rostral to caudal progression receptive field elevations from penetrations A/B to C to D decrease on average from +2°/-5° to -32° to -48°. In the mediolateral dimension, azimuths are greater in lateral MGv (track F and E) than in medial MGv (tracks A-D): the average azimuth value of receptive fields in F is 61°, in E is 33°, and in A, B, C, and D are 12°, 6°, 11°, and 19°, respectively. [Similar variations are seen in the normal MGv, where both mediolateral (Aitkin and Webster, 1972; Calford and Webster, 1981; Imig and Morel,

1985) and rostrocaudal (Rodrigues-Dagaeff et al., 1989) gradients of functional properties exist.]

In the dorsoventral axis, elevations tend to decrease with depth. This is seen most clearly in vertical penetrations located in lateral MGv (Tracks B and E) where the downward progression of receptive field locations takes a less curved trajectory than in medially located penetrations. More specifically, in medially located penetrations (Tracks A and C), reversals in receptive field progressions are seen. [Similar progressions of frequency tuning selectivities are seen in the normal cat MGN: in electrode penetrations oriented at 40° from normal in the coronal plane, C-shaped progressions are seen medially in the nucleus, while constant or monotonically increasing tuning selectivities occur in more lateral penetrations (Morel et al., 1987).] The progression of receptive fields in the ferret MGv is thus consistent with the curved sheet-like lamellae previously described in cat MGv (Morest, 1965), but with a more vertical orientation.

This proposed concentric lamellar organization is further strengthened by results from penetrations oriented +45° from vertical in the coronal plane (Tracks D, F, and G). Both Track D and Track G are oriented orthogonal to the proposed lamellar orientation. They pass from higher azimuthal representation laterally in the nucleus to more central azimuthal representations medially; at the same time, their elevational representation remains fairly constant. [Consistent with the rostro-caudal gradient seen in Tracks A-D, Track G is located in a region of higher elevational representation than Track D.] Track F, located laterally and caudally in MGv, appears to run *along* a lamellar plane, so that receptive fields remain generally restricted to the same region of visual space; consistent with other dorsoventrally running penetrations, the elevation decreases somewhat from F1 to F5.

The remaining receptive fields recorded in the MGv are in large part consistent with these findings (Fig. 4). The receptive fields of visual units recorded at positions indicated in Fig. 4B are plotted in Fig. 4A. Receptive fields of visual units located in lateral lamellae (cells A-J1) have high azimuthal values (>45°). Those with lowest azimuthal values (<15°) lie

medial in the nucleus (cell T). Mid-azimuthal values are found at intermediate locations (cells N-S). However, cells J2, K, L, and M (Fig. 4A, lower case italicized) are not consistent with this proposed topographic organization. While it is apparent that visual topography established in the ferret MGv is not precise, even in the normal MGv "aberrant" frequency selectivities are recorded in topographic frequency progressions (Imig and Morel, 1985).

In summary, our data suggests a systematic mapping of the visual field onto the MGv. Increasing azimuthal locations map from inner lamellae to outer lamellae, while increasing elevational locations map from caudal to rostral *and* from ventral to dorsal.

Visual Topography in the MGm

The topography in the MGm is less clear than in the MGv (Fig. 5). Receptive fields recorded in penetrations through the MGm are shown in Fig. 6A and 6B; the corresponding electrode track positions in the MGm are illustrated in Fig. 6D. Within individual penetrations (Fig. 6A), some topography is indicated. Tracks B and C share similar reversals in topography (from low to high followed by high to low azimuthal coordinates). However, Track A, located more anteriorly in the MGm, exhibits an opposite direction of reversal.

Penetrations which cross the MGv/MGm border encounter similar visual field representations in MGv and MGm. Receptive fields recorded in Track D (continuation of Track D shown in Fig. 3) are similar in location and progression pattern to those recorded previously in the MGv in the same penetration: azimuthal values decrease but elevational values remain constant (about -45° elevation, compare Fig. 3, Track D). In Track G (continuation of Track G shown in Fig. 3), receptive fields are located in a similar region of the visual field (about +20° azimuth, -40° elevation) but reverse in azimuthal progression (from low to high instead of high to low, compare Fig. 3, Track G).

The relative positions of electrode penetrations in the MGm may suggest a rough mapping of azimuth in the mediolateral dimension. From Track B (medial) to Track C (lateral), the average azimuthal value increases from 14° to 38°. This is also suggested by

Track D, in which the azimuthal values decrease as more medially located units are encoutered in the MGm. Some of the other visual units recorded are consistent with this mapping scheme: cells in tracks E and J are located in lateral MGm represent high (>45°) azimuths; those located in medial MGm (tracks H, I, and M) have low (<15°) azimuths, and those (except Track G, L) with intermediate MGm location (Tracks F, K and N) represent intermediate azimuths.

No clear topography is evident in either the rostrocaudal or dorsoventral axes. Track H and Track A (anterior) exhibits higher average elevations (1° and -19°, respectively) than either Track B and Track C (-37° and -42°, respectively) or Track D (-49°). However, the remaining visual units do not support this impression (e.g. Tracks H, I, J, K, N share similar elevational values but are located throughout the rostrocaudal extent of the nucleus). In the dorsoventral axis, downward progressions are more common, but upward progressions also occur (C1 to C2, I3 to I4, G4 to G5). There is no relationship between azimuth and either dorsoventral or rostrocaudal position in the MGm.

Overall, visual mapping in the MGm is poor. At best, there is a rough mapping of azimuth in the mediolateral dimension. Similarly, in the normal MGm, the topography of frequency representation is less precise than that in the MGv (Rouiller et al., 1989).

Visual Topography in the MGd

The limited data we have of visual units in the MGd is shown in Fig. 5C and D. No obvious visual topography could be discerned in the MGd. Receptive fields recorded in single penetrations have similar receptive field locations (except Track H). Track O follows a complex trajectory not seen in the MGv. Units recorded in the MGd and MGm within single penetrations bear no obvious relationship to each other (compare H1, H2 and I1, I2 in Fig. 5C with H3, H4 and I3, I4 shown in Fig. 5B, respectively). Clearly, however, more data are needed to determine either the presence or lack of topography in the MGd.

Discussion

Retinal Topography in MGv of Rewired Ferrets

We have shown previously that following specific neonatal lesions in the developing ferret brain, retinal afferents can be induced to innervate non-visual thalamic structures in the MGN (Sur et al., 1988). As a result, post-synaptic cells in both the MGN and in A1 are visually driven. In this paper, we present data suggesting this retinal projection to the MGv is topographic in nature. In the MGv, low azimuthal representations are found medially and high azimuths laterally. Elevations are mapped in a rostral to caudal gradient as well as in a dorsal to ventral gradient. These findings are consistent with a visual mapping (schematized in Fig. 6) in which 1) a lamellar plane in the MGv represents a single azimuth (inner lamellae representing low azimuths and outer lamellae high azimuths) and 2) within each lamellar plane elevations map in a ventrocaudal (low elevations) to a rostrodorsal (high elevations) gradient. Lines of projection would lie within single lamellar planes orthogonal to the elevational axis (Fig. 6, shaded bar). These data are not consistent with a mapping scheme in which lines of projection run across laminar planes, as is found in the normal LGN.

The visual map in MGv presented in Fig. 3 has been compiled from several animals. This has been necessary due to the difficulty of obtaining extensive data from individual anismals. Nevertheless, it is likely that a complete visual map can be established within a single MGv for two reasons: 1) the distribution of retinal ganglion cells back-filled from injections in the MGN of rewired ferrets is extensive; labelled cells are found throughout the appropriate hemiretina (unpublished observations, see Chapter 1) and 2) we have recorded complete maps of the visual field within single primary auditory cortices of these animals (Roe et al., 1990; also this chapter, part 2). Our composite data indicate unequivocally that complete visual maps can be established in the MGv of rewired ferrets.

Relation to Topographic Organization in the Normal MGv

From anatomical studies of dendritic architecture and afferent innervation patterns to the MGN, Morest (1965) first reported the concentric lamellar organization of the MGv and suggested that these lamellae correspond to the representation of individual sound frequencies. While subsequent physiological studies were consistent with this proposal (Aitkin and Webster, 1972; Calford and Webster, 1981), the precise 3-dimensional tonotopic organization of the nucleus was difficult to establish. Difficulties were related to the often unclear borders between separate subdivisions of the MGN, lack of obvious laminar organization within the MGv as seen in Nissl-stained sections, the curvilinear nature of the isofrequency lamellae, and a non-artifactual scatter in frequency tuning of cells with respect to position in the MGN. However, Morest's proposal was generally confirmed when the three-dimensional organization in the MGv was physiologically detailed by Imig and Morel (1985). In general, vertical electrode penetrations (within single lamellae) recorded similar frequencies; lateral penetrations (in lateral lamellae) recorded low frequencies and medial penetrations (in medial lamellae) recorded hi frequencies.

Within the lamellar planes in the rostrocaudal dimension, there is also evidence for functional variation. In deeply anesthesized cats, the lowest frequencies are represented caudally but not rostrally and highest frequencies rostrally but not caudally in the MGv (Calford and Wester, 1981; Imig and Morel, 1985). [This variation disappears with lighter anesthesia levels (Morel et al., 1987). For dependence of physiological features of central auditory neurons on anesthetic state, see also Abeles and Goldstein, 1970; Purser and Whitfield, 1972.] Other functional gradients in the rostrocaudal dimension have also been reported (including sharpness of tuning, number of responsive cells to simple acoustical stimuli, degree of tonotopicity, temporal response patterns and response latencies) under a state of light anesthesia (Rodrigues-Dagaeff et al., 1989). In summary, there is a clear tonotopic organization in the mediolateral dimension (across lamellar planes), and some evidence for a crude functional gradient in the rostrocaudal dimension. The physiological

organization of MGv is paralleled by a precise pattern of thalamic projections to A1 from MGv along the tonotopic dimension, but a more divergent and convergent projection along the orthogonal dimensions (Anderson et al., 1980; Middlebrooks and Zook, 1983; Brandner and Redies, 1990; Rodrigues-Dagaeff et al., 1989).

In the ferret, no studies are yet available on frequency representation in the normal MGv. However, evidence from studies on the organization of primary auditory cortex (A1) and thalamocortical connectivity in the ferret suggests a systematic mapping in the MGv. In normal primary auditory cortex of the ferret, there is a systematic map of frequency representation in which low frequencies are represented laterally and high frequencies medially (Kelly et al., 1986). Since medial A1 receives direct input from medial MGv and lateral A1 from lateral MGv (Pallas et al., 1990), it is likely that frequencies run from low to high in a lateral to medial gradient in MGv. Thus, low frequencies are represented in outer lamellae and high frequencies in inner lamellae. Since thalamocortical connectivity in the rewired ferrets remains similar to that in normal ferrets (Pallas et al., 1990), we have reason to believe that the structural organization in the MGv of rewired ferrets is not drastically altered by the neonatal lesions.

Developmental Implications

Orientation of Map in Relation to Single Afferent Axons. In the normal ferret retinogeniculate projection, the optic tract courses over and is restricted to the surface of the LGN (Hahm et al., in prep); single retinogeniculate axons dive into the LGN near the line of projection in which their arbors terminate (Roe et al., 1989). In rewired ferrets, both developing and adult, the optic tract is expanded in breadth and courses over the surface of both the LGN and MGN (Pallas et al., unpublished observations). Single retinal fibers terminating in the MGN arise from the optic tract overlying the MGN (Pallas et al., 1989). Importantly, in both the normal LGN and the rewired MGN, the lines of projection defined physiologically (Fig. 1A, 5) specify the projection patterns of single retinal ganglion cell

axons within each nucleus. The difference between the orientation of lines of projection in the normal LGN and rewired MGN has been mentioned before: in the normal LGN, they cut across eye-specific laminae, while in the rewired MGN, they lie within the plane of "isofrequency" lamellae.

Normal auditory input to the MGv arising from the inferior colliculus is also governed by the planes of frequency-specific lamellae. In the normal auditory system, inferior colliculus fibers enter the the MGN ventrally and closely follow the dendritic lamination patterns in the MGN: where the dendritic laminae are planar, the afferents are planar; where the laminae spiral (e.g. pars ovoidea), the afferents spiral (Morest, 1965). According to Morest, in the MGv, "individual fibers (from the inferior colliculus) travel within the same dendritic layer from one zone to the next. They rarely depart from their orientation parallel to the dendritic layers in any zone." This alignment of inferior collicular afferents to dendritic lamellae is likely to underly the frequency specificity of these lamellae. These observations suggest that the development of dendritic orientation (i.e. lamellar organization) and of afferent fiber arbors are intimately associated events.

In the visual system, retinal arbors in the LGN also closely match the dendritic orientation of cells in their target laminae. In the adult LGN, dendrites of A laminae cells are oriented primarily orthogonal to laminar borders; those in the C laminae extend parallel to laminar borders (Sutton et al., 1987). Similarly, terminations of X and Y axons in the A laminae are oriented orthogonal to laminar borders (Sur et al., 1987; Roe et al., 1989), while W axons terminating in the C laminae are extended parallel to the laminae (Mason and Robson, 1979). Moreover, the A and C terminations of *single* Y axons in the LGN are aligned with the orientation of cells in their respective target zones (Sur et al., 1987; Roe et al., 1989). Thus, whereas single inferior collicular axons arborize within and along the lamellar planes, retinogeniculate axons in the A laminae arborize perpendicular to the laminar borders. Thus, the pattern of dendritic orientation within a target nucleus predicts that of its afferent inputs and thereby the orientation of the visual line of projection within the nucleus.

Target Determination of Map Orientation. The development of afferents into target structures is a highly complex and interdependent series of events. It has been shown in many ways in the visual pathway that perturbation of the retinal input (e.g. by lid suture (Sherman and Spear, 1982), enucleation (Garraghty et al., 1988), or TTX blockade of retinal activity (Shatz and Stryker, 1988) can greatly influence the development of the target (the LGN). Likewise, alteration of the target effects the development of afferents [e.g. LGN degeneration following visual cortical ablations and the consequent changes in retinogeniculate afferents (Hahm et al., 1989; Weber et al., 1989); changes in retinal arbors following blockade of post-synaptic activity with NMDA receptor antagonists (Hahm et al., 1990).]

The orientation of the visual map in the MGv argues that the orientation of sensory afferents in a target nucleus, and consequently the orientation of the sensory map in that nucleus, is largely determined by the target. We discuss below other evidence pertaining to the possible causal relationships between presynaptic and postsynaptic elements, specifically in the context of the orientation and polarity of maps in target structures.

In the LGN, some aspects of cellular maturation can proceed independently of afferent input. In the total absence of retinal afferents, relatively normal cytoarchitectonic differentiation occurs despite absence of normal lamination and shrinkage in LGN size. This has been observed in congenitally anopthalmic mice (Cullen and Kaiserman-Abramof, 1976) as well as in animals binocularly enucleated at various stages of development: 1) before retinal innervation (in ferrets, Guillery et al., 1985a), 2) at the initial stage of retinal innervation (in monkeys, Rakic, 1991), 3) following extensive innervation but before retinal afferent segregation (in rodents, Cullen and Kaiserman-Abramof, 1976; Heumann and Rabinowicz, 1980), and 4) following retinal afferent segregation (in tree shrews, Brunso-Bechtold and Vinsant, 1990). Moreover, the LGN without retinal afferents still establishes roughly normal topographical connectivity with visual cortex (Godement et al., 1979; Kaiserman-Abramof et al., 1980; Brunso-Bechtold et al., 1983; Rhoades and Fish, 1983; Guillery et al., 1985b; Rakic and Williams, 1985). The latter observation argues that topography in thalamic

structures and in thalamocortical projections does not require retinal specification. We consider it highly likely that the MGN contains at least some intrinsic topographic cues, and these cues are recognized by retinal afferents in rewired animals.

The possibility remains that retinal afferents alter intrinsic topographic gradients in the MGN. However, a number of studies indicate that the establishment of normal map polarity and orientation is relatively resistant to perturbations of the input. Regeneration of the retinotectal projection following eye rotation results in reinnervation of the same tectal regions by the same retinal cells, thus producing an inverted visual map (Sperry, 1943). Removal of large retinal sectors leads to expansion of the remaining retina onto the tectum in an orientation similar to normal (Schmidt et al., 1978). Tectal tissue rotation experiments suggest that thalamic targets possess some innate polarity cues which guide the orientation retinal fiber population mapping (Chung and Cook, 1975). Retinal axons can innervate their appropriate tectal locus even following disruption of axonal neighbor-neighbor relationships in the optic tract by N-CAM antibodies (Thanos et al., 1984). Moreover, disrupting input with TTX or strobe illumination interferes with normal sharpening of topography, but not its orientation. Thus, whereas sharpening of topography is highly influenced by input patterns, the mechanisms responsible for establishment of map orientation appear quite robust and persist even following extreme disruptions in input. Given these studies, we find it unlikely that retinal afferents alter pre-existing topographic gradients in the MGN.

Conclusion

We have shown that during development afferents of one sensory modality can map in an orderly fashion to a target of a different sensory modality. Our findings suggest that: 1) the MGv contains intrinsic polarity cues (i.e. in the axis orthogonal to the lamellae); 2) retinal afferents are able to recognize these polarity cues and map accordingly; 3) mechanisms responsible for orderly mapping of retinal fibers onto target nuclei (cf. Sperry, 1963) are not sensory-specific (see also Frost, 1981). 4) It is possible that in this primarily W-cell driven

pathway (see Chapter 1), the normal patterns of retinal activity which serve to sharpen topography are absent. This change in afferent activity patterns may contribute to the coarseness of the visual map in MGv.

References

Abeles M, Goldstein MH (1970) Functional architecture in cat primary auditory cortex: columnar organization and organization according to depth. J Neurophysiol 33:172-187.

Aitkin LM, Webster WR (1972) Medial geniculate body of the cat: organization and responses to tonal stimuli of neurons in ventral division. J Neurophysiol 35:365-380.

Anderson RA, Knight PL, Merzenich MM (1980) The thalamocortical and corticothalamic connections of AI, AII, and the anterior auditory field (AAF) in the cat: evidence for two largely segregated systems of connections. J Comp Neurol 194:663-701.

Berman AL, Jones EG (1982) The thalamus and basal telencephalon of the cat. Univ Wisconsin Press, Madison, Wisconsin.

Brandner S, Redies H (1990) The projection from medial geniculate to Field A1 in cat: organization in the isofrequency dimension. J Neurosci 10:50-61.

Brunso-Bechtold JK, Florence SF, Casagrande VA (1983) The role of retinogeniculate afferents in the development of connections between visual cortex and the dorsal lateral geniculate nucleus. Dev Brain Res 10:33-39.

Brunso-Bechtold JK, Vinsant SL (1990) An ultrastructural and morphometric study of the effect of removal of retinal input on the development of the dorsal lateral geniculate nucleus. J Comp Neurol 301:585-603.

Calford MB (1983) The parcellation of the medial geniculate body of the cat defined by the auditory response properties of single units. J Neurosci 3:2350-2364.

Calford MB, Webster WR (1981) Auditory representation within principal division of cat medial geniculate body: an electrophysiological study. J Neurophysiol 45:1013-1028.

Chung S-H, Cooke J (1975) Polarity of structure and of ordered nerve connections in the developing amphibian brain. Nature 258:126-132.

Cullen MJ, Kaiserman-Abramof IR (1976) Cytological organization of the dorsal lateral geniculate nucleate nuclei in mutant anophthalmic and postnatally enucleated mice. J Neurocytol 5:407-424.

Frost DO (1981) Orderly anomalous retinal projections to the medial geniculate, ventrobasal, and lateral posterior nuclei of the hamster. J Comp Neurol 203:227-256.

Garraghty PE, Shatz CJ, Sur M (1988) Prenatal disruption of binocular interactions creates novel lamination in the cat's lateral geniculate nucleus. Vis Neurosci 1:93-102.

Godement P, Saillour P, Imbert M (1979) Thalamic afferents to the visual cortex in congenitally anophthalmic mice. Neurosci Lett 13:271-278.

Guillery RW, LaMantia AS, Robson JA, Huang K (1985a) The influence of retinal afferents upon the development of layers in the dorsal lateral geniculate nucleus of mustelids. J Neurosci 5:1370-1379.

Guillery RW, Ombrellaro M, LaMantia AL (1985b) The organization of the lateral geniculate nucleus and of the geniculo-cortical pathway that develops without retinal afferents. Dev Brain Res 20:221-234.

Hahm J, Roe AW, Pallas S, Sur M (1989) Physiologically identified retinogeniculate X axons in ferrets with neonatal ablation of visual cortex: sizes of terminal arbors depend only partly on target size. Soc Neurosci Abstr 15:495.

Hahm J, Langdon RL, Sur M (1990) Disruption of retinogeniculate afferent segregation by antagonists to NMDA receptors. Nature, *in press*.

Hahm J (1991) Ph.D. Thesis. M.I.T., Cambridge, MA.

Heumann D, Rabinowicz TH (1980) Postnatal development of the dorsal lateral geniculate nucleus in the normal and enucleated albino mouse. Exp Brain Res 38:75-85.

Imig TJ, Morel A (1985) Tonotopic organization in ventral nucleus of medial geniculate body in the cat. J Neurophysiol 53:309-340.

Kaiserman-Abramoff IR, Graybiel AM, Nauta WJH (1980) The thalamic projection to cortical area 17 in a congenitally anopthalmic mouse strain. Neurosci 5:41-52.

Kelly JB, Judge PW, Phillips DP (1986) Representation of the cochlea in primary auditory cortex of the ferret (*Mustela putorius*). Hearing Res 24:111-115.

Law MI, Zahs KR, Stryker MP (1988) Organization of primary visual cortex (area 17) in the ferret. J Comp Neurol 278:157-180.

LeVay S, Stryker MP (1979) The development of ocular dominance columns in the cat. Soc Neurosci Symp 4:83-98.

Mason CA, Robson JA (1979) Morphology of retino-geniculate axons in the cat. Neurosci 4:79-97.

Middlebrooks JC, Zook JM (1983) Intrinsic organization of the cat's meidal geniculate body identified by projections to binaural response-specific bands in the primary auditory cortex. J Neurosci 3:203-224.

Morel A, Rouiller E, de Ribaupierre Y, de Ribaupierre F (1987) Tonotopic organization in the medial geniculate body (MGB) of lightly anesthetized cats. Exp Brain Res 69:24-42.

Morest K (1965) The laminar structure of the medial geniculate body of the cat. J Anat Lond 99:143-160.

O'leary DDM, Fawcett JW, Cowan WM (1986) Topographic targeting errors in the retinocollicular projection and their elimination by selective ganglion cell death. J Neurosci 6:3692-3705.

Pallas SL, Hahm JO, Sur M (1989) Retinal axon arbors in a novel target: morphology of ganglion cell axons induced to arborize in the medial geniculate nucleus of ferrets. Soc Neurosci Abstr 15:495.

Pallas SL, Roe AW, Sur M (1990) Visual projections induced into the auditory pathway of ferrets. I. Novel inputs to primary auditory cortex (A1) from the LP/pulvinar complex and the topography of the MGN-A1 projection. J Comp Neurol 298:50-68.

Purser BD, Whitfield IC (1972) Thalamo-cortical connections and tonotopicity in the cat medial geniculate body. J Physiol 222:161-162.

Rakic P, Williams RW (1986) Thalamic regulation of cortical parcellation: an experimental perturbation of the striate cortex in rhesus monkeys. Soc Neurosci Abstr 12:1499.

Rakic P, Suner I, Williams RW (1991) A novel cytoarchitectonic area induced experimentally within the primate visual cortex. Proc Natl Acad Sci USA 88:2083-2087.

Rhoades RW, Fish SE (1983) Bilateral enucleation alters visual callosal but not corticotectal of corticogeniculate projections in hamster. Exp Brain Res 51:451-462.

Rodrigues-Dagaeff C, Simm G, de Ribaupierre Y, Villa A, de Ribaupierre, Rouiller EM (1989) Functional organization of the ventral division of the medial geniculate body of the cat: evidence for a rostro-caudal gradient of response properties and cortical projections. Hearing Res 39:103-126.

Roe AW, Garraghty PE, Sur M (1989) The terminal arbors of single on-center and off-center X and Y retinogeniculate axons within the ferret's lateral geniculate nucleus. J Comp Neurol 288:208-242.

Roe AW, Pallas SL, Hahm J, Sur M (1990) A map of visual space induced into primary auditory cortex. Science 250:818-820.

Sachs GM, Jacobson M, Caviness VS (1986) Postnatal changes in arborization patterns of murine retinocollicular axons. J Comp Neurol 246:395-408.

Schmidt JT, Cicerone CM, Easter SS (1978) Expansion of the half retinal projection to the tectum in goldfish: an electrophysiological and anatomical study. J Comp Neurol 177:279-300.

Schneider GE (1973) Early lesions of superior colliculus: factors affecting the formation of abnormal retinal projections. Brain Behav Evol 8:73-109.

Shatz CJ, Stryker MP (1988) Prenatal tetrodotoxin infusion blocks segregation of retinogeniculate afferents. Science 242:87-89.

Sherman SM, Spear PD (1982) Organization of visual pathways in normal and visually deprived cats. Physiol Rev 62:738-855.

Sperry RW (1943) Effect of 180° rotation of the retinal field on visuomotor coordination. J Exp Zool 92:263-279.

Sperry RW (1963) Chemoaffinity in the orderly growth of nerve fiber patterns and connections. Proc Natl Acad Sci USA 50:703-710.

Sretevan DW, Shatz CJ, Stryker MP (1988) Modification of retinal ganglion cell axon morphology by prenatal infusion of tetrodotoxin. Nature 336:468-471.

Stryker MP, Harris WA (1986) Binocular impulse blockade prevents the formation of ocular dominance columns in cat striate cortex. J Neurosci 6:2117-2133.

Sur M, Esguerra M, Garraghty PE, Kritzer MF, Sherman SM (1987) Morphology of physiologically identified retinogeniculate X- and Y-axons in the cat. J Neurophysiol 58:1-32.

Sur M, Garraghty PE, Roe AW (1988) Experimentally induced visual projections into auditory thalamus and cortex. Science 242:1437-1441.

Sutton JK, Agee DA, Brunso-Bechtold JK (1987) A golgi study of dendritic development in the dorsal lateral geniculate nucleus (dLGN) of ferrets. Soc Neurosci Abstr 13:591.

Thanos S, Bonhoeffer F, Rutishauser U (1984) Fiber-fiber interaction and tectal cues influence the development of the chicken retinotectal projection. Proc Natl Acad Sci USA 81:1906-1910.

Weber AJ, Kalil RE, Stanford LR (1989) Morphology of single, physiologically identified retinogeniculate Y-cell axons in the cat following damage to visual cortex at birth. J Comp Neurol 282:446-455.

Zahs KR, Stryker MP (1985) The projection of the visual field onto the lateral geniculate nucleus of the ferret. J Comp Neurol 241:210-224.

Figure Legends

Fig. 1. Schematic of thalamic sensory topography. A) The normal LGN is a C-shaped structure composed of the A, A1, and C laminar planes. Within each of these planes (only one is depicted) low azimuths are represented medially and high azimuths laterally (heavy arrow). Elevations are represented in the dorsoventral axis with elevations decreasing in a dorsal to ventral gradient (light arrow). *Single visual locations* are thus represented by projection lines that run orthogonal to laminar planes (shaded bar). B) The normal MGN, seen coronally, is organized in a lamellar fashion. High frequencies are represented in medial lamellae and low frequencies in lateral lamellae (heavy arrow). *Single frequencies* are represented by an entire lamellar plane (one is depicted by shaded plane). C) A retino-MGN mapping scheme similar to that seen in the normal LGN. Each lamellar sheet contains a 2-dimensional topographic map of the visual world, where one visual axis (e.g. azimuth) is mapped rostrocaudally (heavy arrow) and the other (e.g. elevation) dorsoventrally (light arrow). Lines of projection would run orthogonal to lamellar planes. D) A retino-MGN mapping scheme similar to that seen in the normal MGN. One visual axis (e.g. azimuth) is mapped across lamellar borders (heavy arrow). The orthogonal visual axis (e.g. elevation) would map within each lamellar plane in some systematic fashion (one possible orientation for this axis is shown by light arrow). Lines of projection would run within the lamellar plane orthogonal to the second (in this case, elevational) visual axis.

Fig. 2. Receptive field locations of all visual cells recorded in the MGv (filled circles, n=63), the MGm (open circles, n=29), and the MGd (open squares, n=13).

Fig. 3. Visual topography in the MGv as assessed by penetrations in which multiple visual units were recorded. A) Locations (indicated by penetration letter) of visual receptive fields recorded in penetrations through the MGv as depicted in B. Arrows indicate the direction of increasing depth in each penetration. Dashed arrows aide in distinguishing individual tracts. B) Coronal sections (from caudal to rostral) through a typical MGN in a rewired ferret. Electrode penetrations (lines) made through the MGN of different ferrets (n=5) have been drawn in corresponding positions in this representative MGN. Penetrations A, B (F89-29); C (F87-130); D, F, and G (F90-93); E (F87-132) come from a single cases. Only penetrations in which three or more visual units were recorded are depicted. Dots indicate sites along the electrode tract where visual receptive fields were recorded.

Fig. 4. Locations of all visual receptive fields recorded in MGv that are not depicted in Fig. 3. Same conventions as Fig. 3. A) Receptive field locations of cells (identified by letters) recorded at locations indicated in B. Receptive fields that do not support proposed organization (see text) are indicated by italicized lower case letters. Dotted lines demarcate 15° and 45° isoazimuths. B) Locations of recording sites in which receptive fields shown in A were recorded. Units recorded in the same penetration are indicated by numbered letters.

Fig. 5. Locations of all visual receptive fields recorded in MGm (A,B) and MGd (C) and their locations in the thalamus (D). Conventions as in Fig. 3. A) Receptive field progressions in single penetrations through the MGm. B) All other receptive fields recorded in MGm. C) Receptive field locations of cells recorded in the MGd. D) Locations of electrode penetrations through the MGm and MGd.

Fig. 6. Schematic of visual topography in MGv of rewired ferrets. Coronal view of ferret MGv is depicted by oval. Azimuths map across lamellar planes (one curved plane is depicted), with high azimuths represented in lateral lamellae and low azimuths in medial lamellae. Within each isoazimuthal lamella, elevations are mapped in a rostrodorsal (high elevations) to caudoventral (low elevations) gradient. Single points in the visual field would then be represented in rostroventral-to-caudodorsally oriented projection lines (one depicted by shaded strip).

Fig.1

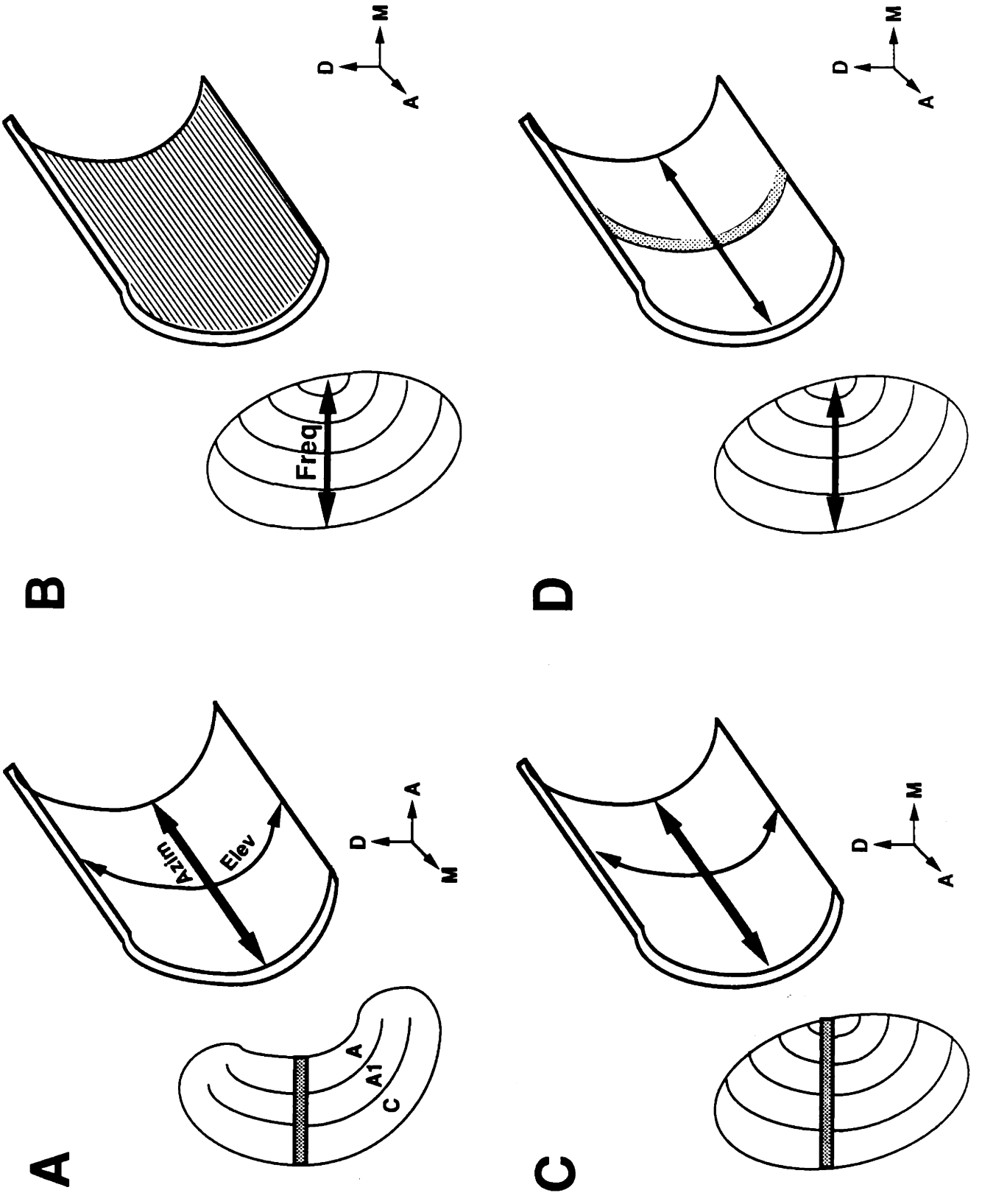

Fig. 2

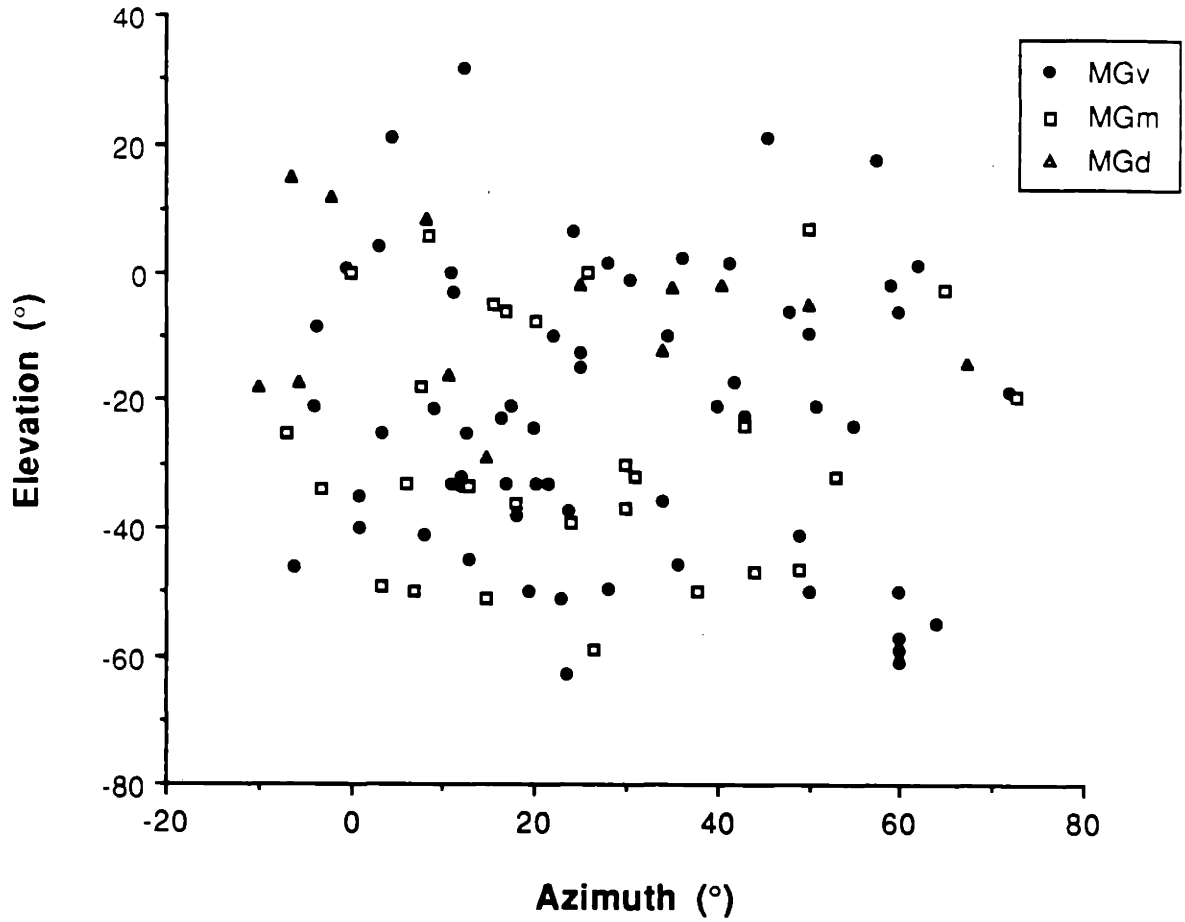

Fig. 3

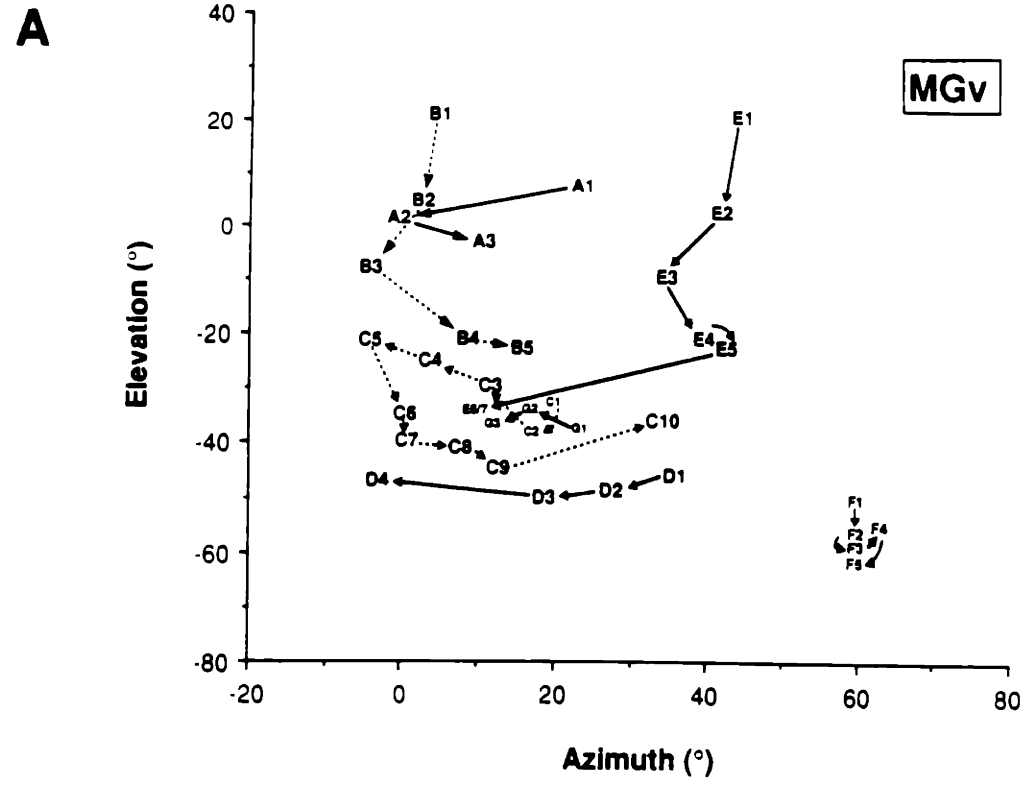
A
MGv
Elevation (°)
Azimuth (°)
40
20
0
-20
-40
-60
-80
-20
0
20
40
60
80
B1
A1
B2
A2
A3
B3
B4
B5
C5
C4
C3
C6
C7
C8
C9
C10
D4
D3
D2
D1
E1
E2
E3
E4
E5
F1
F2
F3
F4
F5

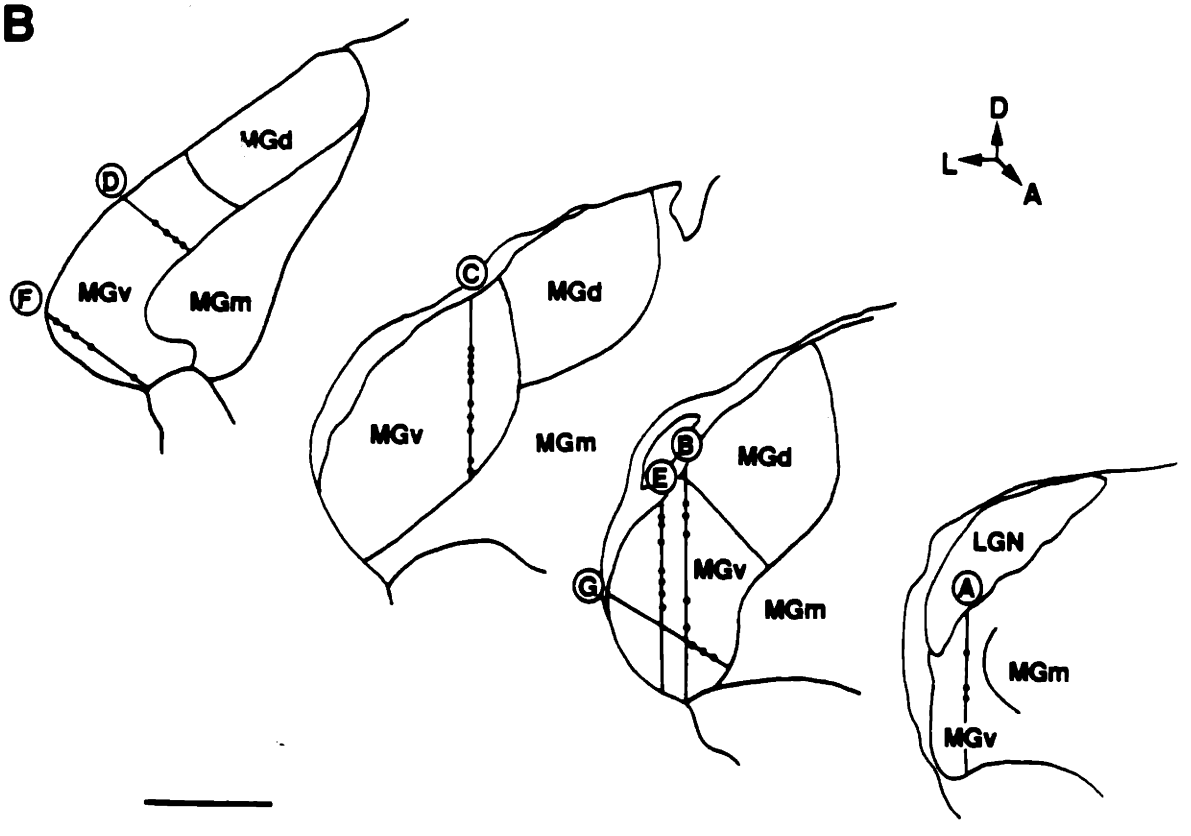
B
D
L
A
MGd
MGv
MGm
LGN

Fig. 4

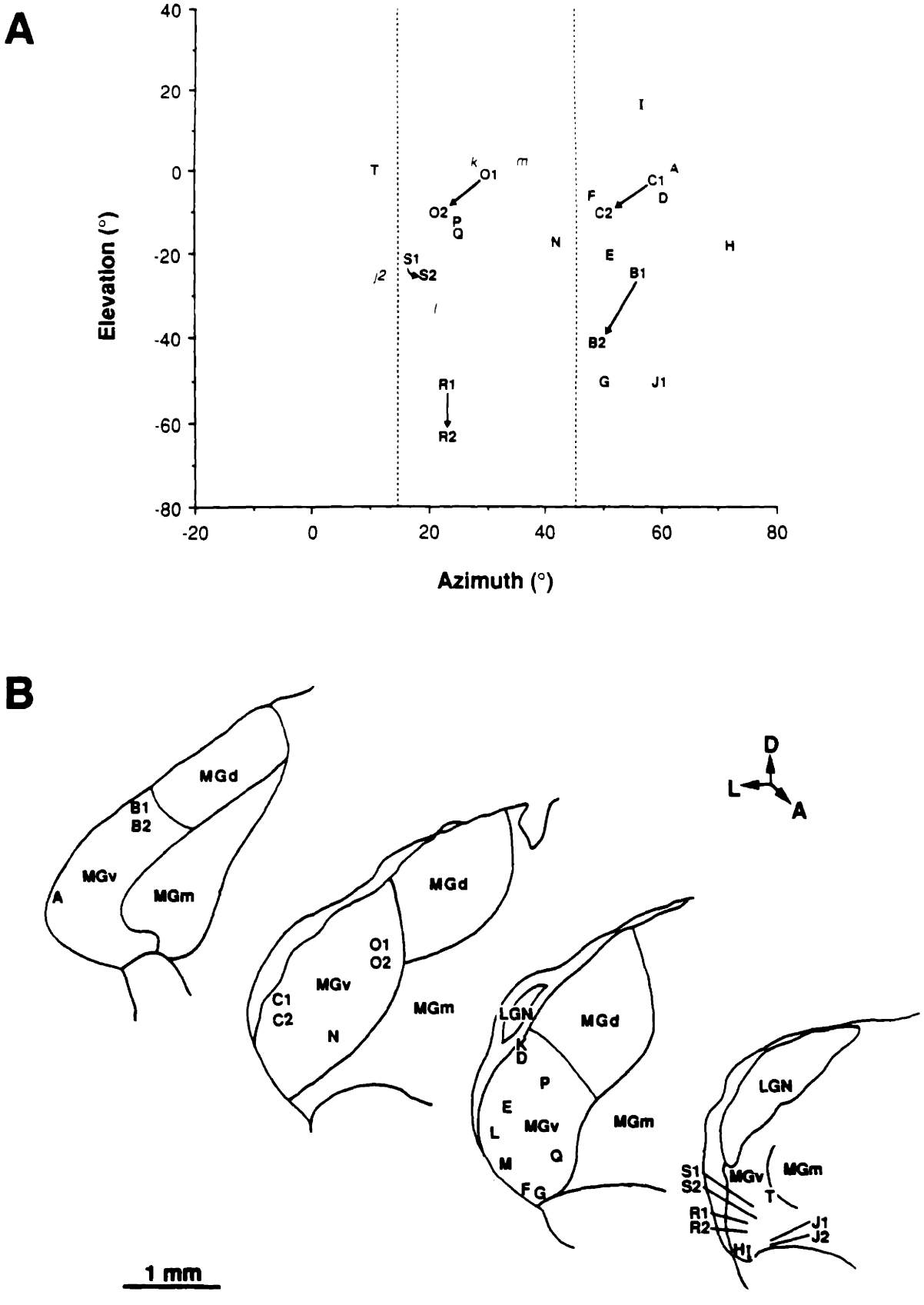
A
Elevation (°)
Azimuth (°)
40
20
0
-20
-40
-60
-80
-20
0
20
40
60
80
T
k
O1
m
I
C1
A
F
D
C2
O2
P
Q
N
E
H
S1
S2
B1
B2
R1
R2
G
J1
B
MGd
B1
B2
MGv
A
MGm
O1
O2
C1
C2
N
LGN
K
D
P
E
L
M
Q
F
G
D
L
A
LGN
S1
S2
MGv
MGm
T
R1
R2
J1
J2
H1
1 mm

Fig. 5

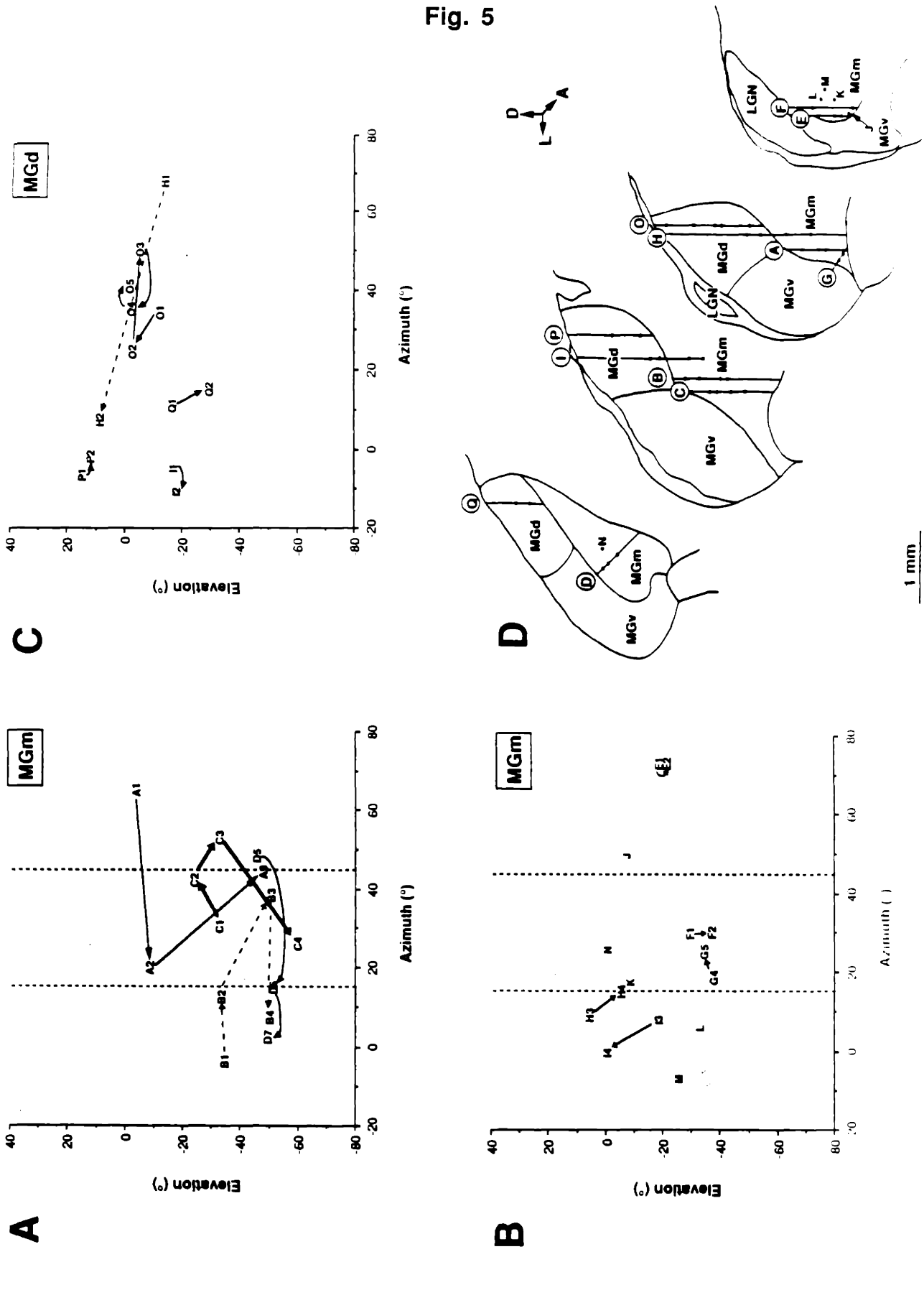
A
MGm
Elevation (°)
Azimuth (°)
B
MGm
Elevation (°)
Azimuth (°)
C
MGd
Elevation (°)
Azimuth (°)
D
MGd
MGm
MGv
LGN
1 mm

Fig. 6

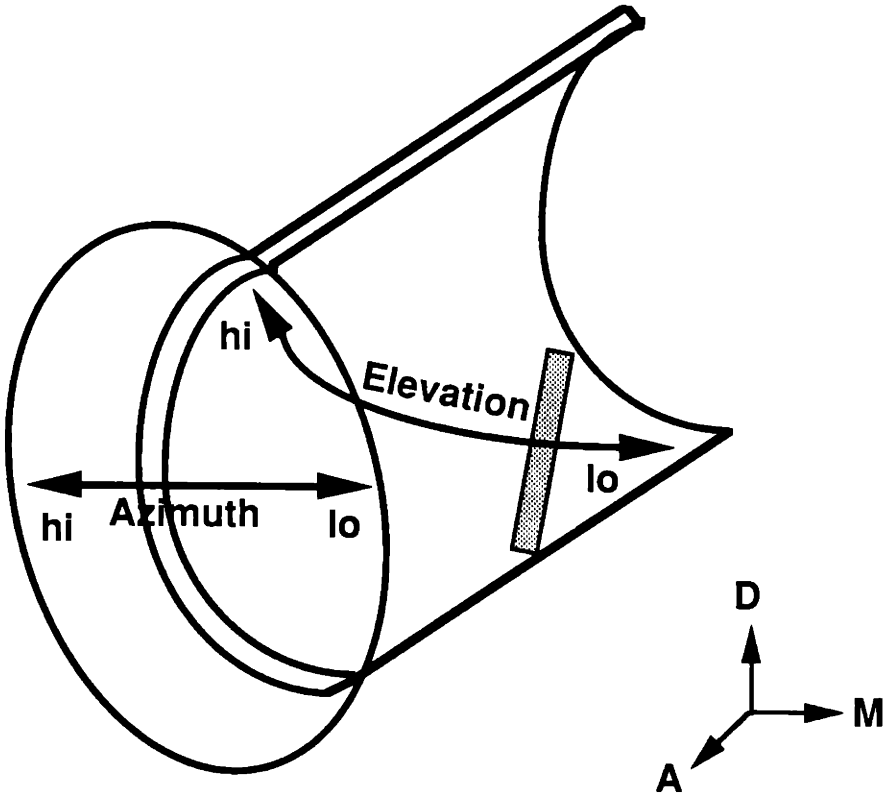

Chapter 2

Part II: Cortical Topography

Experimentally Induced Establishment of Visual Topography in Auditory Cortex

Abstract

We have previously reported that following specific neonatal brain lesions in ferrets, a retinal projection is induced into the auditory thalamus (Sur et al., 1988). Single cells in auditory thalamus (i.e., the medial geniculate nucleus, MGN) and primary auditory cortex (A1) of these ferrets develop visual receptive field properties similar to those in the normal lateral geniculate nucleus (LGN) and primary visual cortex (V1) (Sur et al., 1988; Chapters 1, 2). We now investigate whether the retino-MGN-A1 pathway confers onto its target structures a retinotopic representation of the visual world.

We find that topographically organized retinal maps are established in A1. While these maps are less ordered than visual field maps in V1, we find consistently that azimuthal representations map onto the axis that normally represents varying sound frequency in normal A1. Elevations map within "isofrequency" domains in A1 and can be more variable in their mapping pattern. Intracortical mechanisms may contribute to establishment of elevational topography in the isofrequency axis. Thus, retinal inputs can map in a coherent and visuotopically representative fashion in a non-visual sensory cortex.

Introduction

Topographic sensory representation in any cortical area requires that the topographic organization of the peripheral sensorium be maintained at each subcortical relay and that connectional relationships with cortex respect such topographies. In the visual system, retinotopy is relayed via a point-to-point pattern of thalamocortical connectivity (e.g. Updyke, 1978). In the auditory system, thalamocortical connectivity is topographic in the frequency dimension and highly convergent and divergent in the isofrequency dimension (Anderson et al., 1980; Middlebrooks and Zook, 1983). In the somatosensory system, elongated rods of isorepresentation project to focal loci in primary somatosensory cortex (Jones et al., 1982). Thus anatomical patterns of thalamocortical connectivity appear to predict cortical topography.

We have challenged this notion by constructing (an apparent) dimensional mismatch between peripheral sensorium and cortical target. Specifically, we have rerouted retinal fibers into the auditory pathway, a pathway that is topographically organized along the frequency dimension. The data presented in Part 1 demonstrates that the retinal mapping onto the MGv is retinotopically organized: azimuths are mapped onto the variable frequency axis and elevations are mapped within isofrequency lamellae. The pattern of auditory thalamocortical connectivity (Fig. 1A) would predict a map in auditory cortex that is only retinotopic in the frequency axis (Fig. 1B). In this paper, we present physiological evidence suggesting that a two-dimensional visual map is established in cortex as well. Some of these data has been reported previously (Roe et al., 1990).

Methods

Methods are similar to those described previously in Chapter 2. Briefly, an aberrant retinal projection to the auditory pathway in ferrets was induced by removing normal visual targets and deafferenting the MGN at birth. Once reared to adulthood, operated ferrets were prepared for visual physiological recording. Briefly, animals were anesthetized, paralyzed, and artifically ventilated, and contact lens placed on the eyes. The skull overlying AI was removed and stimulating electrodes were placed straddling the optic chiasm.

Visual units in A1 were recorded with parylene-coated tungsten microelectrodes in penetrations spaced 250-500 um apart. The position of electrode penetrations were recorded by marking on drawings or photographs of the sulcal and vascular patterns on the cortical surface as well as by noting stereotaxic coordinates. In each penetration, units were determined to be visual if they 1) responded to optic chiasm stimulation and 2) responded to flashing or moving spots or bars of light. Cells were qualitatively rated (1-4) for responsivity and receptive fields plotted and characterised (see Chapter 2). Most of these experiments were conducted in conjunction with single-unit recordings (Chapter 2). To maximize extent of cortex mapped, in most penetrations no more than one to two receptive fields were plotted.

At the termination of the experiment, the animal was given an overdose of pentobarbitol and perfused through the heart with saline, followed by fixative (either 1% paraformaldehyde, 2% glutaraldehyde or 10% formalin), and 10% and 20% sugared buffer solutions. Frozen sections were then cut, mounted onto slides, Nissl-stained, and coverslipped.

Data Analysis

Visual representation in A1 was assessed by plotting receptive field locations associated with each penetration. In penetrations in which more than one visual unit was recorded, we considered only the receptive fields recorded in the middle layers of cortex (at

depths between 400-800 um). If multiple units were recorded in the middle layers of a single penetration, the unit with the stronger response index was selected.

To assess topography of visual representation in A1, we constructed two cortical maps in each case, one in which penetrations with similar azimuthal representation were connected by lines and another in which points with similar elevational representation were connected. Drawings were then assessed for the possible presence of azimuthal or elevational mapping gradients. With these lines as guides, idealized isoazimuthal and isoelevational lines were drawn in relation to the cortical penetrations. Approximate magnification factors were calculated from these idealized maps.

Two measures of mapping precision were calculated. 1) We indexed how well the recorded azimuths and elevations at each cortical location matched those of the ideal maps. We defined a "goodness-of-fit" index as the mean difference between the recorded azimuthal/elevational value and the ideal azimuthal/elevational value at that point, normalized by the maximum extent of the map (max value - min value) in that dimension. 2) A Pearson's rank test was used to compare the rank of the actual azimuthal/elevational values recorded with the rank of cortical distance from a fixed reference point (i.e. from the most medial or most caudal penetration).

Results

Topography in A1.

Visual receptive field locations were mapped in primary auditory cortex (AI) in 11 operated ferrets. Penetrations were made in cortex judged to be in A1 [located between the anterior ectosylvian sulcus (AES) and posterior ectosylvian sulcus (PES)] or in adjacent cortical areas. Of four cases in which A1 was relatively extensively mapped, two cases exhibited clear orderly visuotopic maps, one exhibited no discernible topography, and one yielded few sites that were visually responsive. In the remaining 7 cases, a more limited number of penetrations were made. Of these, 4 displayed some evidence of topography and 3 contained none.

Topographic Maps in A1

Fig. 2 illustrates one case (F88-24) in which A1 was fairly extensively mapped. In Fig. 2A, each penetration is indicated by a dot and identified by a letter; X's mark non-responsive penetration sites. The area from which visually responsive cells were recorded is co-extensive with the region of A1 as determined cytoarchitectonically (see Pallas et al., 1990). It was not uncommon for responsive and non-responsive penetrations to be located adjacent each other (e.g. penetration i). No visual units were recorded in the suprasylvian gyrus adjacent to A1 (4 penetrations). The receptive fields recorded in these penetrations span a large extent of the ferret visual field (Fig. 2B), an extent similar to that found in normal visual cortex (see Chapter 2, Law et al., 1988). Azimuths ranged from 6° (unit a) to 65° (unit r); elevations ranged from -37° (unit m) to 13° (unit r).

Two orthogonal representational gradients are apparent in this map. In general, low azimuths are represented medially and high azimuths laterally on the cortical surface. Units with similar azimuthal values (Fig. 2B, connected by arrows) tend to be located at similar mediolateral distances in A1. When these azimuthal values are correlated with mediolateral

distance on the cortical surface, the trend is significant (Pearson correlation coefficient r = 0.74, $p < 0.01$). Furthermore, in a caudal to rostral direction in A1, elevations progress from inferior visual field representations to superior fields (e.g. receptive field progressions a-b, c-e, g-i, j-l, and m-q). This trend is also significantly different from random (Pearson r = 0.46, $p < 0.05$). This visual map in AI is thus two-dimensional and retinotopic, with azimuths mapping in the mediolateral dimension and elevations mapping roughly in the caudal to rostral dimension.

To further assess the topographic organization of this map, we fitted (by eye) idealized isoazimuthal and isoelevational lines (separated by 10° intervals) to these data (Fig. 2C). Lines were drawn to maximize agreement with data as well as to maximize, when possible, regularity in the map. The agreement of recorded azimuths with a regular topographic mapping scheme is fairly good (Fig. 2C, left): only one point (65° at point r) is more than 10° from its ideal location. The mapping of elevations, however, is somewhat less precise (e.g. elevation at point r). To quantify the relative precision of mapping along the the two orthogonal axes, we calculated and compared "goodness-of-fit" indices for azimuths and elevations. The goodness-of-fit index is defined as the mean difference between the recorded value and the ideal value at that cortical position (as determined from idealized contour lines), normalized by the maximal extent of the map in that dimension. This index ranges from 0 to 1, with 0 indicating a perfect fit and values near 1 indicating poor fit. The azimuthal index for this map (x = 0.061, SEM = 0.014, range 0.0 to 0.203) is significantly smaller than elevational index (x = 0.120, SEM = 0.051, range 0.0 to 0.962). [Note: The absolute placement of the idealized contours is not critical to the point of the analysis. We made similar calculations with a slightly different set of contour lines, in which azimuthal contour lines were drawn as regularly spaced (0.45 mm apart) concentric arcs and elevations as radial lines from a single point (Fig. 2C, open square). With these contours, the calculated azimuthal index (x = 0.105, SEM = 0.024, range 0.0 to 0.356) is still lower than the elevational index (x = 0.145, SEM = 0.050, range 0.0 to 0.962).]

Another important aspect of topographic mapping is the amount of cortical area devoted to each locus of visual space. Approximate cortical magnification factors were calculated from the idealized contour lines shown in Fig. 2C. We superimposed the isoazimuthal and isoelevational contours and calculated the cortical magnification factors (mm of cortex/° of visual space) along the -10°, -20°, and -30° isoelevation contours (Fig. 2D). Along each isoelevation, cortical magnification in A1 remains relatively constant from central to peripheral azimuths as well as from superior to inferior elevations (average magnifications along the -10°, -20°, and -30° isoelevations are 0.051 mm/°, 0.052 mm/°, and 0.051 mm/°, respectively). This contrasts significantly with the cortical magnifications in normal V1, which is high for central visual field locations and decreases rapidly with eccentricity (Tusa et al., 1978; Law et al., 1988).

Topographic mapping of the visual field in A1 was also seen in a second case that was fairly extensively mapped (Fig. 3A). In this case, the visually responsive cortical region lies primarily in the anterior half of A1; the visual field representation is correspondingly more restricted (azimuths range from 2° to 68°; elevations range from -18° to 14°). Similar to the previous case, low azimuths are represented medially in cortex and high azimuths laterally (Fig. 3B). From medial to lateral, penetrations c-d, e-h, j-l, m-o, p-q, and r represent approximately 5°, 10°, 20-25°, 35°, 50-55°, and 65° azimuths, respectively. The correlation between azimuth and mediolateral cortical distance is significant (Pearson $r = 0.66$, $p < 0.01$). We did not include points a and b in this calculation because they appear to lie outside A1, possibly in the anterior auditory field or suprasylvian fringe sector (cf. Imig et al., 1982).

Interestingly, in comparison with the previous case, the mapping of elevations is reversed. Within each of the 5°, 10°, 20-25°, 35°, and 50-55° azimuthal progressions, elevations tend to *decrease* from posterior to anterior cortical locations (c-d, g-h, k-l, m-n-o, and p-q). Similar to the previous case, mapping of elevations is cruder than that of azimuths. Correlation between elevations and anteroposterior cortical distance is weakly significant (Pearson $r = -0.39$, $p < 0.1$, points a and b excluded). Goodness-of-fit indices (calculated

from idealized isoazimuthal and isoelevational contours shown in Fig. 3C) for azimuthal values (x =0.094, SEM = 0.035, range 0.0 to 0.561) are again lower than those for elevational values (x = 0.156, SEM = 0.042, range 0.0 to 0.548). [Indices calculated from a perfectly regular idealized map with straight azimuthal (spacing 3.6 mm) and elevational (spacing 5.4 mm) contours are: azimuths (x = 0.221, SEM = 0.051, range 0.051 to 0.831), elevations (x = 0.292, SEM = 0.059, range 0.032 to 0.806).] The poor elevational mapping in this case is in part due to the reversals in topography seen in some receptive field progressions (rows e-h and j-l).

Cortical magnification factors for this map (Fig. 3D) are also relatively constant across azimuths and elevations (average magnifications along each of the 0°, -5°, and -10° isoelevations are 0.039 mm/°, 0.038 mm/°, and 0.037 mm/°, respectively). These magnification values are 20% lower than those of the map in Fig. 2 and reflects the more limited cortical area covered by this map.

In A1 of two other rewired ferrets, no evidence of topography was seen. In one case (F89-59), only 4 out of 19 penetrations in A1 recorded visual units. In the other (F88-77), 12 of 18 penetrations encountered visual cells; however, no topographic pattern could be discerned. Even within single penetrations in this case, receptive field locations jumped by as much as 40° in azimuth. Such scatter was not seen in either of the maps presented in Figs. 2 and 3.

Partial Maps in A1

In the remaining 7 cases, a more limited number of cortical penetrations were made. 4 of these suggested possible topography (Fig. 4). In case F88-34 (Fig. 4A), high azimuths are represented in lateral A1 and lower azimuths are located more medially. Isoazimuthal contours may be highly curved in this case: low isoazimuthal representation (penetrations a-b) is bounded by a highly curved 30° azimuthal contour (c-d-e), which is in turn bounded by a 40-50° contour (f-g would extend between c-d and h-j). Progression h-i-j crosses from lateral

contour to more medial contour. Elevational representation tends to decrease as cortex is traversed in a posterior to anterior direction (except in progression a-b). A similar mapping is suggested by the partial maps shown in Fig. 4B and 4C. Lower azimuths are represented medially (Fig. 4B, a-b) and high azimuths laterally (Fig. 4B, c-d). Elevations map in the orthogonal axis, with high elevations posterior in A1 and lower elevations anterior (Fig. 4B, a-b and c-d; Fig. 4C, a-b-c).

One case displayed a possible rotated visual topography. Units recorded medially had high elevational representation (Fig. 4D, a-b); those recorded laterally represented lower visual fields (Fig. 4D, c-d and e-f). In addition, azimuths (low to high) appeared to map in the posterior to anterior cortical dimension. The rotation may be related to the fact that in this animal A1 was not bounded by an obvious posterior ectosylvian sulcus. A dotted line placed immediately caudal to the caudal-most visual penetration serves only to suggest a possible posterior boundary of A1 in this case; it is possible that the orientation of A1 in this case was altered due to the neonatal lesions of visual cortex.

Discussion

Thalamocortical Connectivity Predicts Azimuthal Topography

Based on the results from thalamic mapping (this chapter, Part 1) and from thalamocortical connectivity (see Fig. 1A), a topographic mapping of the azimuthal dimension of the visual field is predicted (see Fig. 1B, bottom). Our results support this prediction. As predicted by thalamocortical connectivity, azimuths are consistently mapped along the axis that normally maps sound frequency in A1: low azimuths (medial MGv) map medially in A1 and high azimuths (lateral MGv) laterally (Fig. 5). Elevations are mapped in the orthogonal isofrequency dimension and are often less organized and/or more variable in detail (e.g. we find reversals in progressions, maps with opposite polarities, poorer goodness-of-fit indices and Pearson scores).

Sources of Mapping Variability

Variability in Extent of Visual Representation: Neonatal Lesions

There is some inherent variability in the extent of neonatal cortical lesions. More extensive cortical lesions result in a greater induction of retinal afferents (Chapter 1). It is likely that in cases in which few visually responsive neurons were recorded, the visual cortex was not sufficiently ablated to induce significant rerouting of retinal afferents. In cases in which only a portion of the visual field in mapped in A1 (e.g. Fig. 3), it is possible that the complementary visual field representation was not lesioned and that there is only a partial routing of retinal afferents to the auditory thalamus.

Variability in the Mapping of Elevation

Two factors may contribute significantly to the variability in elevational mapping. At the thalamic stage, there is an increased degree of freedom in mapping a line of isoelevation in

the retina onto a plane of isofrequency in the MGN. Receptive field sizes in MGN are significantly larger than those of retinal ganglion cells, suggesting a significant degree of divergence in the retino-MGN pathway (Chapter 1). Also, receptive field progressions in the MGN are not nearly so organized and predictable as those in the LGN, indicating a cruder topography in the input to A1 (this chapter, part 1).

At the thalamocortical level, Middlebrooks and Zook (1983) have shown that within each of the isofrequency laminae in the cat MGv lies approximately five rostrocaudally oriented alternating EE and EI bands, each projecting to each of the 3 EE and 2 EI bands, respectively, in A1. This suggests that within each of the EE and EI systems lies a highly convergent and divergent projection system. However, some evidence indicates that EI bands lie more rostrally in the thalamus than EE bands, and thereby may underly a very crude form of thalamocortical topography in the isofrequency axis (Middlebrooks and Zook, 1983; Brandner and Redies, 1990). We suggest that the visual elevational topography found here is sharper than the suggested anatomical topography along the isofrequency dimension. Figures from both Brandner and Redies (1990) and Middlebrooks and Zook (1983) indicate that only cells in the extreme 10-15% of the isofrequency axis may not have highly convergent input from thalamus. In the visual maps shown here, rough topography is seen along the length of the anterior-posterior axis in A1. Furthermore, the EE and EI bands are seen only in the high frequency representations in MGN and A1. In the low frequency representation, anatomical projections from MGN to A1 are highly distributed.

How, then, is functional topography significantly sharpened from a highly overlapped input? Mapping along the isofrequency dimension must arise via some differential selection/expression mechanism in cortex. It is possible that specific patterns of correlated visual inputs, distinct from normal patterns of auditory inputs, have selectively strengthened or expressed (e.g. via a Hebbian mechanism) those synaptic connections that arise from neighboring points on the retina. Thus, while anatomical connections may appear highly overlapped or distributed, functional connections are quite topographic.

One possibility is that visual inputs during development shape and refine the arborizations of individual thalamocortical axons. Activity-driven synaptic stabilization appears to be phenomenon underlying the sharpening or appropriate segregation of retinogeniculate (Dubin et al., 1986; Sretavan et al., 1988; Shatz and Stryker, 1988), retinotectal (Schmidt and Edwards, 1983; Reh and Constantine-Paton, 1985; Cline et al., 1987) and thalamocortical (Stryker and Harris, 1986) connectivity during development. However, at least in the normal visual system, those connections that are not stabilized functionally are also lost anatomically (Campbell et al., 1984; Campbell and Shatz, 1986). We do not see any evidence of that occurring in this system: thalamocortical connections remain widespread along the isofrequency dimension in rewired ferrets (Pallas et al., 1990).

Another possibility is suggested by physiological studies in auditory, somatosensory, and visual cortex. Recent studies indicate that there is some systematic functional organization along the isofrequency axis, such as sharpness of tuning (Sutter and Schreiner, 1989) and symmetry of tuning as assessed by forward temporal masking (Shamma et al., 1991). This apparent inconsistency between physiological and anatomical is seen in the somatosensory system in which single thalamocortical axons can extend across significantly greater cortical distances than what physiological receptive field sizes would predict (Garraghty et al., 1989; Garraghty and Sur, 1990). Physiological sharpening could result from variations in effectiveness within single terminal arbors, perhaps due to variations in synaptic density (e.g. Garraghty and Sur, 1990) or synaptic efficacy (cf. Burke, 1987) within the arbor. Physiological sharpening could also result from convergence of portions of arbors arising from multiple thalamocortical arbors (in essence a local weighting function). Indeed, such mechanisms have been proposed to underly the dramatic cortical plasticity in adult somatosensory cortex after removal of portions of peripheral inputs (Merzenich et al., 1988; Kaas, 1991) and in adult visual cortex after restricted lesions of the retina (Kaas et al., 1990; Gilbert et al., 1991). Cortical physiological studies suggest that such mechanisms may be present in normal auditory processing. Auditory cortical receptive fields are quite malleable

and exhibit a wide range of expressive capabilities depending, for example, on sensory inputs or state of arousal (e.g. Abeles and Goldstein, 1970). Furthermore, similar to somatosensory (Merzenich et a., 1983; Dykes et al., 1984; Alloway et al., 1989; Jenkins et al., 1990) and motor (Nudo et al., 1990; Jacobs et al., 1991) cortices, receptive field sizes, tuning properties, and cortical sensory maps can be greatly altered by GABA-ergic and cholinergic substances (Muller and Scheich, 1988; Metherate and Weinberger, 1989) as well as changes in central or peripheral input (King and Moore, 1991).

If such dynamic mechanisms are responsible for the establishment of topography in the isofrequency dimension of A1, then it is not surprising that there should be greater variability in elevational representation. Such mechanisms could explain interanimal differences in the polarity of the map, local reversals in elevational representation, and a higher degree of scatter.

Cortical Magnification

In the normal visual pathway, the area of visual cortex representing a degree of visual space falls off exponentially from central to peripheral cortical locations (Tusa et al., 1978). Cortical magnification factors reflect to a large extent the density of retinal ganglion cells at a particular eccentricity (Wassle et al., 1989). Similarly, the visual map in A1 reflects the distribution of its retinal inputs. We have shown in Chapter 1 that the retinal input to the MGN arises from retinal W cells. Consistent with this, cortical magnification factors in A1 remain relatively constant across a wide range of eccentricities, paralleling the relatively uniform distribution of W cells in the retina (Stone, 1965; Fukuda and Stone, 1974). Thus, similar to the normal visual pathway, both retinofugal divergence and thalamocortical divergence must remain relatively constant across eccentricities (cf. Tusa et al., 1978).

Conclusion

In conclusion, one major determinant of the visual map in A1 is the discrete anatomical pattern of projections to the mediolateral dimension of A1 from the mediolateral dimension of the MGN. Visual field azimuths are mapped along this dimension in both the MGN and in A1. The anteroposterior dimension of A1 receives highly convergent and divergent projections from "isofrequency" lamellae in the MGN. We suggest that the mapping of visual field elevation along this dimension in A1 is driven significantly by correlations in input visual activity, so that retinal loci adjacent to each other in elevation come to be mapped topographically adjacent to each other in the anteroposterior dimension. Thus, the topography of the visual map in A1 is established by features of the auditory thalamocortical pathway, on which are overlaid features specific to the visual input (that establish precision and detail in the map). We reach a similar conclusion when we examine the receptive field properties of visual cells in A1 (Chapter 3).

References

Abeles M, Goldstein MH (1970) Functional architecture in cat primary auditory cortex: columnar organization and organization according to depth. J Neurophysiol 33:172-187.

Albus BV (1978) Topographic organization of the projections from cortical areas 17, 18, and 19 onto the thalamus, pretectum and superior colliculus in the cat. J Comp Neurol 173:81-122.

Alloway KD, Rosenthal P, Burton H (1989) Quantitative measurements of receptive field changes during antagonism of GABAergic transmission in primary somatosensory cortex of cats. Exp Brain Res 78:514-532.

Anderson RA, Knight PL, Merzenich MM (1980) The thalamocortical and corticothalamic connections of AI, AII, and the anterior auditory field (AAF) in the cat: evidence for two largely segregated systems of connections. J Comp Neurol 194:663-701.

Brandner S, Redies H (1990) The projection from medial geniculate to Field A1 in cat: organization in the isofrequency dimension. J Neurosci 10:50-61.

Burke RE (1987) Synaptic efficacy and the control of neuronal input-output relations. Trends Neurosci 3:1389-1413.

Campbell G, Shatz CJ (1986) Synapses formed by individual retinogeniculate axons in inappropriate LGN territory during formation of eye-specific layers. Soc Neurosci Abstr 12:589.

Campbell G, So KF, Lieberman AR (1984) Normal postnatal development of retinogeniculate axons and terminals and identification of inappropriately-located transient synapses: electron microscope studies of horseradish peroxidase-labelled retinal axons in the hamster. Neurosci 13:743-759.

Dubin MW, Stark LA, Archer SM (1986) A role for action-potential activity in the development of neuronal connections in the kitten retinogeniculate pathway. J Neurosci 6:1021-1036.

Dykes RW, Landry P, Metherate R, Hicks TP (1984) Functional role of GABA in cat primary somatosensory cortex: shaping receptive fields of cortical neurons. J Neurophysiol 52:1066-1093.

Fukuda Y, Stone J (1974) Retinal distribution and central projections of Y-, X-, and W-cells of the cat's retina. J Neurophysiol 37:749-772.

Imig TJ, Reale RA, Brugge JF (1982) The auditory cortex: patterns of corticocortical projections related to physiological maps in the cat. In: Cortical Sensory Organization, Vol. 3, Multiple Auditory Areas (Woolsey CN, ed). pp. 1-41. Clifton, NJ: Humana Press.

Jacobs, Donoghue (1991) Reshaping of cortical motor map by unmasking latent intracortical connections. Science 251:944-947.

Jenkins WM, Merzenich MM, Ochs MT, Allard T, Guic-Robles E (1990) Functional reorganization of primary somatosensory cortex in adult owl monkeys after behaviorally controlled tactile stimulation. J Neurophysiol 63:82-104.

Jones EG, Friedman DP, Hendry SHC (1982) Thalamic basis of place- and modality-specific columns in monkey somatosensory cortex: a correlative anatomical and physiological study. J Neurophysiol 48:545-568.

Kaas J (1991) Plasticity of sensory and motor maps in adult mammals. Ann Rev Neurosci 14:137-168.

Kelly JB, Judge PW, Phillips DP (1986) Representation of the cochlea in primary auditory cortex of the ferret (*Mustela putorius*). Hearing Res 24:111-115.

King AJ, Moore DR (1991) Plasticity of auditory maps in the brain. Trends Neurosci 14:31-37.

Law MI, Zahs KR, Stryker MP (1988) Organization of primary visual cortex (area 17) in the ferret. J Comp Neurol 278:157-180.

LeVay S, Stryker MP (1979) The development of ocular dominance columns in the cat.

Merzenich MM, Kaas JH, Wall JT, Sur M, Nelson RJ, Felleman (1983) Progression of change following median nerve section in the cortical representation of the hand in areas 3b and 1 in adult owl and squirrel monkeys. Neurosci 10:639-665.

Merzenich MM, Recanzone G, Jenkins WM, Allard TT, Nudo RJ (1988) Cortical representational plasticity. In P Rakic and W Singer (eds): Neurobiology of Neocortex. New York: John Wiley and Sons, pp. 41-67.

Metherate R, Weinberger NM (1989) Acetylcholine produces stimulus-specific receptive field alterations in cat auditory cortex. Brain Res 480:372-377.

Middlebrooks JC, Zook JM (1983) Intrinsic organization of the cat's meidal geniculate body identified by projections to binaural response-specific bands in the primary auditory cortex. J Neurosci 3:203-224.

Muller CM, Scheich H (1988) Contribution of GABAergic inhibition to the response characteristics of auditory units in the avian forebrain. J Neurophysiol 59:1673-1689.

Nudo RJ, Jenkins WM, Merzenich MM (1990) Repetitive microstimulation alters the cortical representation of movements in adult rats. Somatosens Motor Res 7:463-483.

Pallas SL, Roe AW, Sur M (1990) Visual projections induced into the auditory pathway of ferrets. I. Novel inputs to primary auditory cortex (A1) from the LP/pulvinar complex and the topography of the MGN-A1 projection. J Comp Neurol 298:50-68.

Purser BD, Whitfield IC (1972) Thalamo-cortical connections and tonotopicity in the cat medial geniculate body. J Physiol 222:161-162.

Rakic P, Williams RW (1986) Thalamic regulation of cortical parcellation: an experimental perturbation of the striate cortex in rhesus monkeys. Soc Neurosci Abstr 12:1499.

Rhoades RW, Fish SE (1983) Bilateral enucleation alters visual callosal but not corticotectal of corticogeniculate projections in hamster. Exp Brain Res 51:451-462.

Roe AW, Garraghty PE, Sur M (1989) The terminal arbors of single on-center and off-center X and Y retinogeniculate axons within the ferret's lateral geniculate nucleus. J Comp Neurol 288:208-242.

Roe AW, Pallas SL, Hahm J, Sur M (1990) A map of visual space induced into primary auditory cortex. Science 250:818-820.

Schmidt JT, Edwards DL (1983) Activity sharpens the map during the regeneration of the retinotectal projection in goldfish. Brain Res 269:29-39.

Schneider GE (1973) Early lesions of superior colliculus: factors affecting the formation of abnormal retinal projections. Brain Behav Evol 8:73-109.

Shamma Sa, Fleshman JW, Wiser PR (1991) Receptive field organization in ferret primary auditory cortex: spectral orientation columns. J Neurophysiol, *submitted.*

Shatz CJ, Stryker MP (1988) Prenatal tetrodotoxin infusion blocks segregation of retinogeniculate afferents. Science 242:87-89.

Sretavan DW, Shatz CJ, Stryker MP (1988) Modification of retinal ganglion cell axon morphology by prenatal infusion of tetrodotoxin. Nature 336:468-471.

Stone J (1965) A quantitative analysis of the distribution of ganglion cells in the cat's retina. J Comp Neurol 124:337-352.

Stryker MP, Harris WA (1986) Binocular impulse blockade prevents the formation of ocular dominance columns in cat visual cortex. J Neurosci 6:2117-2133.

Sur M, Garraghty PE, Roe AW (1988) Experimentally induced projections into auditory thalamus and cortex. Science 242:1437-1441.

Sutter ML, Schreiner CE (1989) Physiology and topography of cells with multipeaked tuning curves in primary auditory cortex. Soc Neurosci Abstr 15:1116.

Tusa RJ, Palmer LA, Rosenquist AC (1978) The retinotopic organization of area 17 (striate cortex) in the cat. J Comp Neurol 177:213-236.

Wassle H, Grunert U, Rohrenbeck J, Boycott BB (1989) Cortical magnification factor and the ganglion cell density of the primate retina. Nature 341:643-646.

Zahs KR, Stryker MP (1985) The projection of the visual field onto the lateral geniculate nucleus of the ferret. J Comp Neurol 241:210-224.

Figure Legends

Fig. 1. A) Summary of thalamocortical topography in normal and rewired ferrets (from Pallas et al., 1990). Following restricted injections of tracer into A1 in a normal ferret (top), rostrocaudally oriented slabs of back-filled cells are seen in the MGv (left). Injection of one tracer in lateral A1 (low frequency representation, Kelly et al., 1986) labels cells in lateral MGv; injection of a second tracer in medial A1 (high frequency representation) labels cells in medial MGv. In rewired ferrets (right), a similar connectivity pattern is seen: injection of two tracers in different mediolateral positions in A1 results in two segregated bands of rostrocaudally oriented label in MGv. In addition, an enhanced projection from LP to A1 is present in the rewired ferrets. B) Mapping schematic of normal visual (top), normal auditory (middle), and rewired ferret MGN-A1 (bottom) thalamocortical connectivity. Top: In the visual pathway, each point on the retina projects in a roughly point-to-point fashion through the LGN to primary visual cortex (V1). Thus, a 2-dimensional map of visual space exists in V1 (indicated schematically by arrows showing the mapping of visual field azimuth and of elevation along orthogonal axes on the cortex. Middle: In the auditory pathway, each point on the cochlea projects, through intermediate relays, to a slab of cells along the isofrequency axis in the MGN. Each isofrequency slab in the MGN projects in highly overlapping fashion to its corresponding isofrequency slab in primary auditory cortex (A1). The cortex thus contains a 1-dimensional map of the cochlea along the variable frequency axis (marked "frequency"). [Within the isofrequency axis in MGN and A1, separate clusters of neurons receive either excitation from both ears (EE neurons) or excitation from the contralateral ear and inhibition from the ipsilateral ear (EI neurons). Each EE (or EI) slab in the MGN projects to all of the EE (or EI) slabs in A1. Bottom: In rewired ferrets, we induce input from the retina, a 2-dimensional sensory surface, into the MGN. MGN-A1 connectivity in rewired ferrets, which is similar to that in

normal ferrets (see A), would predict a topographic map along the frequency dimension, but not along the convergently/divergently mapped isofrequency dimension of A1.

Fig. 2. Mapping data recorded in case F88-24. A) Electrode penetrations were made in A1 of a rewired ferret (shaded region). This region, bounded by the anterior and posterior ectosylvian sulci (AES and PES, respectively), is shown enlarged at right. Penetrations in which visual responses were obtained (n=18) are indicated by dots and identified by letters. Locations of non-visual penetrations (n=9) are marked by X's. Arrows connect penetrations in which receptive fields with similar azimuths were recorded as shown in B. Caudal is up and lateral to right. Open square indicates point from which alternative ideal map was drawn (see text). B) Receptive field locations of visual units recorded in each of the corresponding penetrations (a-r) shown in A. Arrows connect visual units with similar azimuthal representations in a posterior to anterior progression on the cortical surface. Low azimuths map medially and high azimuths laterally; low elevations map posteriorly and high elevations map anteriorly. VM: vertical meridian, HM: horizontal meridian. See text. C) Azimuthal (left) and elevational (right) coordinate of the receptive field location recorded at each penetration site (dots) is indicated by small numbers. Idealized isoazimuthal (left) and isoelevational (right) contours (dotted lines, large bold numbers) were fitted to these points. Other conventions as in A. D) Cortical magnification factors calculated along two lines of isoelevation (-10° and -20°). Magnification factors are fairly constant across a wide range of azimuths as well as across elevations.

Fig. 3. Mapping data recorded in case F88-61. Conventions as in Fig. 9. A) Visual receptive fields were recorded in 18 penetrations (dots, letters) in A1; 13 locations

were not visual responsive (X's). Arrows connect penetrations in which receptive fields with similar azimuths were recorded as shown in B. B) Receptive field locations of visual units recorded in each of the corresponding penetrations (a-r) shown in A. Arrows connect visual units with similar azimuthal representations in a posterior to anterior progression on the cortical surface. Low azimuths map medially and high azimuths laterally. In contrast to map shown in Fig. 9, low elevations tend to map anteriorly and high elevations posteriorly. C) Azimuthal (left) and elevational (right) coordinate of each receptive field location (dots) is indicated (small numbers). Idealized isoazimuthal (left) and isoelevational (right) contours (dotted lines, large bold numbers) were fitted to these points. D) Cortical magnification factors calculated along two lines of isoelevation (0° and -10°). Magnification factors are fairly constant across a wide range of azimuths as well as across elevations.

Fig. 4. Four partial maps. Conventions same as Fig. 2A, B. Increasing azimuths map from medial to lateral in cases F88-34 (A) and F85-76 (B). Decreasing elevations tend to map from posterior to anterior in cases F88-34 (A), F85-76 (B), and F90-38 (C). Open circles in B indicate penetrations in which response to visual flash was recorded, but receptive field could not be localized. D) Possible rotated map. Increasing azimuths map from posterior to anterior and decreasing elevations from medial to lateral. No posterior ectosylvian sulcus was evident in this case. Dotted line represents suggested location of posterior A1 boundary.

Fig. 5. Schematic of visual topography in A1. Receptive fields of visual units (A-D, cf. Chapter 3) recorded at cortical positions in A1 (top) have visual field locations shown (bottom). Central azimuths are represented in medially located isofrequency bands in A1; peripheral azimuths in lateral isofrequency bands. Elevations, although more

variable in topography, map in the orthogonal dimension of A1. (AES: anterior ectosylvian sulcus, PES: posterior ectosylvian sulcus).

Fig. 1

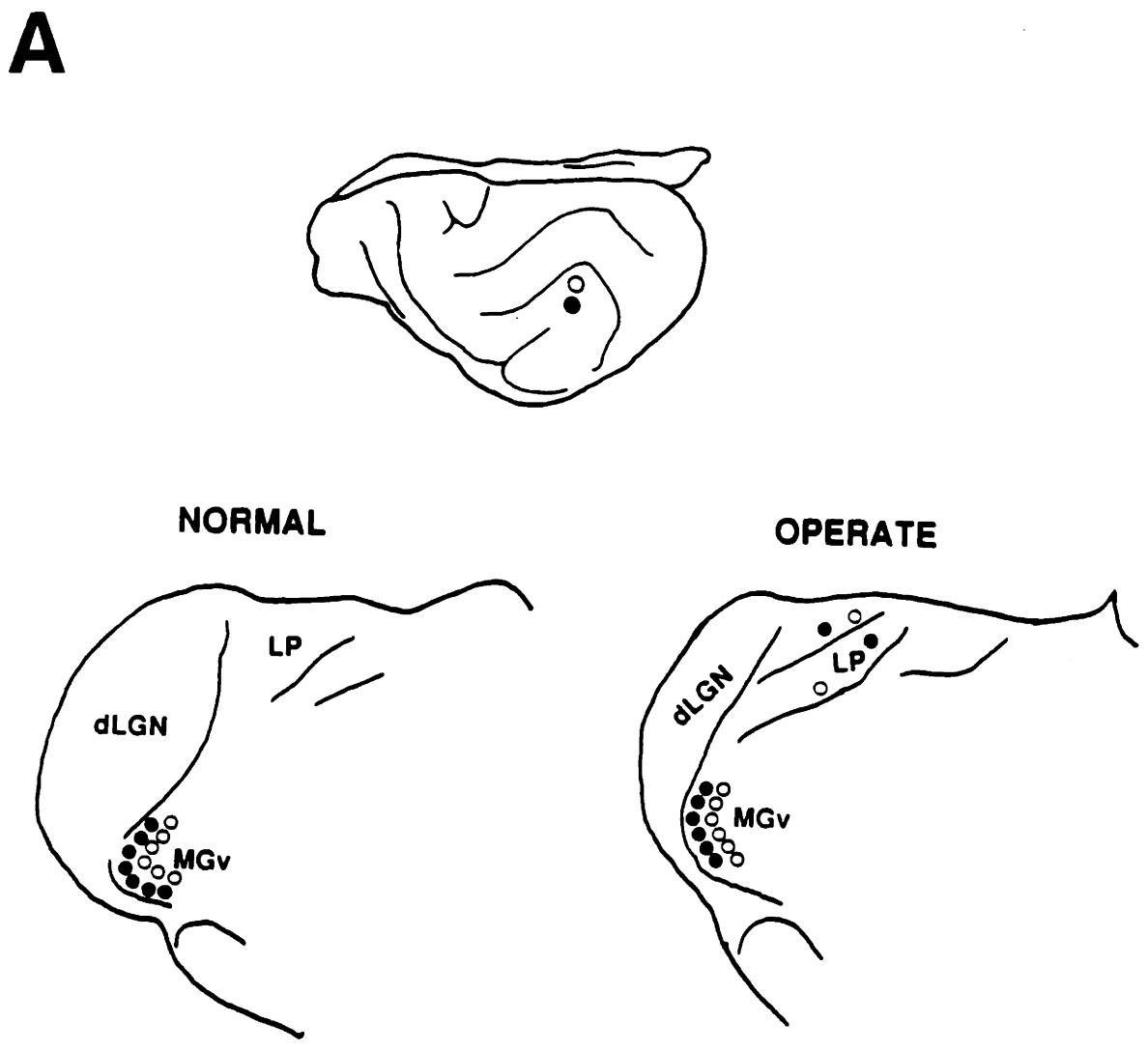

Fig. 1B

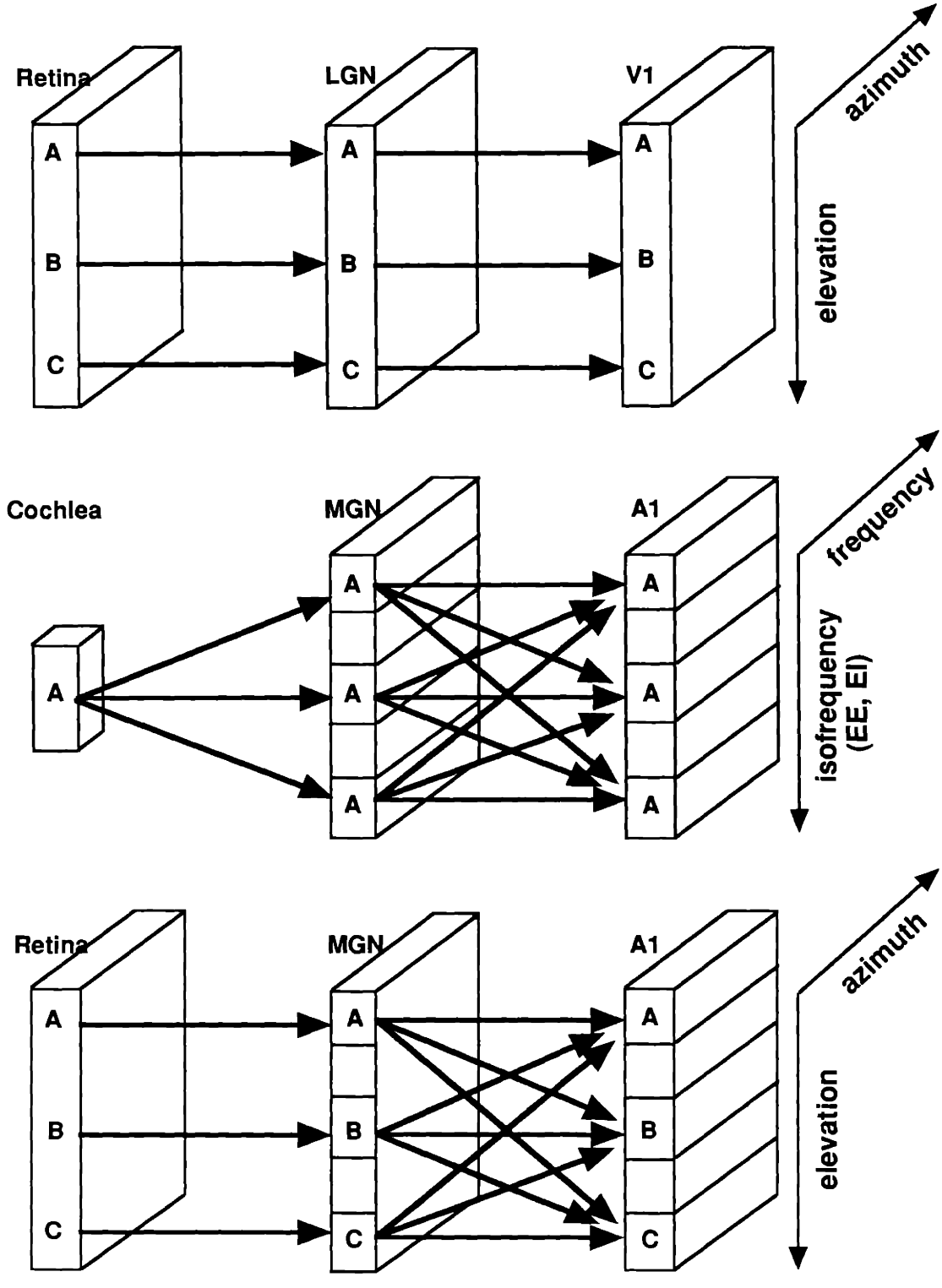
Retina
LGN
V1
A
B
C
azimuth
elevation
Cochlea
MGN
A1
frequency
isofrequency
(EE, EI)
Retina
MGN
A1
azimuth
elevation

Fig. 2

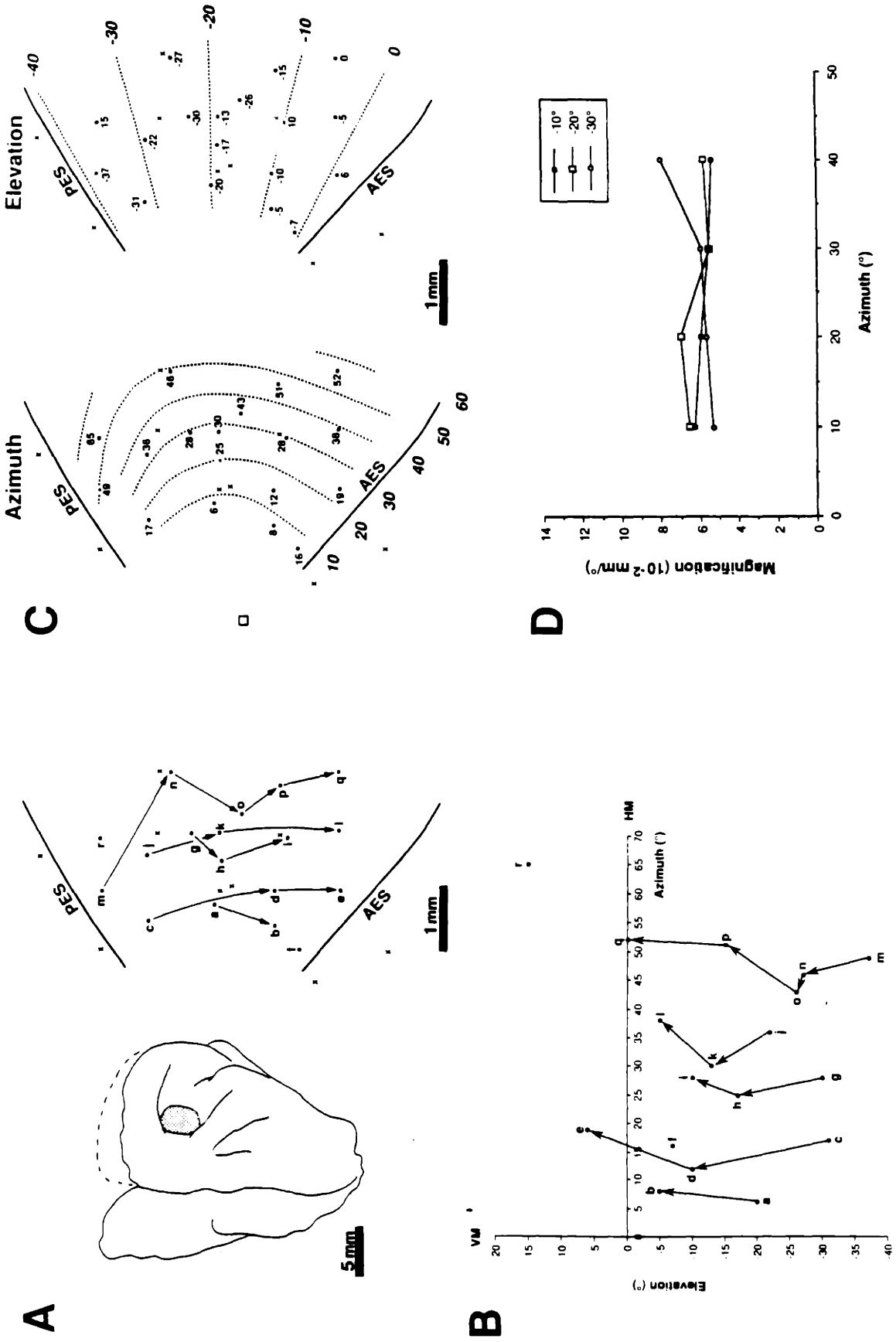
A
pES
AES
5mm
1mm
B
VM
HM
Azimuth (°)
Elevation (°)
C
Elevation
Azimuth
pES
AES
1mm
D
-10°
-20°
-30°
Magnification (10-2 mm/°)
Azimuth (°)

Fig. 3

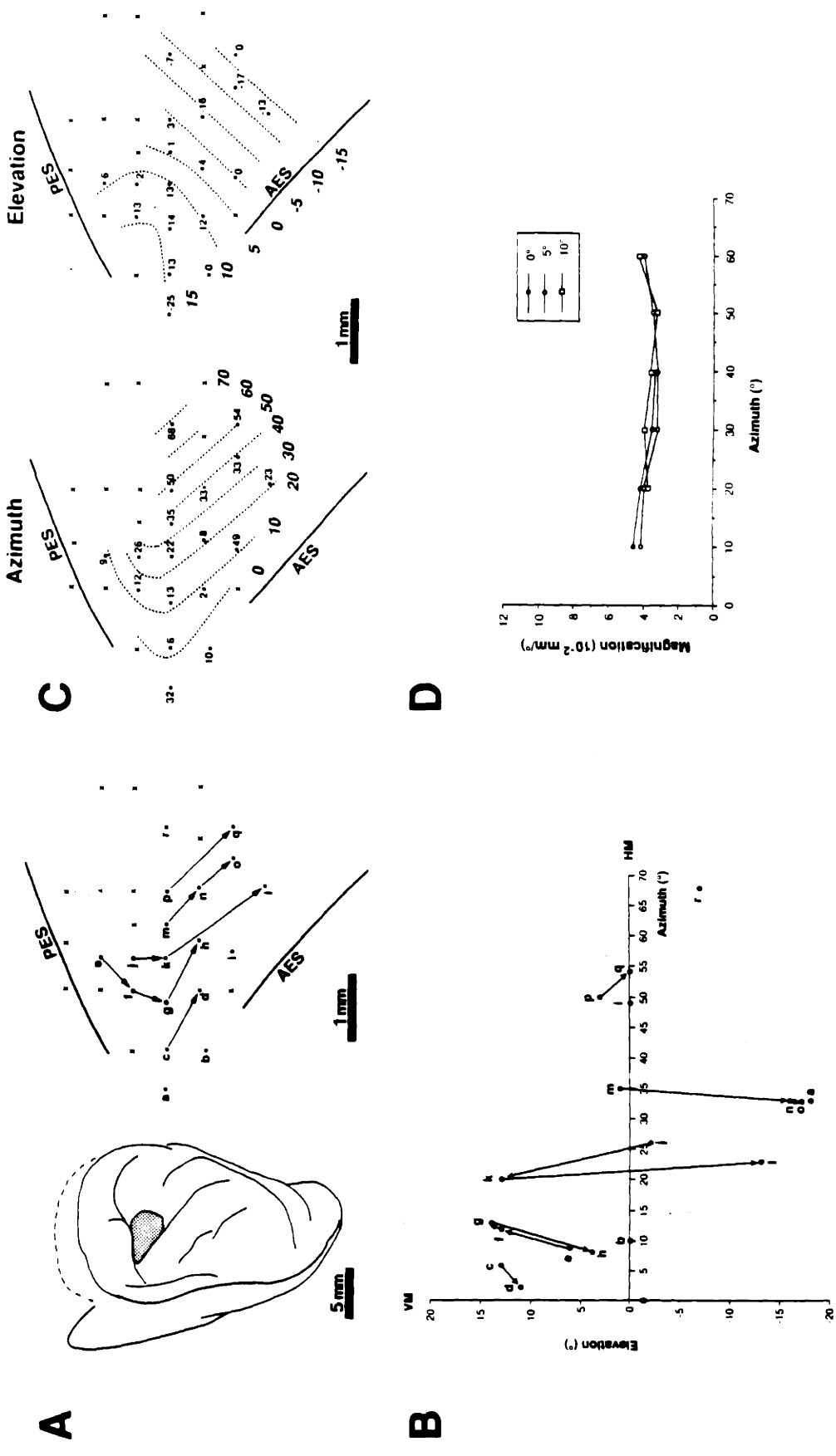
A
B
C
D
PES
AES
1mm
5mm
Elevation
Azimuth
Elevation (°)
Azimuth (°)
Magnification (10⁻² mm/°)
0°
5°
10°

Fig. 4

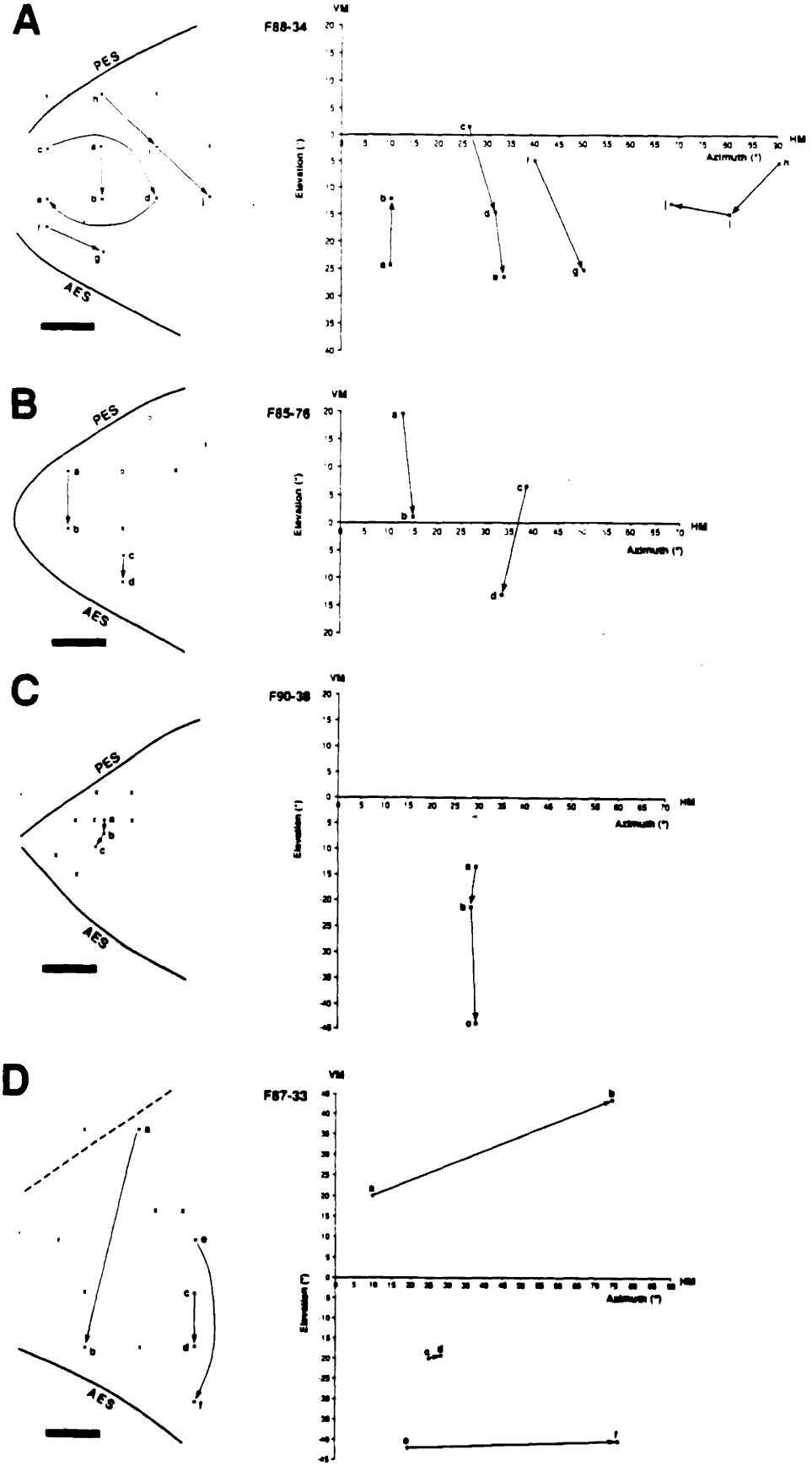
A
PES
AES
F88-34
VM
HM
Azimuth (°)
Elevation (°)
B
PES
AES
F85-76
VM
HM
Azimuth (°)
Elevation (°)
C
PES
AES
F90-38
VM
HM
Azimuth (°)
Elevation (°)
D
AES
F87-33
VM
HM
Azimuth (°)
Elevation (°)

Fig. 5

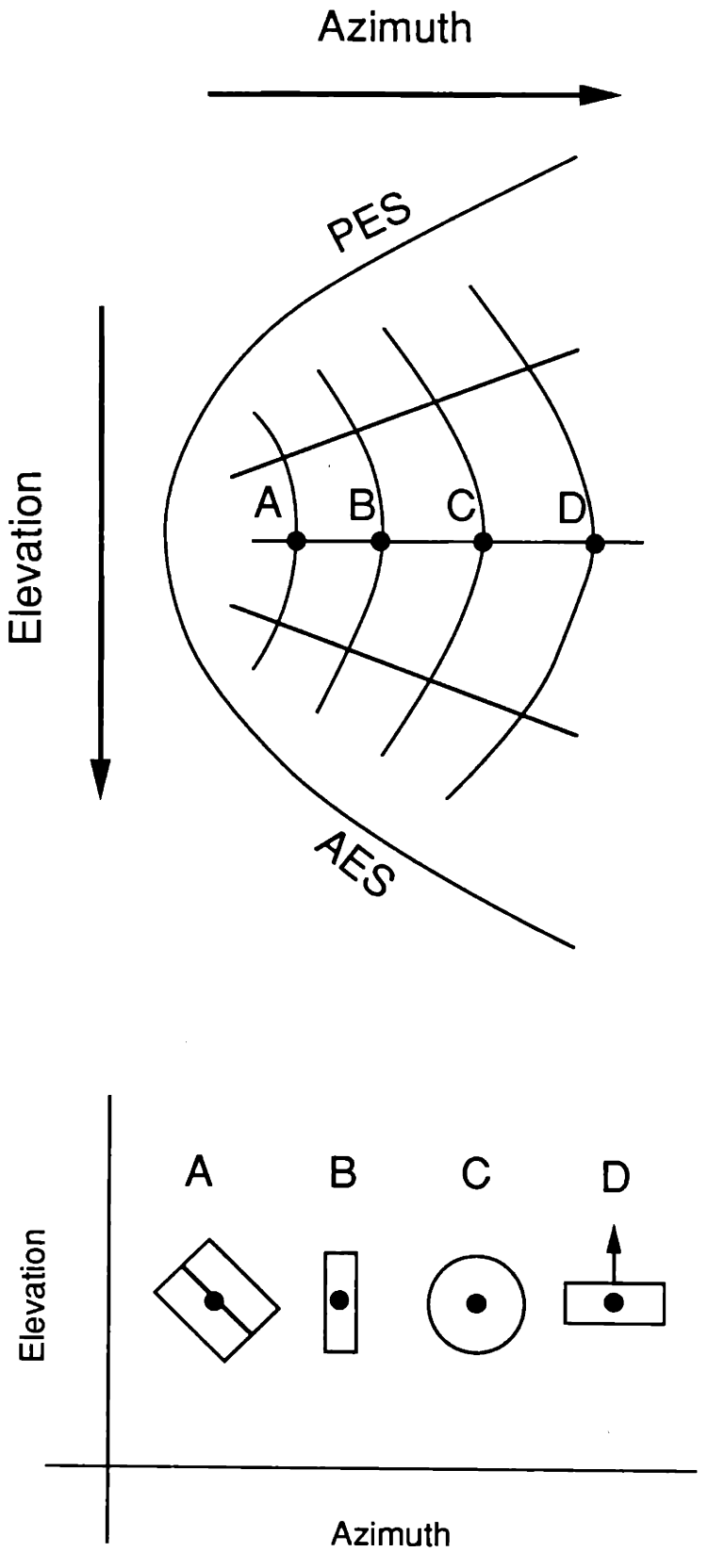

Chapter 3

Visual Projections Routed to the Auditory Pathway in Ferrets: Receptive Fields of Visual Neurons in Primary Auditory Cortex

Abstract

Do sensory cortices of different sensory modalities perform similar functional transformations on their input? One way to address this question is provide two sensory cortices with the same input and observe whether or not their outputs differ. We have used such an approach with an experimental preparation in which retinal input is provided to primary auditory cortex in ferrets. As reported previously, following neonatal surgical manipulations, retinal W cells are able to reroute to auditory thalamus in ferrets and provide visual driving to cells in auditory cortex (Sur et al., 1988). We have now examined the resulting visual response properties of single cells in auditory cortex (A1) and compared them to those in normal visual cortex (V1). Both differences and similarities were observed. Differences (large receptive field size, long latencies to electrical stimulation, and poor responsivity) were related to W type input characteristics. Similarities were related to intracortical circuitry: similar to cells in V1, A1 cells exhibit orientation and direction selectivities and have simple/complex receptive field organizations. Furthermore, the degree of orientation and directional selectivity, as well as the proportions of simple, complex, and non-oriented cells found in A1 and V1 were similar. The similarities in receptive field properties between A1 and V1 argue that certain intracortical circuits may be common to all sensory cortices.

Introduction

In the mammalian central nervous system, many properties of sensory processing are unique and specific to the needs of a particular sensory modality. For example, each sensory pathway receives input from considerably different sensory epithelia and contains different numbers and types of subcortical processing stations. The visual and auditory systems, in particular, exhibit fundamental differences in organization. In the visual system, a two-dimensional map of visual space is transmitted from the retina to primary visual cortex via a single subcortical waystation, the lateral geniculate nucleus (LGN). In the auditory system, primary auditory cortex contains a one-dimensional map of spectral frequency transmitted from the cochlea via multiple subcortical nuclei. In contrast to the point-to-point (i.e., spatial coordinate preserving) connectivity between the LGN and V1, the thalamocortical anatomy between the auditory thalamus (medial geniculate nucleus, MGN) and A1 preserves frequency specificity in one dimension, but is highly convergent and divergent in the orthogonal dimension (Anderson et al., 1980; Middlebrooks and Zook, 1983; Merzenich et al., 1984). Thus, major differences exist between the inputs to visual and auditory cortex, both in terms of anatomical connectivity and in terms of computational strategies (see Discussion Chapter).

At the same time, there are strong parallels in thalamic and cortical organization. When examined at the ultrastructural level, both MGN and LGN contain characteristic triadic arrangements between afferent terminals, inhibitory interneurons, and postsynaptic relay neurons (Guillery, 1969; Morest,1975; Majorossey and Kiss, 1976). Cortical laminae in A1 and V1 are characterized by similar patterns of inputs, outputs, as well as laminar cell type composition (e.g., Jones; Winguth and Winer, 1986; DeFelipe and Jones, 1988). Furthermore, similar intralaminar projection patterns suggest common intracortical synaptic connectivities (e.g., Gilbert and Wiesel, 1979; Mitani and Shimokouchi, 1985). These parallels in anatomical organization may suggest that sensory systems, at least at the thalamic and cortical stages, perform stereotypical transformations on the input they receive. Such

commonalities could underly the [essence] of thalamic and cortical function in sensory processing.

There is as yet no direct *functional* evidence for such common circuitries across sensory domains. It is inherently difficult to compare functional transformations in sensory systems with such vastly different inputs, such as the visual and auditory systems. For example, what would be the functional correlate of "orientation tuning" in the auditory cortex? One way to eliminate the difficulties associated with differences in inputs is to probe two sensory structures with the same type of input.

In this paper, we have taken such an approach to explore possible functional commonalities between two primary cortical regions, primary visual cortex and primary auditory cortex. We have replaced auditory input with visual input in the auditory pathway, and subsequently studied the resulting visual response properties in auditory cortex. We have previously demonstrated that retinal afferents in the ferret can be induced to innervate non-visual thalamic structures, specifically the auditory thalamus (medial geniculate nucleus, MGN). These afferents provide visual driving to cells in primary auditory cortex, A1, of the ferret (Sur et al., 1988) and establish a rough two-dimensional visual topography there (Roe et al., 1990). We now examine both qualitatively and quantitatively the physiological response properties of single visual units in A1 and compare them to those in primary visual cortex (V1) of normal ferrets.

Methods

Rewired Ferrets: Neonatal Surgery to Route Retinal Projections to the MGN

To induce retinal innervation of non-visual thalamic structures, it is necessary to remove normal retinal targets and to make alternative target space available (Schneider, 1973). In this case, we remove or greatly reduce the two major retinal targets (the lateral geniculate nucleus, LGN, and the superior colliculus, SC) and deafferent the auditory thalamus, the medial geniculate nucleus (MGN).

Procedures are similar to those described previously (Pallas et al., 1990). Briefly, timed pregnant pigmented ferret jills were bred in our colony or purchased from a commercial supplier (Marshall Farms). Within 24 hours of parturition, ferret kits were removed and anesthetized by deep hypothermia. All surgery was performed under sterile conditions. A 1 cm midline incision was made in the scalp and the skull exposed. After removing a small piece of overlying skull, the SC was ablated by heat cautery. To induce massive retrograde degeneration of the LGN, large regions of visual cortex (including Areas 17, 18, and often 19) were lesioned by cauterizing through the skull. Fibers running in the brachium of the inferior colliculus were transected at the mid-SC level, thereby denervating the MGN. All lesions were made unilaterally (bilateral lesions significantly reduced survival rates). On completion of surgery, the skin was sutured and the kit revived under a heat lamp. A single dose of antibiotic (0.01 cc amoxycillin, 100 mg/ml) was given subcutaneously and antibacterial ointment was applied to the wound. The kit was then returned to the mother for rearing.

These lesions result in induction of developing retinal afferents into the MGN (Sur et al., 1988). Since the normal thalamocortical connectivity from the MGN to primary auditory cortex (A1) is retained (Pallas et al., 1990), an aberrant visual pathway from the retina to MGN to A1 is established by adulthood (Sur et al., 1988).

Visual Physiology in Adult Ferrets

Surgical Preparation

Normal and rewired adult ferrets were prepared for visual physiology with procedures similar to those described previously (Roe et al., 1988). Animals were anesthetized, paralyzed, and respirated. Following induction of anesthesia with ketamine hydrochloride (30 mg/kg) and xylazine (2 mg/kg), a cannula (24g) for anesthetic and paralytic delivery was implanted in either the femoral or the jugular vein, and an endotracheotomy was performed. Animals were then placed in a stereotaxic apparatus, paralyzed, and artificially respired (rate 30-40/min, volume 25-30cc) with a 70/30 mixture of nitrous oxide/oxygen. Ferrets received a constant intravenous infusion of a 5% dextrose solution containing ketamine hydrochloride (10 mg/kg/hr) for anesthesia and gallamine hydrochloride (3.6 mg/hr/kg) for muscular paralysis. End-tidal CO_2 was maintained at 4.0%, heart rate monitored, and body temperature maintained at 38°C with a heating pad. Supplemental halothane (1%) was supplied during all surgical procedures. The skull and dura overlying visual cortex in normal animals and auditory cortex in lesioned animals were removed. Stimulating electrodes were lowered into the optic chiasm and cemented in place. Drops of atropine sulfate and phenylephrine hydrochloride were applied to the eyes to dilate the pupils. Eyes were fitted with zero power contact lens and focussed on a tangent screen 114 cm in front of the animal. Optic disks were plotted by reflection onto the tangent screen, and locations of receptiv fields inferred therefrom.

Recording and Data Collection

In 18 lesioned and 13 normal adult ferrets, we used parylene insulated tungsten microelectrodes (2-3 megaohm impedances) to record extracellularly from cells in A1 of lesioned and V1 of normal animals. Recording penetrations were made in A1 and V1 on the basis of sulcal patterns (Kelly et al., 1986, Law et al., 1988). In lesioned ferrets, penetrations were placed between the anterior and posterior limbs of the ectosylvian sulcus

(Kelly et al., 1986) and in normal ferrets, in the caudal half of the lateral sulcus (Law et al., 1988). Penetrations were usually spaced 250-500 μm apart. Unit activity was assessed every 50-100 μm in each penetration for 1) response to electrical stimulation of the optic chiasm and 2) response to visual stimulation. In two lesioned animals and one normal animal, broad-band auditory stimuli (clicks or white noise) were delivered through earphones. Visually responsive units were plotted and characterized on the tangent screen with a hand-held projection lamp. In addition to receptive field location and size, a number of other response characteristics were also examined. These included ocular dominance, orientation, direction, and velocity selectivities, spatial organization of 'on' and 'off' responses, presence or absence of summation and end-stopping, and strength of response. When possible, oriented cells were classified as simple or complex (Hubel and Wiesel, 1962). Electrolytic lesions (5μA for 5 sec) were placed at the bottom of selected penetrations.

The tuning characteristics of a subset of these units were studied quantitatively. For quantitative determination of orientation, direction, and velocity tuning preferences, moving bar stimuli, either projected with an optic bench or generated on a Tektronix monitor driven by a "Picasso" stimulus generator, were swept at different orientations (usually at 30° intervals) and velocities (from 5°/s to 100°/s) over the receptive field. Spike responses of the cell under study were isolated with a pulse-shape discriminator (Ealing). For each category of stimulus, 15 cycles of response were collected and summed by the Unkelscope Program run on an IBM PC 286 computer and post-stimulus time (PST) histograms generated on-line. Spike responses were also stored on tape and PST histograms analyzed off-line. Background activity was collected in the absence of visual stimulation.

Histology

Following the completion of data collection, the animal was sacrificed with an intravenous or intraperitoneal overdose of pentobarbital (65 mg/kg) and perfused through the heart with saline followed by fixative (1% paraformaldehyde, 2% glutaraldehyde) and 10%

and 20% sucrose solutions. The brain was then removed from the cranium and stored in 30% sucrose overnight. After brain sulcal patterns were recorded photographically, frozen sections were cut at 50 μm and stained with cresyl violet. Lesions and recording tracks were identified and located with respect to the borders of A1.

Data Analysis

For each cell that was studied quantitatively, peak response minus background was calculated for every stimulus condition. From these, orientation, velocity, and bar size tuning curves were plotted and selectivity indices calculated. The orientation index was defined as 1 - (Orthogonal response/Best response) and the direction selectivity index defined as 1 - (Non-preferred direction response/Preferred direction response). These are normalized indices, with 1.0 indicating a highly selective and 0 a non-selective cell. In addition, orientation widths were determined at $1/\sqrt{2}$ height (cf. Schiller et al., 1976b). Unless otherwise specified, statistical tests employed the Mann-Whitney U test (MW-U).

Results

As we have reportedly previously, cells recorded in A1 of rewired ferrets are responsive to visual stimuli (Sur et al., 1988; Roe et al., 1990). We have now studied in detail the response properties of visual cells in A1 of lesioned ferrets and compared them to visual response properties in V1 of normal adult ferrets.

Four-hundred and ninety-five visual units were recorded from A1 of lesioned ferrets and 153 visual units from V1 of normal ferrets (see Table 1). Nearly all cells responded to electrical stimulation of the optic chiasm. 194 (39%) of the cells in A1 and 105 (69%) of the cells in V1 had receptive fields that could be clearly localized and plotted on the tangent screen. While only a subset of the electrically driven cells were driven visually, nearly every visually driven cell could be driven by electrical stimulation of the optic chiasm. Almost all visually responsive units (95% in A1, 93% in V1) were driven by chiasm stimulation as well. As will be described below, a subset of these visual cells were further characterised and their responses studied quantitatively (see Table 1). Of the units that were tested for auditory responsiveness (n=35 in A1 of two lesioned ferrets, n=22 in V1 of one normal ferret), none responded either to clicks or to white noise. These same auditory stimuli produced robust responses in normal primary auditory cortex (n=37 in one normal ferret).

We have not attempted to conduct a laminar analysis of our data. However, we can ascertain that visual units were recorded throughout cortical layers in both A1 and V1 (Fig. 1). Our recording depths in both A1 and V1 ranged from 0-2000 μm with the majority of cells (91% of all cells in A1, 80% of all cells in V1) recorded from the superficial 1000 μm. Histological reconstruction revealed that electrode tracts in A1 were oriented approximately 30-45° from surface normal. At these angles, a recording depth of 2000 μm in A1 corresponds to cortical depths ranging between 1000 μm (45° angle) and 1414 μm (30° angle). Therefore, cells were recorded throughout the ≈1 mm thickness of ferret A1, with a large majority recorded in the superficial 500-707 μm. Electrode penetrations in V1 ranged from 0-

90° (due to folding back of lateral sulcus) and in almost all cases traversed the entire cortical thickness.

Differences Between Response Features of Cells in A1 and V1

There were three major differences between the characteristics of visual units in A1 and V1: responsivity, receptive field size, and latency to optic chiasm stimulation. As will be discussed later, these differences arise primarily from the properties of retinal and thalamic input to A1 and V1.

Responsivity

The first salient difference between visual units in A1 and V1 was their responsiveness to visual stimulation. Most cells in V1 responded in robust and consistent fashion to visual stimuli. In contrast, cells in A1 were much more difficult to drive, exhibited labile responses, and responded with fewer spikes. These cells were qualitatively rated during recordings on a 4-point scale where 1 indicates poor responsiveness and 4 good responsiveness. This index reflects both robustness (qualitative determination of response strength, i.e. number of spikes) as well as reliability of response. (Units that were driven only by electrical stimulation were not rated. 38 A1 cells recorded in early experiments also were not rated.) Of 105 V1 cells and 156 A1 cells that were rated, 93% of units in V1 were rated 4 and 68% of units in A1 were rated 1 (Fig. 2).

Other observations may also be explained, at least in part, by the poorer responsivity of A1 units. Whereas 69% (105/153) of V1 units had receptive fields that could be readily localized, only 39% (192/495) of the receptive fields in A1 were locatable (see Table 1). Two of the units in A1 were visually responsive only to very strong stimuli, such as on/off flashes at the eye or to turning on and off of room lights. Only half of the visual cells in A1 (100/194)

responded sufficiently well to flashing or moving bars of light so that receptive field borders could be reliably determined (Table 1). For the same reason, other receptive field characteristics were also difficult and time-consuming to determine (see below).

Receptive Field Size

A second prominent difference between A1 and V1 cells is the size of their receptive fields. Receptive field sizes (calculated as the average of the length and width of the receptive field) of visual cells in A1 are significantly larger than those of V1 cells, their mean diameter (mean = 10.9°, n=87) reaching almost 3 times that of V1 cells (mean = 3.9°, n=102) (Fig. 3A). 64% of the cells in A1 had receptive fields larger than the largest receptive fields recorded in V1. In addition, 13% of cells in A1 had receptive fields that were large (15-30° in diameter) and whose borders were difficult to determine precisely (Fig. 3A: large, diffuse).

The difference in the receptive fields sizes are not eccentricity related. While the distribution of receptive field eccentricities recorded in A1 and V1 is significantly different ($p < .0001$) (Fig. 3B), receptive field sizes in A1 are still larger when eccentricity-matched populations are compared (Fig. 3C). This was also true for eccentricity-matched samples below 15° (A1, n=18; V1, n=53; Mann Whitney-U, $p < .0001$) and below 45° (A1, n=78; V1, n=101; Mann Whitney-U, $p < .0001$).

Latency

Cells in A1 and V1 also differ in their latencies to optic chiasm stimulation. When the latencies of all cells in A1 and V1 are compared (Fig. 4A), those recorded in A1 (mean = 6.8 msec) are significantly longer than those in V1 (mean = 4.4 msec). In both A1 (Fig. 4B) and V1 (Fig. 4C), the latencies recorded for the subpopulation of visually responsive cells (A1, n=194; V1, n=77) were representative of all units recorded. Thus, the large proportion of long latencies recorded in A1 cannot be attributed solely to the greater proportion of cells with

poor visual responsiveness. There were no correlations between cortical depth and latency, receptive field size, or responsivity.

Similarities Between Cells in A1 and V1: Tuning Characteristics

Of the visual cells recorded in A1 of rewired ferrets, a portion were sufficiently responsive to allow further characterizations, including determination of cell class, ocular dominance, and orientation, direction, and velocity selectivities. As mentioned previously, reliably responding visual cells were much more frequently encountered in V1 than in A1; this difference is illustrated by the higher percentage of cells in V1 (25%, n=38) than in A1 (5%, n=24) whose responses were quantified.

Ocular Dominance

To determine a cell's ocular dominance (OD), we compared (with an audio monitor) the ipsilateral and the contralateral monocular responses to visual stimulation of its receptive field. We subsequently rated the cell on a scale from 1-7, with 1 indicating complete contralateral dominance, 7 complete ipsilateral dominance, and 4 equal dominance by the two eyes (Hubel and Wiesel, 1962). In V1, we recorded predominantly contralaterally dominated cells (Fig. 5): 65% of all units tested exhibited complete contralateral dominance (OD group 1) and only 10% exhibited an ipsilateral dominance (OD groups 5, 6, or 7). [A few cells (n=3) to which we did not give an ocular dominance rating were not responsive to monocular stimulation but exhibited noticeably enhanced responses to binocular stimulation.] This significantly heavier contralateral representation in the mustelid visual cortex has been previously reported and is due both to its extensive monocular segment as well as a true contralateral bias in its binocular segment (LeVay et al., 1987; Law et al., 1988; Zahs and Stryker, 1988; Redies et al., 1990).

In A1, a similar ocular dominance distribution was seen: 66% of the visual cells rated were completely contralaterally dominated (OD 1) and 7% exhibited ipsilateral preference (OD 5, 6, or 7). Approximately 30% of units recorded in both A1 and V1 are binocular (OD 2-6). These two ocular dominance distributions are not significantly different [$\chi^2(.95) = 4.6$, df = 6].

Cells recorded in A1 and V1 with any ipsilateral contribution had receptive fields in the binocular segment. The receptive fields of 5 cells in V1 (1 contralaterally, 2 ipsilaterally, 2 binocularly driven) and 5 cells in A1 (all contralaterally driven) fell in the ipsilateral hemifield. This may be a reflection of inappropriate location of some retinal ganglion cells with respect to the nasotemporal division in the ferret retina (Vitek et al., 1985).

Receptive Field Types

V1 Cells. Receptive fields of cells in V1 of normal ferrets were classified as simple or complex, if oriented, or as non-oriented, and in general resembled those described previously in cats (Hubel and Wiesel, 1962) and ferrets (Zahs and Stryker, 1988; Law et al., 1988). Most simple cells (n=20) exhibited two or three spatially segregated contrast-specific subfields, responding to either onset or offset of optimally oriented flashing bars and/or to moving light or dark contrast edges of optimal orientation. Responses within a single subfield exhibited spatial summation to flashing bars of increasing size. Some cells which we classified as simple (n=4) exhibited spatial summation but had only a single on or off region (Zahs and Stryker, 1988; cf. Palmer and Davis, 1981 and Schiller et al., 1976a). Complex cells (n=50) had only a single oriented response field to flashing bars or moving contrast edges of the appropriate orientation and typically responded both to the onset and offset of light and/or to edges of either light or dark contrast. Complex cells typically were equally responsive to small as well as large bars within their receptive fields. Two cells which we classified as complex responded only to very small moving or flashing oriented bars within their receptive fields and were silenced by bars illuminating the entire receptive field. These

cells may correspond to "special complex" cells described in previous studies (Gilbert, 1977; Palmer and Rosenquist, 1974). End-inhibition was seen in both simple (n=8) and complex cells (n=10). Non-oriented cells (n=27) had either circular or elongated receptive fields with weak or absent inhibitory surrounds.

There appears to be a true species difference between ferret and cat visual cortex in terms of the prevalence of non-oriented cells. While cat (Hubel and Wiesel, 1962) and mink (LeVay et al., 1987) visual cortex lack non-oriented cells, approximately one quarter of cells recorded in ferret V1 are non-oriented. A previous study of receptive fields in ferret V1 reported only that "most single neurons...were orientation-selective" (Law et al., 1988). It is unlikely that our findings represent recordings from geniculocortical afferents since 1) afferents were recognized by their higher level of spike activity, 2) geniculate neurons do not have elongated receptive fields (Esguerra et al., 1986; Price and Morgan, 1987), 3) non-oriented units were recorded at all depths, and 4) some of the non-oriented units were recorded for considerable periods of time during quantitative characterization (see below). While it is possible that some of the recording sites were influenced by multi-unit activity, the presence of orientation selectivity would still be detected at such sites since visual cortical cells within a single columnar locale share similar orientation selectivities (LeVay et al., 1987; Law et al., 1988; Redies et al., 1990).

A1 Cells. In A1, as mentioned above, receptive fields were larger. In general, receptive field organization was more difficult to determine due to weakness and lability of response. Despite this, similar receptive field structures were observed. We were able to classify approximately one-half (52/100) of the cells in A1 as simple, complex, or non-oriented. Similar to those in V1, simple cells in A1 (n=16) displayed orientation selectivity and had one (n=4), two (n=6), or three (n=4) spatially segregated subfields. Borders between subfields were not as sharp as those in V1, but were nonetheless clearly present. Complex cells (n=24) were oriented, exhibited either on, off, or on/off responses throughout their receptive fields, and responded equally well to small and large bars. End-stopping was seen

in 1 simple and 5 complex cells. In one case (simple cell), the degree of end-inhibition was quite dramatic: extending a light bar by 10% beyond the receptive field border reduced the cell's response by 50%. Non-oriented receptive fields (n=12) were either circular or elongated with weak or absent inhibitory surrounds.

Relative proportions

Not only do simple, complex, and non-oriented cell types occur in A1, they also occur in proportions similar to that found in V1. In both the A1 and the V1 populations recorded, approximately 50% of the cells were complex, 25% simple, and 25% non-oriented (Fig. 6). While we do not claim that these figures reflect actual cell class composition in A1 and V1, at no time did we attempt to "find" cells of any particular class. Our sampling was based solely on units with appropriate strength and consistency of response. We found no statistically significant correlations, in either A1 or V1, between receptive field type and receptive field size, latency to optic chiasm stimulation, or depth. Neither were there any correlations between cell type and orientation, direction, or velocity selectivities.

Tuning Characteristics of Single Units in A1 and V1

To determine orientation tuning, we first examined responses to flashing bars at various orientations. For cells not responsive to standing flashes, we made a qualitative assessment of orientation selectivity with moving or "jiggling" bars or moving edges. We also tested for response to moving spots; however, moving spots were generally not an effective stimulus. For quantitative determination of orientation selectivities, moving bars were used as stimuli. In almost all cases, the quantitative characterization of the optimal orientation agreed with our qualitative assessments. For some cells in A1, quantitative collection of multiple stimulus sweeps revealed orientation tuning not obvious from responses to single sweeps assessed by ear.

An example of an orientation selective cell in V1 is shown in Fig. 7A. This cell is a simple cell and responds optimally to a bar oriented at -45° from vertical, sweeping in either direction. A second example is shown in Fig. 7B. This complex cell prefers bars oriented at +45° from vertical and is slightly directional for upwards movement.

Cells in A1 were also characterised similarly. Fig. 8A illustrates the orientation selectivity of a non-directional simple cell in A1 that preferred horizontally oriented bars. A directionally selective simple cell is shown in Fig. 8B. This cell responds best to downward sweeping bars oriented 30° from vertical. As can be seen from these plots, cells in A1 respond with fewer spikes overall than those in V1 and their responses are modulated less strongly above background levels.

Orientation Tuning

The orientation tuning of 38 cells in V1 and 24 cells in A1 was studied quantitatively. For each of these cells, two measures of orientation tuning were calculated: orientation selectivity and orientation tuning width. The orientation selectivity index is defined as: 1 - (Orthogonal response/Best response) (cf. Felleman and Van Essen, 1987). A cell whose response in the best orientation is twice the level of that in the orthogonal orientation would have an orientation selectivity index of 0.5; one whose best response in 1.5 times that in the orthogonal orientation would have an index of 0.33. Therefore, we consider those units with indices below 0.3 to be unoriented, those with indices from 0.3-0.5 to be broadly oriented, and those with indices above 0.5 to be sharply oriented. Both A1 and V1 contained cells exhibiting a range of orientation tuning indices, ranging from unoriented to sharply oriented. In fact, no significant difference was seen in the proportions of cells with low, broad, or sharp orientation tuning characteristics of cells in A1 and V1 (Fig. 9A). Approximately 40% of units in A1 (3 simple, 6 complex) and V1 (6 simple, 8 complex) were sharply oriented (index > 0.5); 33% of units in A1 (5 simple, 3 complex) and 26% in V1 (3 simple, 7 complex) were broadly oriented (index 0.3 - 0.5).

Orientation tuning widths (defined as the width of the orientation tuning curve at $1/\sqrt{2}$ peak height) were also determined. For both A1 and V1 cells, orientation tuning widths ranged from narrow tuning (< 30°) to very broad tuning (> 90°) (Fig. 9B). While a greater percentage of cells in V1 than in A1 had tuning widths of 30° - 59°, these distributions were not significantly different. Thus, neither measure of orientation tuning reveals any quantitative difference between A1 and V1 with respect to orientation tuning.

Direction Selectivity

A directionality index was calculated from the responses obtained at the preferred orientation of each cell; this index was defined as: 1 - (Non-preferred/Preferred response). The frequency distribution of these indices in A1 and V1 also proved to be similar (Fig. 10). Interestingly, V1 contained a higher proportion (40%) of non-directional (directionality index < 0.3) cells than A1 (21%). A1 also contained a greater proportion (25%) of highly directional cells (index > 0.6) than V1 (15%). These two distributions were not significantly different (Mann Whitney-U, $0.5 < p < 0.1$). No relationship was seen between cell class and directionality in either A1 or V1: directionality indices for each of the simple, complex, and non-oriented cells classes ranged from non-directional to highly directional.

Velocity Selectivity

One of the more unexpected findings from this study was that the velocity tuning preferences of cells in A1 were similar to those of cells in V1. The velocity selectivity of each cell was studied by collecting responses to optimally oriented light stimuli swept at several velocities, generally between 5°/s and 100°/s, over its receptive field. 29 V1 cells (9 simple, 11 complex, and 9 non-oriented) and 18 A1 cells (6 simple, 9 complex, and 3 non-oriented) were studied in this fashion. The stimulus orientation chosen for non-oriented cells was arbitrary.

Examples of velocity tuning preferences are shown in Fig. 11A (A1, right column; V1, left column) and are similar to those previously described in cat visual cortex (e.g. Orban et al., 1981). Most cells were tuned to either slow (< 15°/s, curves 1 and 2), medium (15-50°/s, curve 3), or fast (> 50°/s, curve 4) velocities. A few of these exhibited velocity high-pass or low-pass characteristics (curve 5). We recorded a few cells that responded equally well to slow and to fast stimulus velocities but not to medium velocities (curve 6). Cells exhibiting broad selectivities were also encountered (curve 7). Thus, both A1 and V1 exhibit a range of velocity tuning preferences. Furthermore, these tuning preferences are found in similar proportions in these two areas. Approximately 45% of the cells recorded in A1 and V1 are tuned to slow, 35% to medium, and less than 10% to fast velocities (Fig. 11B). No consistent relationship was seen between velocity tuning preference and cell type.

Discussion

We have reported previously that retinal projections can be induced to innervate auditory thalamus in ferrets following specific neonatal lesions and that these projections provide visual driving to cells in primary auditory cortex (A1) of these lesioned ferrets (Sur et al., 1988; Pallas et al., 1990; Roe et al., 1990) . We now report on the detailed receptive field properties of these visual cells in A1 and compare them to those of visual cells recorded in primary visual cortex (V1) of normal ferrets. We consider the comparison between A1 and V1 appropriate in that both areas, being the major direct cortical recipient of visual thalamic input, are "primary visual cortices".

Three main differences emerge between visual cells in A1 and V1. In comparison to visual cells in V1, those in A1 are more poorly responsive to visual stimulation, have longer latencies to electrical stimulation of the optic chiasm, and have larger receptive field sizes. We suggest that these differences result primarily from characteristics of the retinal and thalamic input to each of these cortices (see discussion below).

The most striking result of this study is that the reponse properties of at least the most visually responsive cells in A1 bear strong resemblances to those in V1. A1, like V1, contains cells that are orientation- and direction-selective. In addition, the distribution of quantitatively assessed orientation selectivities recorded in A1 and V1 are similar. Simple and complex cells, some of which were end-stopped, were found in both A1 and V1. Moreover, similar proportions of simple, complex, or non-oriented cells were recorded in A1 and V1. Both A1 and V1 contain contralaterally biased ocular dominance distributions. Finally, there were no qualitative or significant quantitative differences in direction or velocity selectivities. These similarities between visual response properties in A1 and V1 directs some of our discussion (see below) towards underlying parallels in intracortical circuitry across sensory modalities.

Sources of Visual Input to A1 in Lesioned Ferrets

It is important to consider at the outset what the sources of visual input to A1 are in rewired ferrets. It is possible, for example, that there are novel cortico-cortical projections to A1 in lesioned animals that arise from unlesioned visual cortical areas, and that the features of visual integration (such as orientation selectivity, direction selectivity, and binocularity) that we ascribe to processing within A1 are already present in these cortical inputs.

The issue has been addressed by making injections of retrograde tracers into A1 in rewired ferrets, and comparing the cortical and thalamic inputs with those to A1 in normal ferrets (Pallas et al., 1988; Pallas et al., 1990). In brief, the cortical areas that project to A1 in lesioned animals are the same areas that project to A1 in normal animals, and do not include any visual cortical areas.

The overwhelming proportion of thalamic input to A1 in rewired animals arises from the MGN (Pallas et al., 1990). In addition, a sparse input arises from the LP/Pulvinar complex to A1 in rewired ferrets (Pallas et a., 1990). However, it is unlikely that these projections contribute to the visual responses of A1 neurons: 1) the projections are much sparser than the projections from the MGN and 2) they arise from cells that lie deep within the LP/Pulvinar region and that show almost no overlap with retinal projections in these animals.

Contribution of Inputs to Response Properties in A1

We have found that visual cells in A1 are poorly responsive, have large receptive field sizes, and long latencies to optic chiasm stimulation. These characteristics are already present in and can be predicted by the retinal and thalamic input to A1. We have shown previously that the auditory thalamus in rewired ferrets receives retinal ganglion cell input of the W cell type (Chapter 1; Sur et al., 1988; Pallas et al., 1989). Retinal W cells have "sluggish" responsiveness to visual stimuli and are characterized by large, often diffuse, receptive fields,

some of which have center-surround organization but many of which do not (Wilson et al., 1976; Fukuda et al., 1984; Stanford, 1987). Similar receptive field properties are found in postsynaptic visual cells in the MGN in rewired ferrets (Sur et al., 1988). Large receptive field sizes of A1 cells may be due to both the W cells that form the retinal source of inputs and to the pattern of highly convergent and divergent thalamocortical connectivity typical of the auditory system and shown to be retained in these rewired ferrets (Pallas et al., 1990; cf. Anderson et al., 1980; Middlebrooks and Zook, 1983). Poor responsivity of cells in A1 is consistent with its W type input. In addition, we cannot rule out abnormal synaptic configurations of retinal axons on MGN cells or additional inhibitory mechanisms within MGN or A1 that decrease the responsiveness of MGN and A1 cells in lesioned animals.

Retinal W cells also have slowly conducting, poorly myelinated axons (Cleland and Levick, 1974ab) and predict the relatively long latencies to optic chiasm stimulation found both in the MGN (Sur et al., 1988) and in A1. Some of the latencies to optic chiasm stimulation in A1 are quite long (>10 msec). In Area 19 of normal adult cats, a cortical region which receives primarily W input via the C laminae of the LGN, the longest latencies reported do not exceed 8 msec (Kimura et al., 1980). One possible source of this discrepancy may lie in the relative heterogeneity of the W cell class. Tonic W cells have medium sized somata, and project to the C laminae of the LGN ; phasic W cells have small somata, finer and slower conducting axons, and project predominantly to the superficial layers of the superior colliculus (Berson, 1987; Stanford, 1987). Our evidence indicates that the W cell population providing input to A1 is comprised of cells from both the larger W1 as well as the smaller W2 cell population (Roe et al., 1987). Thus, some of the longest latencies recorded in A1 may arise from the more slowly conducting W2 population that do not project to Area 19 via the LGN in normal animals.

Intracortical Mechanisms in A1 and V1

We find a high degree of similarity between response properties in A1 and those in V1. Single cells in A1 exhibit receptive field organizations, orientation selectivities, direction selectivities, and velocity preferences quite similar to those found in V1 cells. Furthermore, A1 and V1 contain similar proportions of cells with simple, complex, and non-oriented receptive field. These findings are somewhat surprising in view of the fact that A1 and V1 receive significantly different types of input from the retina.

V1 in normal cats and ferrets is dominated by X and Y inputs from the retina relayed through the LGN. Previous studies devoted to examining the contribution of X and Y inputs to receptive field properties of simple and complex cells in primary visual cortex have shown that neither the simple nor the complex cell classes are exclusively X- or Y-driven (Ferster 1990ab; Malpeli, 1983; Malpeli et al., 1981; Mullikin et al., 1984; Tanaka, 1983). The results of this study demonstrate 1) that X and Y input are not necessary for and 2) that W cell input is sufficient for the generation of simple/complex receptive field types. We argue that these properties are, therefore, not dependent on input cell type (i.e., X, Y, or W), but are generated via intracortical circuitries activated by a minimum of visual input.

Similarly, the generation of other receptive field properties such as tuning for orientation and direction is likely to be intracortically mediated. Visual cells in the MGN have circular or elongated receptive fields with weak or absent inhibitory surrounds and lack orientation selectivity (Sur et al., 1988; Chapter 1). Thus, it is unlikely that orientation tuning properties of A1 cells arise from properties already present at either the retinal or MGN level. The finding that slightly, but not significantly (MW-U, $0.5 < p < 0.1$) more A1 cells are directionally selective than V1 cells may be related to the existence of some directionally selective W cells in the retina (Cleland and Levick, 1974ab). Whether orientation and direction selectivity arise from convergence of thalamocortical input (e.g., Hubel and Wiesel, 1962) and/or from inhibitory intracortical mechanisms (e.g., Sillito, 1975) cannot be

addressed with these data. However, the highly divergent thalamocortical connectivity in the auditory system could make specific convergence of thalamocortical inputs a less tenable basis for orientation or direction tuning. Intracortical origins of orientation and direction selectivity have also been demonstrated in other studies such as the persistence of orientation and direction selectivity following inactivation of A layers in the LGN (Malpeli, 1983) and loss of direction selectivity following selective lesions of superficial cortical layers (Eysel et al., 1987). These cortical receptive field properties are thus likely to arise from intracortical circuits common to both V1 and visually innervated A1.

That many cortical cells in A1 are tuned for relatively high velocities may be surprising given that retinal and LGN W cells generally prefer slow moving stimuli (Cleland and Levick, 1974ab; Stone and Fukuda, 1974; Sur and Sherman, 1982). However, retinal and LGN W cells can have temporal frequency resolutions of up to 30-40 hz (Stanford, 1987).

Another significant finding in this study relates to binocularity. In rewired ferrets, the retino-MGN projection arises from both eyes and terminates in a non-overlapping manner in the MGN (Roe et al., in prep). Furthermore, out of 125 visual units recorded in the MGN of rewired ferrets, none were driven binocularly (Roe et al., in prep). Thus in A1, as in V1, binocularity is a visual property that is generated in cortex. In view of the highly divergent thalamocortical connectivity from the MGN to A1 (in both normal and rewired ferrets, Pallas et al., 1990), we find it remarkable that single cells in A1 are driven by retinal ganglion cells from the two eyes with corresponding receptive field locations. This finding adds support to the idea that correlated activity from the two eyes plays a primary role in synaptic stabilization/selection of thalamocortical synapses or of synapses driven by thalamocortical input (cf. Chapman et al., 1989; Meister et al., 1990; Mastronarde, 1983a,b).

Possible Functional Commonalities between Visual and Auditory Cortices

In this study, we have demonstrated that visual responses in A1 have receptive field properties similar, at least to the degree to which we have examined them, to those in normal V1. One possible interpretation of this data is that sensory cortices of different modalities share similar internal circuitries and perform similar functional transformations on their input. There is a compelling historical precedent for the view that sensory cortices subserving different modalities share similar internal structures (e.g. Mountcastle, 1978; DeFelipe and Jones, 1988). Anatomically, commonalities exist between the thalamocortical and corticocortical connectivities of visual, auditory, and somatosensory cortices (Peters and Jones). Intracortical lamina-specific cell morphologies and interlaminar projection patterns in auditory and visual cortex are similar (Gilbert and Wiesel, 1979; Winer, 1984; Mitani et al., 1985; Matsubara and Phillips, 1988). Functional parallels have been suggested, for example, by similarities in the patterns of interlaminar connectivities as assessed electrophysiologically and anatomically (Mitani and Shimokouchi, 1985; Ferster and Lindstrom, 1982). However, it is difficult compare in a functional manner two cortical structures that represent such different sensory domains: visual cortex contains a two dimensional representation of visual space and auditory cortex a one dimensional representation of sound frequency (Sur et al., 1990).

One parallel which we will attempt to draw involves the generation of orientation selectivity. Orientation selectivity is a central defining feature of primary visual cortex; assessing its presence or absence in A1 of rewired animals was a major motivating force behind this study. The finding that orientation tuning is indeed generated in A1 naturally leads us to question what the auditory correlate of "orientation" selectivity might be. For this purpose, it is instructive to consider the nature of frequency representation in normal A1 and the tuning characteristics of its cells.

Orientation Selectivity in Auditory and Visual Cortex

One of the most revealing studies in this regard has been that of Schreiner and Langner (1988a). They showed that individual auditory neurons respond best not only to a particular spectral frequency, but also to a particular frequency of temporal amplitude modulation (it is primarily the temporal frequency envelope, not the spectral frequency, which determines "pitch"). Thus, the response of a neuron in the MGN to a specific auditory stimulus is very similar to the result obtained by applying the appropriate spectral frequency filter (centered on the characteristic frequency of the cell) and the appropriate temporal modulation frequency filter (centered on the cell's best temporal modulation frequency) to that stimulus (Schreiner and Langner, 1988a; cf. Dreher and Sanderson, 1973 for similar analysis of LGN cells). This proposal (Schreiner and Langner, 1988a) that individual auditory neurons can be relatively completely characterized by filters in two domains (frequency and time) bears a striking parallel to the characterization of visual neurons as two-dimensional spatial filters (Enroth-Cugell and Robson, 1966). To further bolster this idea of a spectro-temporal filter, in the inferior colliculus of the cat a two dimensional map has been described, one axis of which maps spectral frequency and the orthogonal axis which maps best amplitude modulation frequency (Schreiner and Langner, 1988b). Although in primary auditory cortex, a map of best amplitude modulation per se has not been found, there is evidence for a systematic map of forward temporal masking in primary auditory cortex (i.e. the influence of a previous tone on a the response to a second tone) in the axis orthogonal to the frequency axis (Shamma et al., 1990). While further investigation is needed, these studies indicate that the second dimension of auditory cortex may contain a systematic map of some aspect of temporal patterning of auditory stimuli. In any case, it is clear that auditory cortical neurons are selective for both sound frequency and the temporal sound patterns (Schreiner, 1990).

The proposal that properties related to the temporal domain constitute the second axis of representation in normal A1 is further supported by responses of synaptically related thalamic and cortical neurons in the auditory system to specific time varying stimuli

(Creutzfeldt et al., 1980). In contrast to MGN cells which respond more-or-less faithfully to the detailed aspects of auditory input, auditory cortical cells respond only to the dynamic portions of the temporal stimulus envelope. Like the spatial differentiation that edge detectors perform in visual cortex (Marr and Hildreth, 1980; Hochstein, 1984; Richter and Ullman, 1986), cortical auditory neurons compute a temporal differentiation. Similar comparisons can be made for somatosensory cortical neurons (Hellweg et al., 1977). Thus, when considering what might be the auditory correlate of "orientation" selectivity, it may be instructive to consider the frequency and the time domains as the relevant axes of differentiation.

Predictions for Normal Auditory Cortical Processing

This kind of analysis leads to specific predictions about cortical processing in the auditory system and is intricately related to the way in which orientation selectivity arises in normal visual cortex. We will consider two leading models of orientation selectivity generation in visual cortex.

Additive Model. An additive model of orientation selectivity involves convergence of thalamic inputs (Hubel and Wiesel, 1962; Ferster, 1986, 1987; Chapman et al., 1989), while a subtractive model invokes inhibitory intracortical circuits (Sillito, 1975; Greuel et al., 1988). In the additive model, geniculate receptive fields can be defined by x,y spatial coordinates (where x signifies a specific range of azimuths and y a specific range of elevations) and can be combined to produce a cortical receptive field whose orientation is defined by the slope of the line joining x_0, y_0 to x_2, y_2 (Fig. 12A). In the auditory system, receptive fields in the MGN defined by f,t spectrotemporal coordinates (where f signifies a specific range of frequencies and t a specific range or pattern of temporal modulations) may converge to produce an auditory cortical receptive field defined by a line joining f_0, t_0 to f_2, t_2 (Fig. 12B). In other words, auditory cortical cells should respond to simultaneous activation of MGN cells with coordinates falling on the line joining f_0, t_0 to f_2, t_2. Cells with "orientations" falling along different lines would be activated by different stimulus conditions. For example, a cell whose

"orientation" is defined by a varying f and a constant t would prefer neurons selective for frequency sweeps or multiple tone sequences with constant temporal amplitude modulations. Indeed, some auditory cortical cells are tuned to specific directions and rates of frequency modulation (cf. Whitfield and Evans, 1965; Mendelson and Cynader, 1985). An orientation defined by a varying t and constant f would perhaps exhibit selectivity for a broader range of (or for a stimulus composed of a number of) different temporal amplitude modulations all presented at a single spectral frequency. In support of this, cells in auditory cortex respond to specific rates and amplitudes (height of intensity change) of amplitude modulation (Phillips and Hall, 1987). Finally, some cells should respond best to stimuli composed of a number or a range of different frequencies as well as of different temporal modulation preferences. Finally, if "orientation" selectivity is organized in primary auditory cortex in a manner similar to that found in primary visual cortex, then this model predicts that there should be some organized progression of orientations with slopes $\Delta f/\Delta t$ across auditory cortex.

Subtractive Model. There is also evidence supporting the subtractive model of orientation tuning. Loss or change of orientation tuning specificity in visual cortical cells follows local application of GABA antagonists such as bicuculline (Sillito, 1975) and other excitatory agents such as ACh, norepinephrine, NMDA, and glutamate (Fregnac et al., 1988; Greuel et al., 1988). In addition, the presence of lateral inhibitory/modulatory mechanisms has been demonstrated by modulation of orientation tuning with the presence of differing orientations outside the receptive field (Gilbert and Wiesel, 1989a; Fox et al., 1990). In an analagous manner, the frequency tuning curves of auditory cortical neurons can be broadened, sharpened, or become multipeaked under the influence of GABAergic, glutaminergic, and cholinergic substances (Müller and Scheich, 1988; Ashe et al. 1989; McKenna et al., 1989; Metherate and Weinberger, 1989). As yet, no pharmacological studies have yet been made on temporal modulation tuning. However, the report that auditory cortical neurons have a much narrower selectivity range for temporal amplitude modulations than their thalamic counterparts (Creutzfeldt et al., 1980; Schreiner and Langner, 1988a) may indicate the presence of a

cortical tuning mechanism that relies on inhibition. In addition, lateral inhibitory mechanisms may underly modulation of responsiveness (diminishment or enhancement) and tuning by frequencies outside the frequency response area of an auditory cortical cell as well as by previous and subsequent stimuli (i.e. modulation by temporal patterns of sound) (Espinosa and Gerstein, 1988; McKenna et al., 1989; Shamma et al., 1990). Findings such as these have shifted our attention from the vertical columnar organization of sensory cortex to that of an integrated horizontal network and parallels studies in other cortical areas as well (Jenkins et al., 1990; Georgopoulous et al., 1982; cf. Vogels, 1990). More specifically, it is possible that orientation selectivity of visual neurons in A1 of lesioned ferrets arises by inhibitory mechanisms similar to those in normal V1, and that operate in normal A1 as well.

The fact that evidence has accumulated for both additive and subtractive models suggests that they are not mutually exclusive of each other. In any event, the parallels that have been drawn between possible mechanisms in visual cortex and those in auditory cortex are strong and supports the view that sensory cortices subserving different modalities can perform similar transformational roles.

The Establishment of Cortical Circuitries During Development

The question remains as to whether we have demonstrated that normal auditory and visual cortices employ common intracortical mechanisms, or whether the revealed similarities are due to the novel establishment of "visual" circuits in auditory cortex by instructive visual inputs during development. The first interpretation lends a more passive role to sensory afferent input, implying that visual input to A1 simply accesses/activates similar cortical circuits. The second interpretation lays heavy emphasis on the instructive role of afferent input during development. In the following discussion, we consider two contrasting models of the nature-nurture dilemma, afferent specification and target specification during

development. Each is considered in a mutally exclusive manner and each is potentially consistent with our findings in A1 of rewired ferrets. We conclude this section with a proposal which attempts to integrate both views.

Target Specification of Cortical Circuitry. In the previous section, we presented hypotheses about possible parallels in intracortical processing in auditory and visual cortex. The interpretation that intracortical circuitries are common across sensory cortices is consistent with the view that the establishment of cortical circuitries during development is to a large extent independent of afferent input characteristics. In this case, sensory cortex, regardless of modality, follows *a* characteristic sensory cortical developmental program. Sensory cortices of different modalities would then be indistinguishable during development as well as in the adult (Fig. 13A). In principle, cortical features such as orientation selectivity and simple cell receptive field organizations can emerge from a network of unoriented cells even in the absence of sensory input (Linsker, 1986). Such independence from the type of input is consistent, for example, with the fact that receptive field properties such as orientation tuning and simple/complex receptive field organizations are already present in the young, visually inexperienced visual cortex (Hubel and Wiesel, 1963; Albus and Wolf, 1984; Braastad and Heggelund, 1985). Indeed, the fact that "normal" receptive field properties are found in A1 of rewired ferrets suggest that the development of many cortical receptive field properties are not dependent on class-specific (X, Y, or W) patterns of sensory input, and develop, in fact, despite its relatively weak source of retinal input (W type) and despite the different pattern of thalamocortical connectivity (Pallas et al., 1990). In this view, intracortical circuits in A1 are established regardless of sensory input type. [That is not to say that normal cortical circuits develop in the total absence of sensory input; a minimal amount of sensory input may be required to trigger events which result in establishment of cortical circuits.]

There is also other evidence to suggest that the development of synaptic arrangements between pre- and post-synaptic elements in the brain is to a large extent target-controlled. Perhaps the most directly relevant evidence comes from a similar experimental preparation in

the hamster. When retinal afferents are redirected to either MGN or the somatosensory thalamus (VB) of operated hamsters, the resulting synaptic arrangements between the retinal terminals and target (either MGN or VB) relay cells resembles that of the normal target nucleus (Campbell and Frost, 1988). In our experimentally rewired ferrets, visual inputs during development do not change the pattern of auditory thalamocortical connectivity (Pallas et al., 1990). In the visual system, single Y cells in the retina that project to both LGN and SC exhibit strikingly different synaptic connectivities in each target (Sterling, 1973; Behan, 1981; Wilson et al., 1984; Hamos et al., 1987). Other examples of target-directed differentiation of synaptic circuitry can also be found in the cerebellum (Mugnaini, 1970; Palay and Chan-Palay, 1974), the cochlear nucleus (Fekete et al., 1982; Ryugo and Rouiller, 1988), peripheral nervous system (Landis, 1985), and work on striatal transplants (Bjorklund et al., 1987). These examples suggest that, at least in some systems, development of synaptic arrangement between the pre- and post-synaptic elements is target-controlled.

Afferent Specification of Cortical Circuitry. Another, and equally compelling, interpretation of these data is that sensory activity provided by sensory input during development is instructive in establishing specific cortical circuitries and thereby their functional properties. The temporal patterns of sensory activity are unique to each sensory modality and may actively instruct the development of specific cortical circuits from an initially naive cortical template (Fig. 13B). This is an attractive hypothesis in view of the significant literature on activity-dependent mechanisms during development and has been recently discussed in the context of this experimental preparation (Sur et al., 1990; Pallas, 1990).

It is clear that the development of functional properties of visual cortical cells can be modified by abnormal visual input. Studies using abnormal visual rearing conditions (for review, see Sherman and Spear, 1982), activity blockade (Stryker and Harris, 1986; Chapman et al., 1989), and post-synaptic activity perturbation (Kasamatsu and Pettigrew, 1979; Reiter and Stryker, 1988; Bear et al., 1990) during development have shown that changing the quality and quantity of activity can greatly influence the establishment of ocular

dominance in visual cortex. Other cortical receptive field properties are also affected. For example, binocular lid suture and dark rearing produce dramatic reductions in the number of cells with normal receptive field properties (Wiesel and Hubel, 1965; Fregnac and Imbert, 1978). Rearing in striped environments of a single orientation results in a higher incidence of cells with similar orientation (Blakemore and Cooper, 1970; see, however, Movshon and Van Sluyters, 1981). Analogous findings have been made in the auditory system (King and Moore, 1991).

In this context, the functional similarity of visually innervated auditory cortex to normal visual cortex would be the first clear demonstration of cross-modal induction of modality-specific cortical circuitry by peripheral input. If significant differences exist in the intracortical circuitry of normal primary visual cortex and normal primary auditory cortex, these findings would suggest that inputs do not simply influence, but actually "instruct" the establishment of cortical circuits. At the time that the lesions are made in the ferret, posterior cerebral cortex is still quite immature. In primary visual cortex, only the deeper cortical layers (layers 4, 5, and 6) have migrated into place and geniculocortical afferents are still waiting in the subplate (McConnell, 1988; Peduzzi, 1988; Jackson et al., 1989; cf. Shatz and Luskin, 1986). Primary auditory cortex is likely to be at a similar (or slightly more advanced) stage of development (Romand,1983). Thus in the rewired ferrets, we have replaced auditory input with visual input at a time when cortical circuits have not yet been fully established. We speculate that, at this point in development, auditory cortex is quite receptive to instruction by afferent input (regardless of modality). It is possible that similar lesions made at an earlier stage of development would produce an even more dramatic change in organization of the auditory pathway, such as changing the divergent nature of auditory thalamocortical connectivity to a point-to-point connectivity (cf. Sur et al., 1990).

A Proposal. A great deal of effort has been devoted to examining the columnar organization of cerebral cortex and the contribution of this organization to cortical function. However, it is becoming increasingly clear that horizontal intracortical connections also play a

key role in generating receptive field properties. As mentioned previously, there is evidence to suggest that orientation and direction selectivity are local network properties, the specific expression of which are mediated by lateral intracortical connections (Eysel, Gilbert and Wiesel, Van Essen, Singer). In other words, a local network that generates "orientation" embodies the full range of potential orientations of any cell within that network. It is possible, therefore, that the establishment during development of a basic network that is able to potentially endow orientation selectivity upon single cells is distinct from the actual establishment of orientation selectivity of any single cell during development.

Our proposal then is as follows:

1) The establishment of a basic, highly laterally interconnected intracortical network that is able to confer specific selectivities onto single cells, takes place regardless of modality, submodality (e.g. X, Y, or W), or pattern of sensory input during development (this paper, Metin and Frost, 1989; Luhmann et al., 1990; Callaway and Katz, 1991b).

2) The extent, or "weight", of any network is influenced by external factors during development. Horizontal intracortical connectivities become more specific and more refined during normal development (Callaway and Katz, 1991a). Sensory experience does not preventing the emergence of this horizontal network, but does alter the details, such as pruning of individual intracortical arbors and dendritic branches during development (Luhmann et al., 1986; Callaway and Katz, 1990b). This results in differences in the detailed patterns of horizontal intracortical connectivities in the adult A1 and V1 (compare Matsubara et al., 1988 and Gilbert and Wiesel, 1989b). We propose that these changes in horizontal connectivities do not determine whether or not a neuron develops properties such as orientation selectivity, but rather the degree to which its orientation selectivity can be modulated by other inputs (cf. Gilbert and Wiesel, 1989b).

3) In the adult, the specific pattern of sensory input at any particular moment selects or expresses from the network the characteristics that any single neuron will express (Fig.

13C). This idea finds support in work on use-dependent modification of cortical function, dramatic modification of cortical receptive field properties by intracortical infusion of pharmacological agents, lesion induced adult plasticity, and other examples of experience-induced plasticity in the adult brain (Merzenich et al. 1984; Greuel et al., 1988; Gilbert and Wiesel, 1989a; Mioche and Singer, 1989; Jenkins et al., 1990; King and Moore, 1991; see also Anderson and Van Essen, 1987).

In conclusion, it is possible that the establishment of certain, basic cortical transformations is independent of input activity pattern, while the fine-tuning of these basic circuits can be modulated by experience during development and their expression modulated by sensory inputs in the adult.

References

Albus K, Wolf W (1984) Early post-natal development of neuronal function in the kitten's visual cortex: a laminar analysis. J Physiol 348:153-185.

Andersen RA, Knight PL, Merzenich MM (1980) The thalamocortical and corticothalamic connections of AI, AII, and the anterior auditory field (AAF) in the cat: evidence for two largely segregated systems of connections. J Comp Neurol 194:663-701.

Anderson CH, Van Essen DC (1987) Shifter circuits: a computational strategy for dynamic aspects of visual processing. Proc Natl Acad Sci USA 84:6297-6301.

Ashe JH, McKenna TM, Weinberger NM (1989) Cholinergic modulation of frequency receptive fields in auditory cortex: II. Frequency-specific effects of anticholinesterases provide evidence for a modulatory action of endogenous Ach. Synapse 4:44-54.

Bear MF, Kleinschmidt A, Gu Q, Singer W (1990) Disruption of experience-dependent synaptic modifications in striate cortex by infusion of an NMDA receptor antagonist. J Neurosci 10:909-925.

Behan M (1981) Identification and distribution of retinocollicular terminals in the cat: an electron microscopic autoradiographic analysis. J Comp Neurol 199:1-15.

Berson DM (1987) Retinal W-cell input to the upper superficial gray layer of the cat's superior colliculus: a conduction-velocity analysis. J Neurophysiol 58:1035-1051.

Bjorklund A, Lindvall O, Isaacson O, Brundin P, Wictorin K, Strecker RE, Clarke DJ, Dunnet SB (1987) Mechanisms of action of intracerebral neural implants: studies on nigral and striatal grafts to the lesioned striatum. Trends Neurosci 10:509-516.

Braastad BO, Heggelund P (1985) Development of spatial receptive field organization and orientation selectivity in kitten striate cortex. J Neurophysiol 53:1158-1178.

Callaway EM, Katz LC (1991a) Emergence and refinement of clustered horizontal connections in cat striate cortex. J Neurosci 10:1134-1153.

Callaway EM, Katz LC (1991b) Effects of binocular deprivation on the development of clustered horizontal connections in cat striate cortex. Proc Natl Acad Sci 88:745-749.

Campbell G, Frost DO (1988) Synaptic organization of anomalous retinal projections to the somatosensory and auditory thalamus: target-controlled morphogenesis of axon terminals and synaptic glomeruli. J Comp Neurol 272:383-408.

Chapman B, Zahs KR, Stryker MP (1989) Receptive fields of geniculocortical afferents tend to be aligned along preferred orientation of cortical cells. Soc Neurosci Abst 15:1055.

Cleland BG, Levick WR (1974a) Brisk and sluggish concentrically organized ganglion cells in the cat's retina. J Physiol 240:421-456.

Cleland BG, Levick WR (1974b) Properties of rarely encountered types of ganglion cells in the cat's retina and an overall classification. J Physiol 240:457-492.

Creutzfeldt O, Hellweg FC, Schreiner CE (1980) Thalamocortical transformation of responses to complex auditory stimuli. Exp Brain Res 39:87-104.

DeFelipe J, Jones EG (1988) Cajal on the Cerebral Cortex: An Annotated Translation of the Complete Writings. New York: Oxford.

Dreher B, Sanderson KJ (1973) Receptive field analysis: responses to moving visual contours by single lateral geniculate neurons in cat. J Physiol Lond 234:95-118.

Dreher B, Leventhal AB, Hale PT (1980) Geniculate input to cat visual cortex: a comparison of area 19 with areas 17 and 18. J Neurophysiol 44:804-826.

Duysens J, Orban GA, Van der Glas HW, Maes H (1982a) Functional properties of area 19 as compared to area 17 of the cat. Brain Res 231:279-291.

Duysens J, Orban GA, Van der Glas HW, de Zegher FE (1982b) Receptive field structure of area 19 as compared to area 17 of the cat. Brain Res 231:293-308.

Enroth-Cugell C, Robson JG (1966) The contrast sensitivity of retinal ganglion cells of the cat. J Physiol 187:517-552.

Esguerra M, Garraghty PE, Russo GS, Sur M. (1986) Lateral geniculate nucleus in normal and monocularly deprived ferrets: X- and Y- cells and cell body size. Soc Neurosci Abstr 12:10.

Espinosa IE, Gerstein GL (1988) Cortical auditory neuron interactions during presentation of 3-tone sequences: effective connectivity. Brain Res 450:39-50.

Eysel UT, Worgotter F, Paper HC (1987) Local cortical lesions abolish lateral inhibition at direction selective cells in visual cortex. Exp Brain Res 68:606-612.

Fekete DM, Rouiller EM, Liberman MC, Ryugo DK (1982) The central projections of intracellularly labeled auditory fibers in cats. J Comp Neurol 229:432:450.

Felleman DJ, Van Essen DC (1987) Receptive field properties of neurons in Area V3 of Macaque monkey extrastriate cortex. J Neurophysiol 57:889-920.

Ferster D (1986) Orientation selectivity of synaptic potentials in neurons of cat primary visual cortex. J Neurosci 6:1284-1301.

Ferster D (1987) Origin of orientation-selective EPSPs in simple cells of cat visual cortex. J Neurosci 7:1780-1791.

Ferster D (1990a) X- and Y-mediated synaptic potentials in neurons of areas 17 and 18 of cat visual cortex. Visual Neurosci 4:115-133.

Ferster D (1990a) X- and Y-mediated current sources in areas 17 and 18 of cat visual cortex. Visual Neurosci 4:135-145.

Fox JM, Delbruck T, Gallant JL, Anderson CH, Van Essen DC (1990) Modulation of classical receptive field responses by moving texture backgrounds in monkey striate cortex: spatial and temporal interactions. Soc Neurosci Abst 16:1270.

Fregnac Y, Shulz D, Thorpe S, Bienenstock E (1988) A cellular analogue of visual cortical plasticity. Nature 333:367-370.

Frost DO, Metin C (1985) Induction of functional retinal projections to the somatosensory system. Nature 317:162-164.

Fukuda Y, Hsiao CF, Watanabe M, Ito H (1984) Morphological correlates of physiologically identified Y-, X-, and W-cells in cat retina. J Neurophysiol 52:999-1013.

Georgopoulos AP, Kalaska JF, Caminiti R, Massey JT (1982) On the relations between the direction of two-dimensional arm movements and cell discharge in primate motor cortex. J Neurosci 2:1527-1537.

Gilbert CD (1977) Laminar differences in receptive field properties of cells in cat primary visual cortex. J Physiol 268:391-421.

Gilbert CD, Wiesel TN (1979) Morphology and intracortical projections of functionally characterised neurones in the cat visual cortex. Nature 280:120-125.

Gilbert CD, Wiesel TN (1989a) The influence of contextual patterns on orientation selectivity in V1 of the cat. Soc Neurosci Abst 15:324.

Gilbert CD, Wiesel TN (1989b) Columnar specificity of intrinsic horizontal and corticocortical connections in cat visual cortex. J Neurosci 9:2432-2442.

Greuel JM, Luhmann HJ, Singer W (1988) Pharmacological induction of use-dependent receptive field modifications in the visual cortex. Science 242:74-77.

Guillery RW (1969) The organization of synaptic interconnections in the laminae of the dorsal lateral geniculate nucleus of the cat. Z Zellforsch 96:1-38.

Hamos JE, Van Horn SC, Raczkowski D, Sherman SM (1987) Synaptic circuits involving an individual retinogeniculate axon in the cat. J Comp Neurol 259:165-192.

Hata Y., Tsumoto T., Sato H., Hagihara K., and Tamura H. (1988) Inhibition contributes to orientation selectivity in visual cortex of the cat. Nature 335:815-817.

Hellweg FC, Schultz W, Creutzfeldt OD (1977) Extracellular and intracellular recordings from cat's cortical whisker projection area: thalamo-cortical response transformation. J Neurophysiol 40:463-479.

Hochstein S (1984) Zero-crossing detectors in primary visual cortex. Biol Cybern 51:195-199.

Hubel DH, Wiesel TN (1962) Receptive fields, binocular interaction, and functional architecture in the cat's visual cortex. J. Physiol. 160:106-154.

Hubel DH, Wiesel TN (1963) Receptive fields of cells in striate cortex of very young, visually inexperienced kittens. J Neurophysiol 26:994-1002.

Jackson CA, Peduzzi JD, Hickey TL (1989) Visual cortex development in the ferret. I. Genesis and migration of visual cortical neurons. J Neurosci 9:1242-1253.

Jenkins WM, Merzenich MM, Ochs MT, Allard T, Guic-Robles E (1990) Functional reorganization of primary somatosensory cortex in adult owl monkeys after behaviorally controlled tactile stimulation. J Neurophysiol 63:82-104.

Kasamatsu T, Pettigrew JD (1979) Preservation of binocularity after monocular deprivation in the striate cortex of kittens treated with 6-hydroxydopamine. J Comp Neurol 185:139-162.

Katz LC, Callaway (1990) Development of interlaminar connections of layer 4 neurons in cat striate cortex. Soc Neurosci Abstr 16:1129.

Kelly JB, Judge PW, Phillips DP (1986) Representation of the cochlea in primary auditory cortex of the ferret (*Mustela putorius*). Hearing Res 24:111-115.

King AJ, Moore DR (1991) Plasticity of auditory maps in the brain. Trends Neurosci 14:31-37.

Kimura M, Shiida T, Tanaka K, Toyama K (1980) Three classes of area 19 cortical cells of the cat classified by their neuronal connectivity and photic responsiveness. Vision Res 20:69-77.

Law MI, Zahs KR, Stryker MP (1988) Organization of primary visual cortex (Area 17) in the ferret. J Comp Neurol 278:157-180.

Leventhal AG, Zhou Y, Ault SJ, Thompson KG (1990) Cortical contribution to the orientation sensitivity of relay cells in the cat lateral geniculate nucleus. Soc Neurosci Abst 15:176.

Linsker R (1986) From basic network principles to neural architecture: emergence of orientation-selective cells. Proc Natl Acad Sci 83:8390-8394.

Luhmann HJ, Millan LM, Singer W (1986) Development of horizontal intrinsic connections in cat striate cortex. Exp Brain Res 63:443-448.

Luhmann HJ, Singer W, Martinez-Millan L (1990) Horizontal interactions in cat striate cortex: I. Anatomical substrate and postnatal development. Eur J Neurosci 2:344-357.

Majorossey K, Kiss A (1976) Specific patterns of neuron arrangement and of synaptic articulation in the medial geniculate body. Exp Brain Res 26:1-177.

Malpeli JG, Schiller PH, Colby CL (1981) Response properties of single cells in monkey striate cortex during reversible inactivation of individual lateral geniculate laminae. J Neurophysiol 46:1102-1119.

Malpeli JG (1983) Activity of cells in area 17 of the cat in absence of input from layer A of lateral geniculate nucleus. J Neurophysiol 49:595-610.

Marr D, Hildreth E (1980) Theory of edge detection. Proc R Soc Lond B 207:187-217.

Mastronarde DN (1983a) Correlated firing of cat retinal ganglion celss. I. Spontaneously active in puts to X- and Y-cells. J Neurophysiol 49:303-324.

Mastronarde DN (1983b) Correlated firing of cat retinal ganglion celss. II. Responses of single X- and Y-cells to single quantal events. J Neurophysiol 49:325-349.

Matsubara JA, Phillips DP (1988) Intracortical connections and their physiological correlates in the primary auditory cortex (A1) of the cat. J Comp Neurol 268:38-48.

McConnell SK (1988) Fates of visual cortical neurons in the ferret after isochronic and heterochronic transplantation. J Neurosci 8:945-974.

McKenna TM, Ashe JH, Weinberger NM (1989) Cholinergic modulation of frequency receptive fields in auditory cortex: I. Frequency-specific effects of muscarinic agonists. Synapse 4:30-43.

McKenna TM, Weinberger NM, Diamond DM (1989) Responses of single auditory cortical neurons to tone sequences. Brain Res 481:142-153.

Meister M, Wong RL, Baylor DA, Shatz CJ (1990) Synchronous bursting activity in ganglion cells of developing mammalian retina. Invest Ophthalmol Vis Sci Suppl 31:115.

Mendelson JR, Cynader MS (1985) Sensitivity of cat primary auditory cortex (A1) neurons to the direction and rate of frequency modulation. Brain Res 327:331-335.

Merzenich MM, Jenkins WM, Middlebrooks JC (1984) Observations and hypotheses on special organizational features of the central auditory nervous system. In: Dynamic Aspects of Neocortical Function (Edelman GM, Gall WE, Cowan WM, eds). pp. 397-424. New York: Neurosciences Research Foundation.

Metherate R, Weinberger NM (1989) Acetylcholine produces stimulus-specific receptive field alterations in cat auditory cortex. Brain Res 480:372-377.

Metin C, Frost DO (1989) Visual responses of neurons in somatosensory cortex of hamsters with experimentally induced retinal projections to somatosensory thalamus. Proc Natl Acad Sci USA 86:357-361.

Middlebrooks JC, Zook JM (1983) Intrinsic organization of the cat's medial geniculate body identified by projections to binaural response-specific bands in the primary auditory cortex. J Neurosci 3:203-224.

Mioche L, Singer W (1989) Chronic recordings from single sites of kitten striate cortex during experience-dependent modifications of receptive-field properties. J Neurophysiol 62:185-197.

Mitani A, Shimokouchi M (1985) Neuronal connections in the primary auditory cortex: an electrophysiological study in the cat. J Comp Neurol 235:417-429.

Mitani A, Shimokouchi M, Itoh K, Nomura S, Kudo M, Mizuno N (1985) Morphology and laminar organization of electrophysiologically identified neurons in the primary auditory cortex in the cat. J Comp Neurol 235:430-447.

Morest K (1975) Synaptic relationships of Golgi Type II cells in the medial geniculate body of the cat. J Comp Neurol 162:157-194.

Mugnaini E (1970) Neurones as synaptic targets. In: Excitatory Synaptic Mechanisms (Anderson P, Jansen JKS, eds). pp. 149-169. Oslo: Universitesvorlaget.

Müller CM, Scheich H (1988) Contribution of GABAergic inhibition to the response characteristics of auditory units in the avian forebrain. J Neurophysiol 59:1673-1689.

Mullikin WH, Jones JP, Palmer LA (1984) Receptive field properties and laminar distribution of X-like and Y-like simple cells in cat area 17. J Neurophysiol 52:350-371.

Orban GA, Kennedy H, Maes H (1981) Response to movement of neurons in areas 17 and 18 of the cat: velocity sensitivity. J Neurophysiol 45:1043-1058.

Palay SL, Chan-Palay V (1974) Cerebellar Cortex: Cytology and Organization. Berlin: Springer.

Pallas SL (1990) Cross-modal plasticity in sensory cortex. In: The Neocortex: Ontogeny and Phylogeny (Finlay BL, Innocenti G, Scheich H, eds). pp. 205-218. New York: Plenum.

Pallas SL, Hahm JO, Sur M (1989) Retinal axon arbors in a novel target: morphology of ganglion cell axons induced to arborize in the medial geniculate nucleus of ferrets. Soc Neurosci Abst 15:495.

Pallas SL, Roe AW, Sur M (1990) Visual projections induced into the auditory pathway of ferrets. I. Novel inputs to primary auditory cortex (A1) from the LP/pulvinar complex and the topography of the MGN-A1 projection. J Comp Neurol 298:50-68.

Palmer LA, Davis TL (1981) Receptive field structure in cat striate cortex. J Neurophysiol 46:260-276.

Palmer LA, Rosenquist AC (1974) Visual receptive fields of single striate cortical units projecting to the superior colliculus in the cat. Brain Res 67:27-42.

Pasternak T, Leinen LJ (1986) Pattern and motion vision in cats with selective loss of cortical directional selectivity. J Neurosci 6:938-945.

Peduzzi JD (1988) Genesis of GABA-immunoreactive neurons in the ferret visual cortex. J Neurosci 8:920-931.

Phillips DP, Hall (1987) Responses of single neurons in cat auditory cortex to time-varying stimuli: linear amplitude modulations. Exp Brain Res 67:479-492.

Price DJ, Morgan JE (1987) Spatial properties of neurones in the lateral geniculate nucleus of the pigmented ferret. Exp Brain Res 68:28-36.

Ramoa AS, Shadlen M, Freeman RD (1987) Dark-reared cats: unresponsive cells become visually responsive with microiontophoresis of an excitatory amino acid. Exp Brain Res 65:658-665.

Redies C, Diksic M, Rimi H (1990) Functional organization in the ferret visual cortex: a double-label 2-deoxyglucose study. J Neurosci 10:2791-2803.

Reiter HO, Stryker MP (1988) Neural plasticity without action potentials: less active inputs become dominant when kitten visual cortical cells are pharmacologically inhibited. Proc Natl Acad Sci USA 85:3623-3627.

Richter J, Ullman S (1986) Non-linearities in cortical simple cells and the possible detection of zero crossings. Biol Cybern 195-202.

Roe AW, Garraghty PE, and Sur M (1987) Retinotectal W-cell plasticity: experimentally induced retinal projections to auditory thalamus in ferrets. Soc Neurosci Abst 13:1023.

Roe AW, Garraghty PE, Sur M (1988) The terminal arbors of single on-center and off-center X and Y retinogeniculate axons within the ferret's lateral geniculate nucleus. J Comp Neurol 288:208-242.

Roe AW, Pallas SL, Hahm JO, Sur M (1990) A map of visual space induced into primary auditory cortex. Science 250:818-820.

Roe AW, Pallas SL, Kwon YH, Sur (1990) Visually innervated auditory cortex in ferrets generates visual response properties similar to those in normal visual cortex. Soc Neurosci Abst 16:984.

Romand R (1983) Development of auditory and vestibular systems, Academic Press.

Ryugo DK, Rouiller EM (1988) Central projections of intracellularly labeled auditory nerve fibers in cats: morphometric correlations with physiological properties. J Comp Neurol 271:130-142.

Saito H, Tanaka K, Fukada Y, Oyamada (1988) Analysis of discontinuity in visual contours in area 19 of the cat. J Neurosci 8:1131-1143.

Schiller PH, Finlay BL, Volman SF (1976a) Quantitative studies of single-cell properties in monkey striate cortex. I. Spatiotemporal organization of receptive fields. J Neurophysiol 39:1288-1319.

Schiller PH, Finlay BL, Volman SF (1976b) Quantitative studies of single-cell properties in monkey striate cortex. II. Orientation specificity and ocular dominance. J Neurophysiol 39:1320-1333.

Schneider GE (1973) Early lesions of superior colliculus: factors affecting the formation of abnormal retinal projections. Brain Behav Evol 8:73-109.

Schreiner CE, Langner G (1988a) Coding of temporal patterns in the central auditory nervous system. In: Auditory Function: Neurobiological Bases of Hearing (Edelman GE, Gall WI, and Cowan WM, eds). pp 337-361. New York: John Wiley and Sons.

Schreiner CE, Langner G (1988b) Periodicity coding in the inferior colliculus of the cat. II. Topographical organization. J Neurophysiol 60:1823-1840.

Shamma SA, Fleshman JW, Wiser PR (1991) Receptive field organization in ferret primary auditory cortex: spectral orientation columns. J Neurophysiol, *submitted.*

Shatz CJ, Luskin MB (1986) The relationship between the geniculocortical afferents and their cortical target cells during development of the cat's primary visual cortex. J Neurosci 6:3655-3668.

Sherman SM, Spear PD (1982) Organization of visual pathways in normal and visually deprived cats. Physiol Rev 62:738-855.

Sillito AM (1975) The contribution of inhibitory mechanisms to the receptive field properties of neurons in the striate cortex of the cat. J Physiol 250:305-322.

Simons DJ, Land PW (1987) Early experience of tactile stimulation influences organization of somatic sensory cortex. Nature 326:694-697.

Stanford LR (1987) W-cells in the cat retina: correlated morphological and physiological evidence for two distinct classes. J Neurophysiol 57:218-244.

Sterling P (1973) Quantitative mapping with the electron microscope: retinal terminals in the superior colliculus. Brain Res 54:347-354.

Stone J, Fukuda Y (1974) Properties of cat retinal ganglion cells: a comparison of W-cells with X- and Y-cells. J Neurophysiol 37:722-748.

Stryker MP, Harris WA (1986) Binocular impulse blockade prevents the formation of ocular dominance columns in cat visual cortex. J Neurosci 6:2117-2133.

Suga N, Niwa H, Taniguchi I, Margoliash D (1987) The personalized auditory cortex of the mustached bat: adaptation for echolocation. J Neurophysiol 58:643-654.

Sur M, Sherman SM (1982) Linear and nonlinear W-cells in C-laminae of the cat's lateral geniculate nucleus. J Neurophysiol 47:869-884.

Sur M, Garraghty PE, Roe AW (1988) Experimentally induced projections into auditory thalamus and cortex. Science 242:1437-1441.

Sur M, Pallas SL, Roe AW (1990) Cross-modal plasticity in cortical development: differentiatioin and specification of sensory neocortex. Trends Neurosci 13:227-233.

Tanaka K (1983) Cross-correlation analysis of geniculostriate neuronal relationships in cats. J Neurophysiol 49:1303-1318.

Tanaka K, Ohzawa I, Ramoa AS, Freeman RD (1987) Receptive field properties of cells in area 19 of the cat. Exp Brain Res 65:549-558.

Vitek DJ, Schall JD, Leventhal AG (1985) Morphology, central projections, and dendritic field orientation of retinal ganglion cells in the ferret. J Comp Neurol 241:1-11.

Vogels R (1990) Population coding of stimulus orientation by striate cortical cells. Biol Cybern 64:25-31.

Whitfield IC, Evans EF (1965) Responses of auditory cortical neurons to stimuli of changing frequency. J Neurophysiol 28:655-672.

Wilson JR, Friedlander MJ, Sherman SM (1984) Fine structural morphology of identified X- and Y-cells in the cat's lateral geniculate nucleus. Proc R Soc Lond B 221:411-436.

Wilson PD, Rowe MH, Stone J (1976) Properties of relay cells in the cat's lateral geniculate nucleus: a comparison of W-cells with X- and Y-cells. J Neurophysiol 39:1193-1209.

Winer JA (1984) Anatomy of layer IV in cat primary auditory cortex (A1). J Comp Neurol 224:535-567.

Zahs KR, Stryker MP (1988) Segregation of ON and OFF afferents to ferret visual cortex. J Neurophysiol 59:1410-1429.

Figure Legends

Fig. 1. Depth from cortical surface (in μm) at which units in A1 (dark bars, n=485) and V1 (light bars, n=134) were recorded. (Depths of 19 units from early experiments in V1 were not recorded.) Note that electrode penetrations were not necessarily perpendicular to cortical surface (see text).

Fig. 2. Distribution of responsivity indices of cells in A1 (dark bars) and V1 (light bars). These distributions are significantly different ($p < .0001$). Out of total of 194 cells, 38 recorded from early experiments in lesioned animals were not rated for responsivity.

Fig. 3. A) Receptive field diameters (defined as average of width and height of receptive field) of cells in A1 (dark bars) and V1 (light bars). Receptive field sizes in A1 (mean = 10.9°, dark arrowhead) are significantly larger ($p < .0001$) than those in V1 (mean = 3.9°, light arrowhead). B) Distribution of receptive field locations recorded in A1 (dark diamonds) and V1 (light squares). In A1, significantly many more fields were recorded representing peripheral regions of the visual field than in V1 ($p < .0001$). C) Taking into consideration only receptive fields whose eccentricities are below 30° reveals that A1 cells still have much larger receptive fields ($p < .0001$).

Fig. 4. Latencies of cells in A1 and V1 to electrical stimulation of the optic chiasm. A) Cells in A1 (dark bars, n=485, mean = 6.8 msec) have significantly longer latencies to chiasm stimulation than those in V1 (light bars, n=124, mean = 4.4 msec) ($p < .0001$). B) Latencies of visually responsive cells in A1 (shaded bars, n=184, mean = 6.9 msec) are similar to those of all cells recorded in A1($p > .13$). C) Similarly, visually responsive cells in V1 (shaded bars, n=77, mean = 4.3 msec) have latencies similar to all cells recorded in V1 ($p > .7$).

Fig. 5. Ocular dominance distributions of visual cells recorded in A1 (dark bars) and in V1 (light bars). These two distributions are not significantly different [$\chi^2(.95) = 4.6$, df = 6]. Of 105 visual V1 units, 29 cells were not rated for ocular dominance (22 recorded in early experiments in which ocular dominance was not assessed, 3 "stereo" cells (see text), and 4 poorly responsive cells). In A1, of 194 visual cells, 110 were rated with confidence.

Fig. 6. Percentage of simple, complex, and non-oriented cells in A1 (dark bars) and V1 (light bars). These distributions are not significantly different [$\chi^2(.95) = 3.7$, df = 2].

Fig. 7. Orientation tuning of 2 cells in V1. Post-stimulus time histograms collected of cell responses to sweeping bars at different orientations and directions (indicated by bars with arrows). Plotted are the peak responses (minus background) to each stimulus. A) A simple cell with an orientation tuning index of 0.57, an orientation tuning width of 63°, and a directionality index of 0.25. B) An end-stopped complex cell with an orientation tuning index of 0.73, an orientation tuning width of 65°, and a directionality index of 0.38.

Fig. 8. Orientation tuning of 2 cells in A1. Conventions same as in Fig. 5. A) An end-stopped complex cell with orientation tuning index 0.73, orientation tuning width 65°, and directionality index 0.38. B) A simple cell with orientation tuning index 0.63, orientation tuning width 47°, and directionality index 0.71.

Fig. 9. Orientation tuning of cells in A1 (dark bars) and in V1 (light bars). A) Distribution of orientation tuning indices [index defined as (1 - Best response/Orthogonal response)] in A1 (mean = 0.41) and V1 (mean = 0.39) are similar ($p > 0.65$). B) Distributions of

orientation tuning widths (defined as width at height of $1/\sqrt{2}$) in A1 (mean = 65.3°) and V1 (mean = 72.5°) are not significantly different ($p > 0.90$).

Fig. 10. Directionality indices of cells in A1 (dark bars) and in V1 (light bars). A1 mean = 0.45, V1 mean = 0.36. These two distrubitions are not significantly different ($0.5 < p < 0.1$).

Fig. 11. A) Examples of velocity tuning curves in V1 (left column) and A1 (right column). In each column, curves 1 and 2 are tuned for slow (<15°/s), curves 3 for medium (15°-50°/s), and curves 4 for fast (>50°/s) velocities. Curves 5 display hi-pass or lo-pass, curves 6 U-shaped, and curves 7 velocity broad-band characteristics. B) Distributions of cells in A1 (dark bars) and V1 (light bars) with peak velocity preferences near 6°/s, 13°/s, 25°/s, 50°/s, 100°/s, as well as those displaying broad-band (BB) and U-shaped (slow/fast) tuning curves. These distributions are not significantly different ($p > 0.8$). A1 mean = 27.9°/s, V1 mean = 24.6°/s.

Fig. 12. Schematic of additive model of orientation selectivity in visual cortex (A) and auditory cortex (B). Circles, representing receptive fields of thalamocortical input, fall along a line representing the orientation selectivity of a cortical cell. Insets are schematize receptive fields of corresponding thalamic cells. Vertical axis represents response magnitude; horizontal axis represents azimuth (x_i in A), elevation (y_i in A), frequency (x_i in B), or temporal parameter (y_i in B).

Fig. 13. Models of development of intracortical circuitry (see text).

Table 1. Number of Units Recorded in V1 and A1

	V1		A1	
Total	153	(%)	495	(%)
Electrically Driven	124	(95)[a]	485	(98)
Visually Driven	105	(69)	194	(39)
Visually and Electrically Driven	77	(59)[b]	184	(37)
Receptive Field Size Determined	101	(66)	100	(20)
Ocular Dominance Determined	76	(50)	110	(22)
Cell Class Determined	101	(66)	52	(11)
Quantitatively Characterized	38	(25)	24	(5)
Driven by Auditory Stimuli	0	(0)	0	(0)

[a]Percentage calculated from a total of 131 cells for which chiasm latencies were assessed. In one experiment, chiasm latencies were not assessed (22 cells).

[b]Percentage calculated from a total of 83 cells. Excludes visually responsive cells for which chiasm latencies were not assessed (22 cells).

Fig. 1

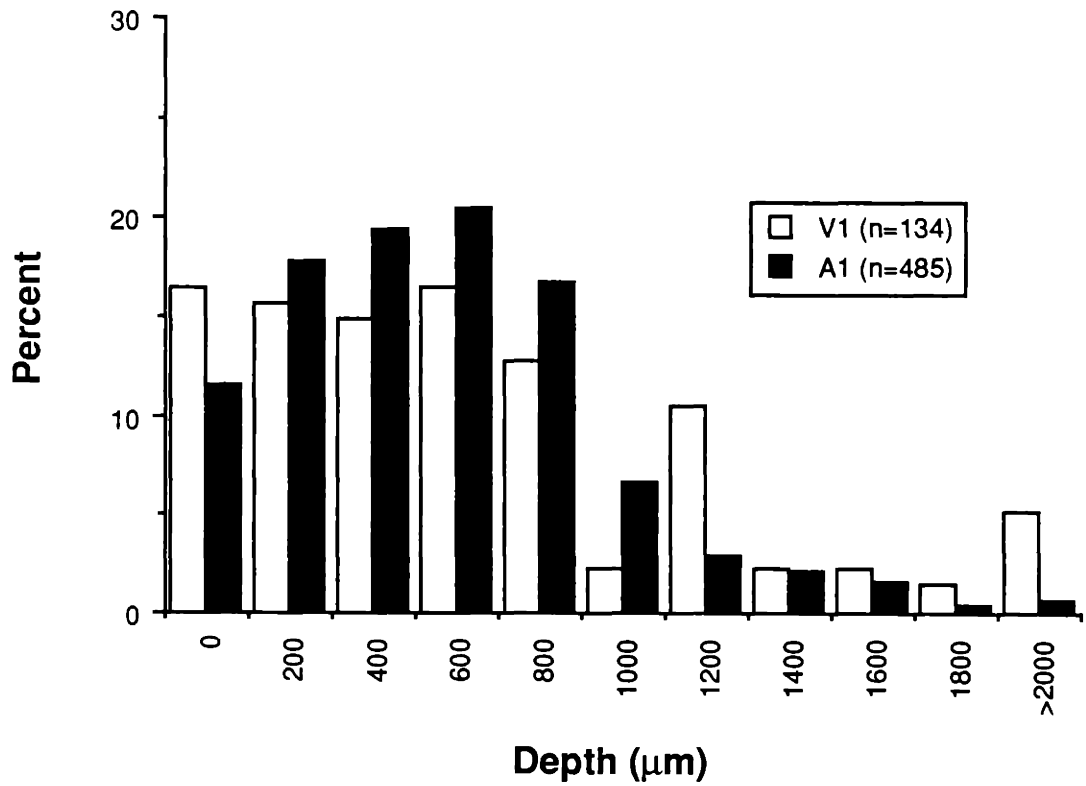
30
20
10
0
Percent
V1 (n=134)
A1 (n=485)
0
200
400
600
800
1000
1200
1400
1600
1800
>2000
Depth (μm)

Fig. 2

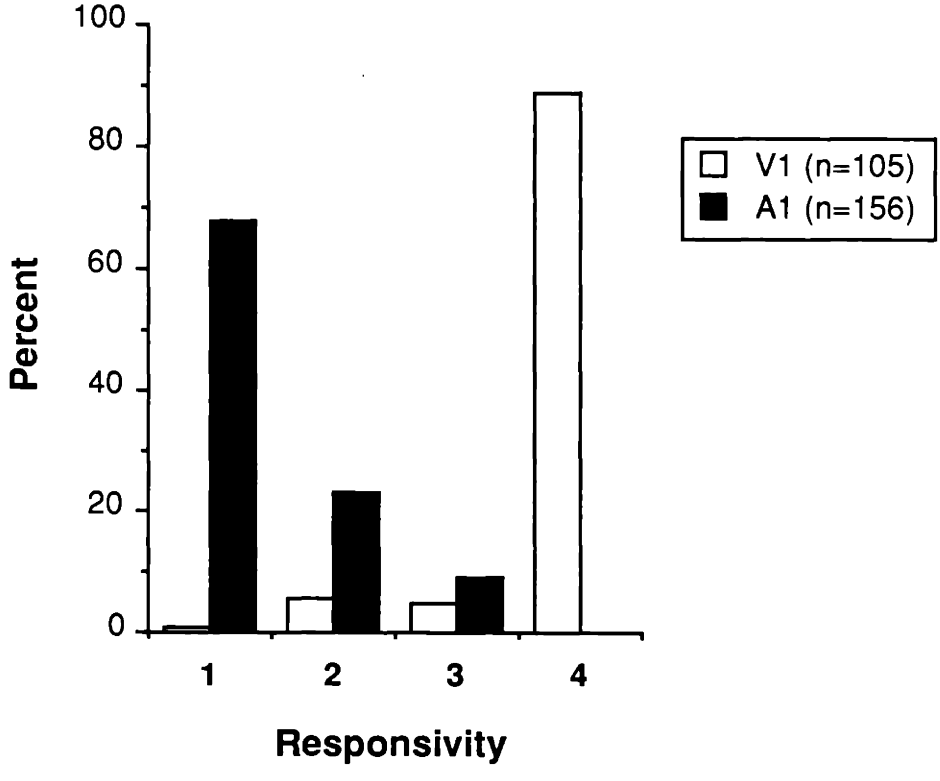

Fig. 3

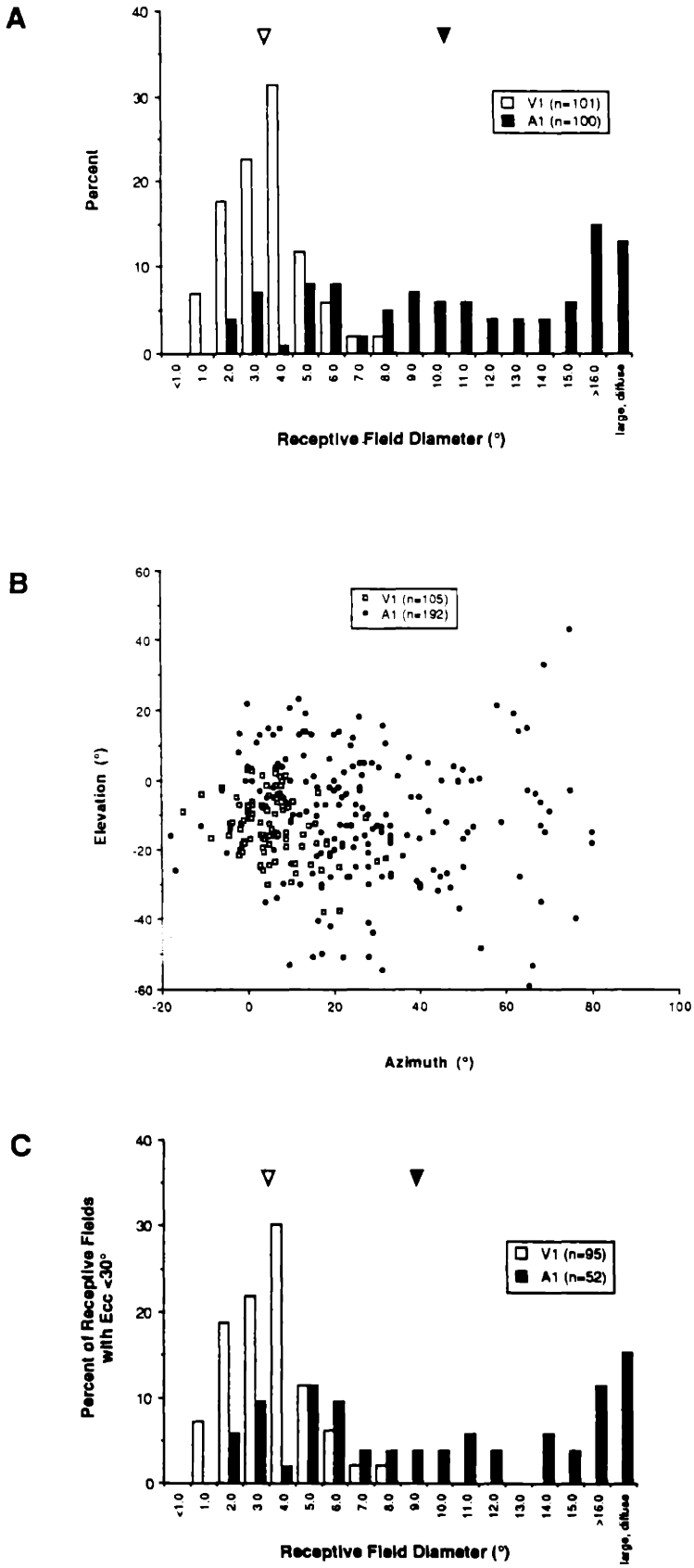
A
Percent
V1 (n=101)
A1 (n=100)
Receptive Field Diameter (°)
B
Elevation (°)
V1 (n=105)
A1 (n=192)
Azimuth (°)
C
Percent of Receptive Fields with Ecc <30°
V1 (n=95)
A1 (n=52)
Receptive Field Diameter (°)

Fig. 4

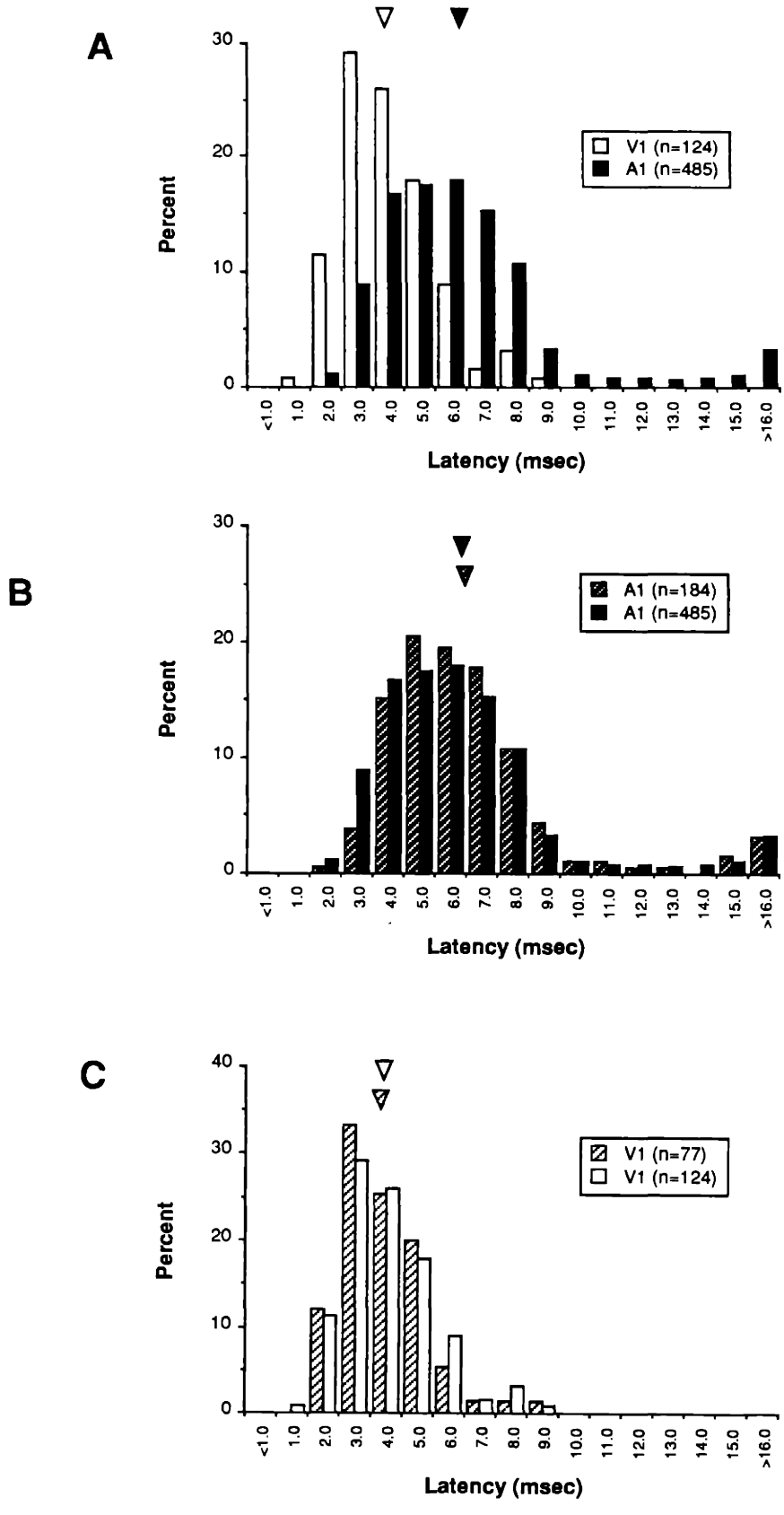
A
Percent
30
20
10
0
V1 (n=124)
A1 (n=485)
<1.0
1.0
2.0
3.0
4.0
5.0
6.0
7.0
8.0
9.0
10.0
11.0
12.0
13.0
14.0
15.0
>16.0
Latency (msec)
B
Percent
A1 (n=184)
A1 (n=485)
Latency (msec)
C
Percent
40
V1 (n=77)
V1 (n=124)
Latency (msec)

Fig. 5

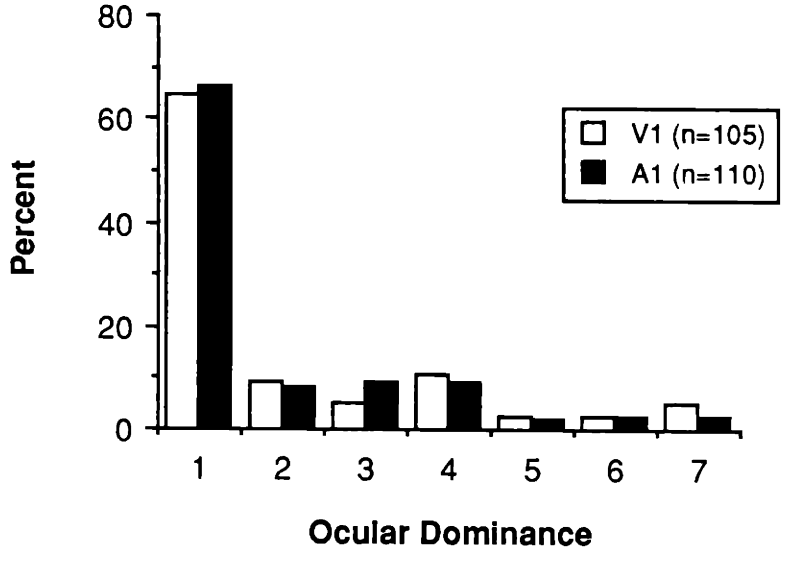
80
60
40
20
0
Percent
V1 (n=105)
A1 (n=110)
1
2
3
4
5
6
7
Ocular Dominance

Fig. 6

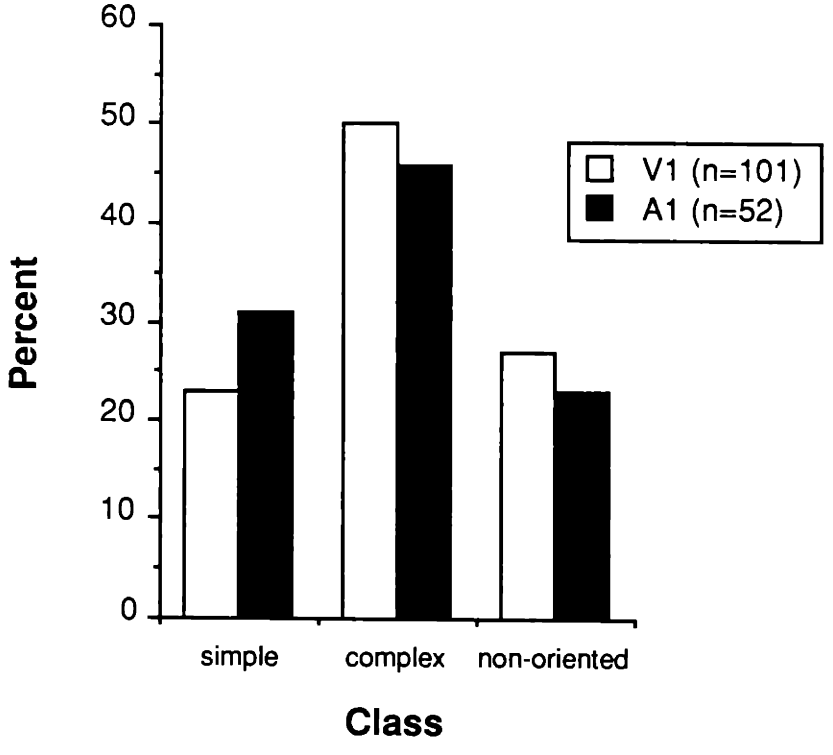
60
50
40
30
20
10
0
Percent
V1 (n=101)
A1 (n=52)
simple
complex
non-oriented
Class

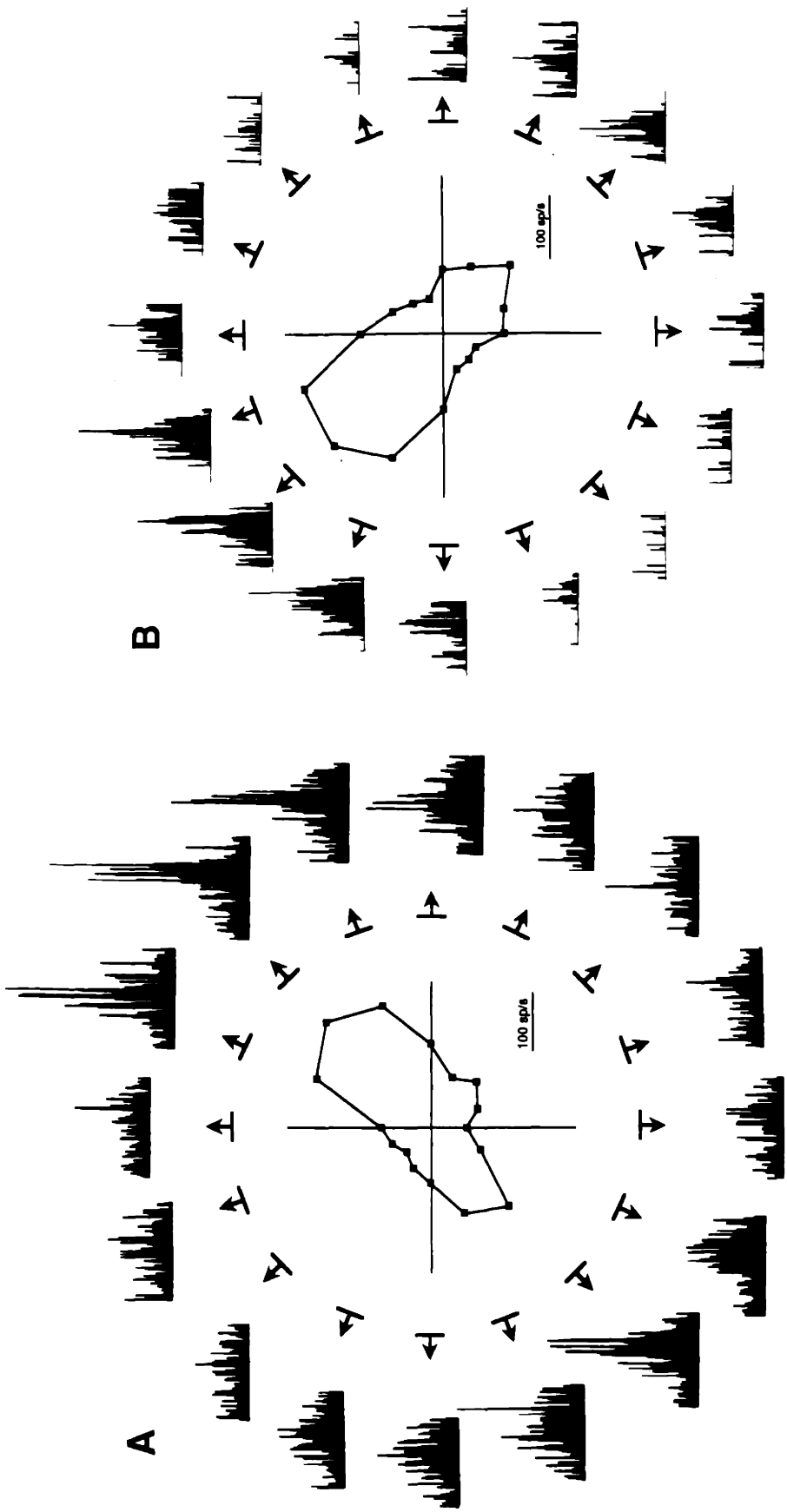

Fig. 7

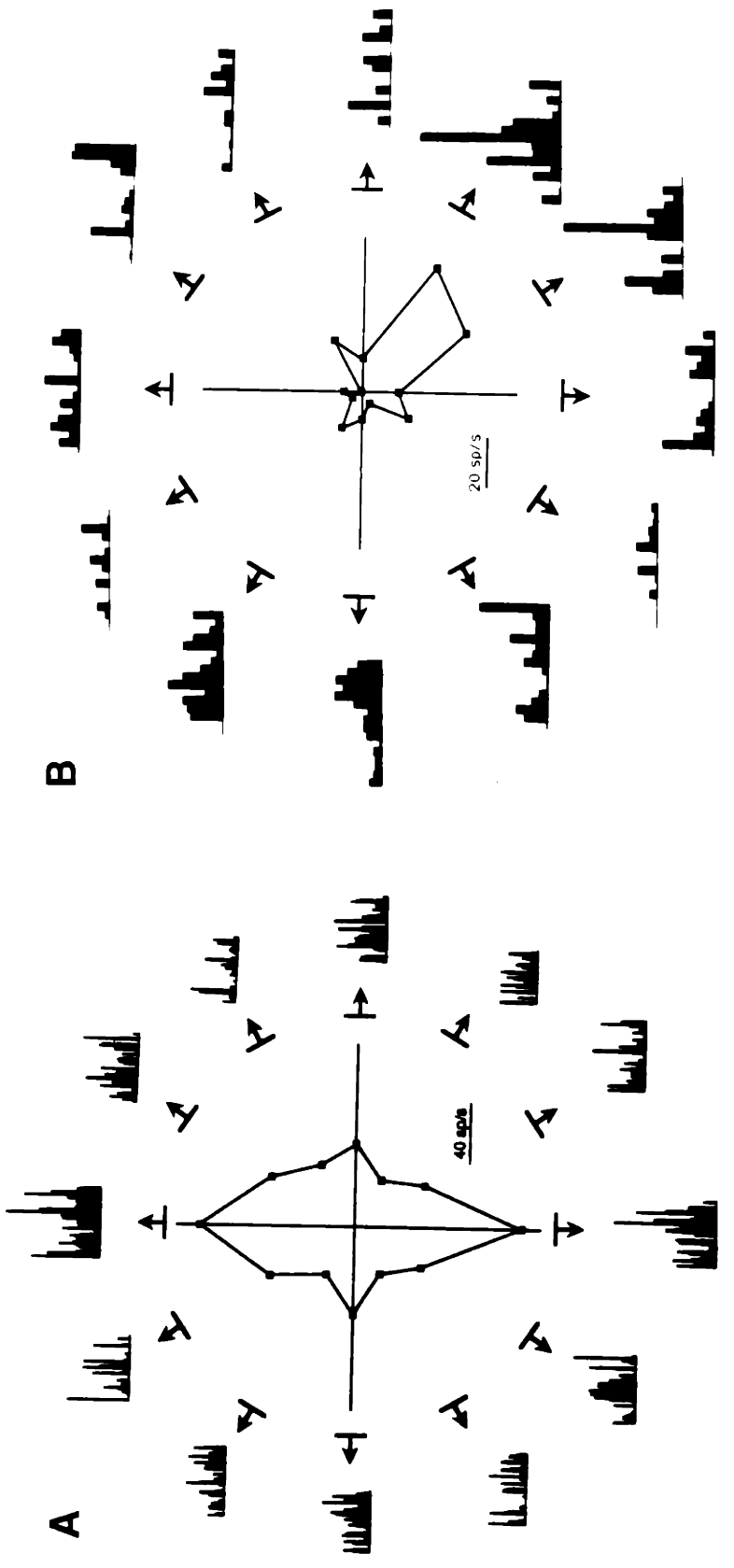

Fig. 8

Fig. 9

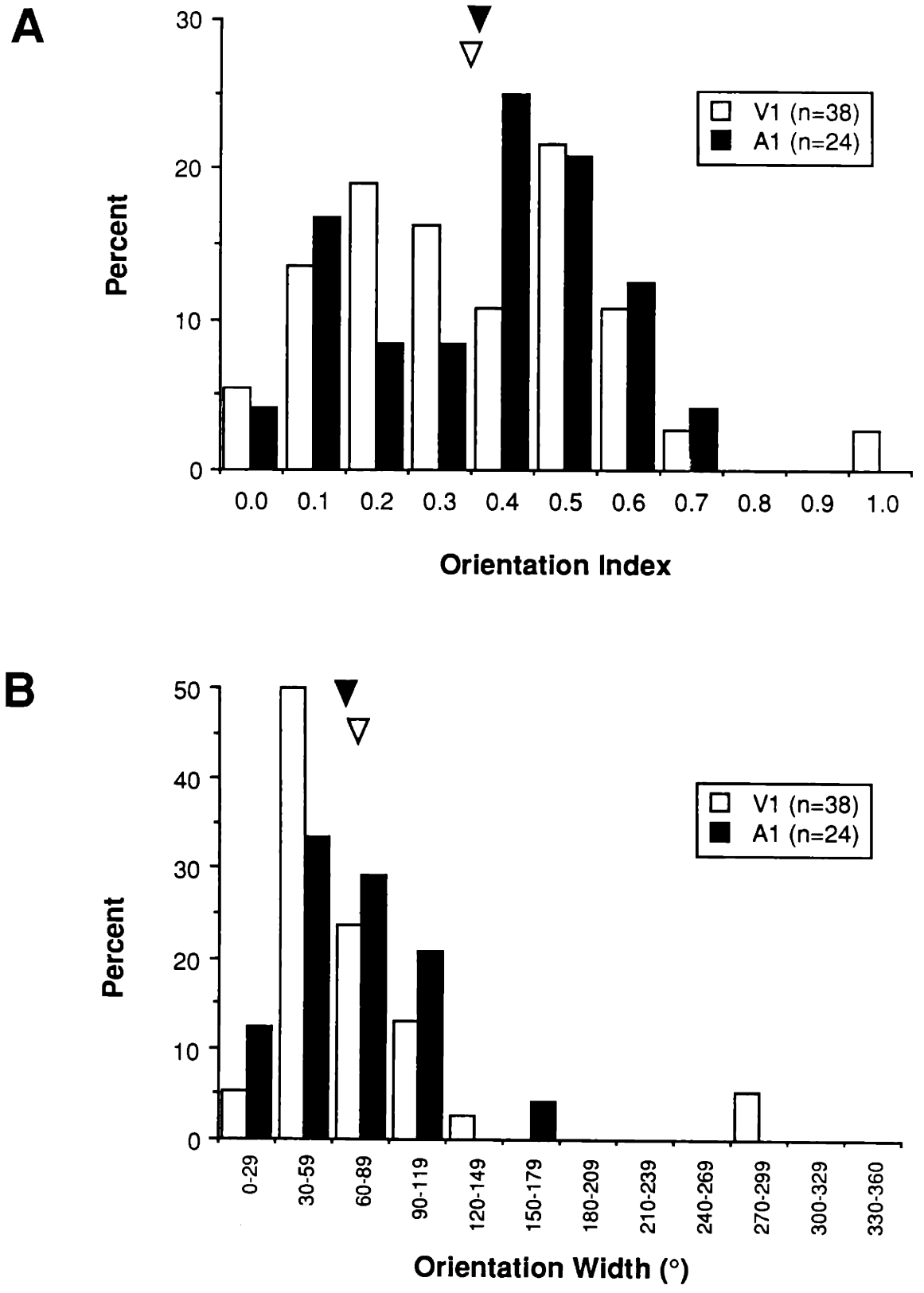
A
30
20
10
0
Percent
V1 (n=38)
A1 (n=24)
0.0
0.1
0.2
0.3
0.4
0.5
0.6
0.7
0.8
0.9
1.0
Orientation Index
B
50
40
30
20
10
0
Percent
V1 (n=38)
A1 (n=24)
0-29
30-59
60-89
90-119
120-149
150-179
180-209
210-239
240-269
270-299
300-329
330-360
Orientation Width (°)

Fig. 10

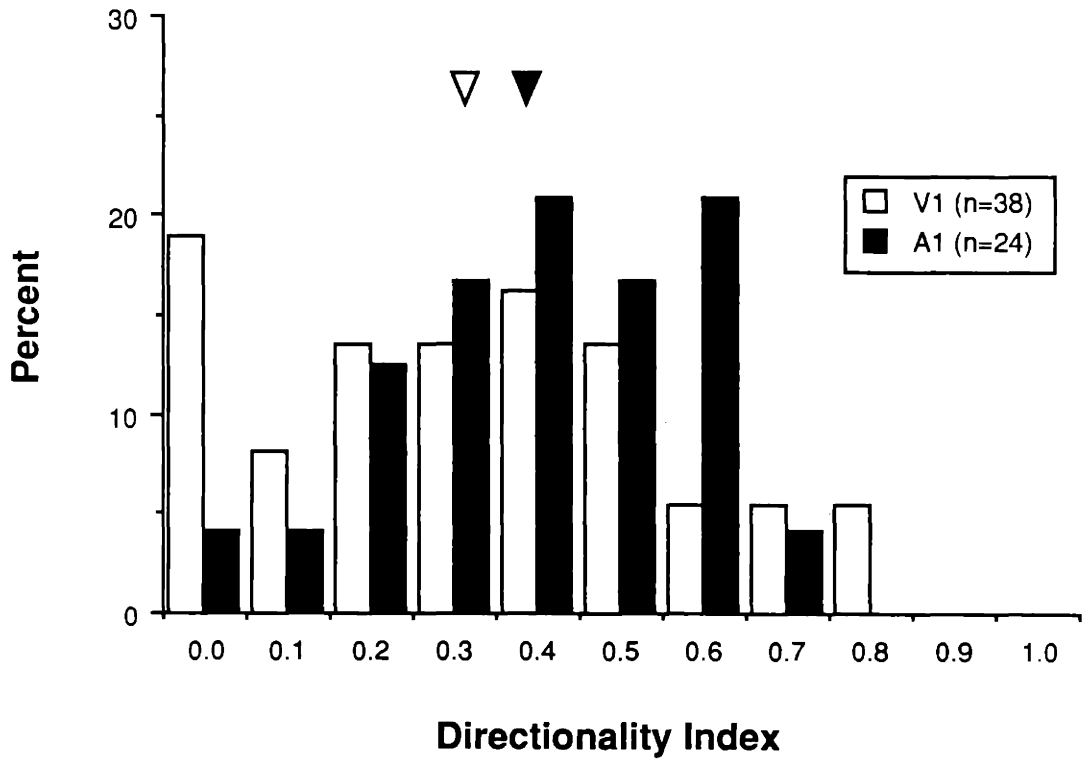
30
20
10
0
Percent
V1 (n=38)
A1 (n=24)
0.0
0.1
0.2
0.3
0.4
0.5
0.6
0.7
0.8
0.9
1.0
Directionality Index

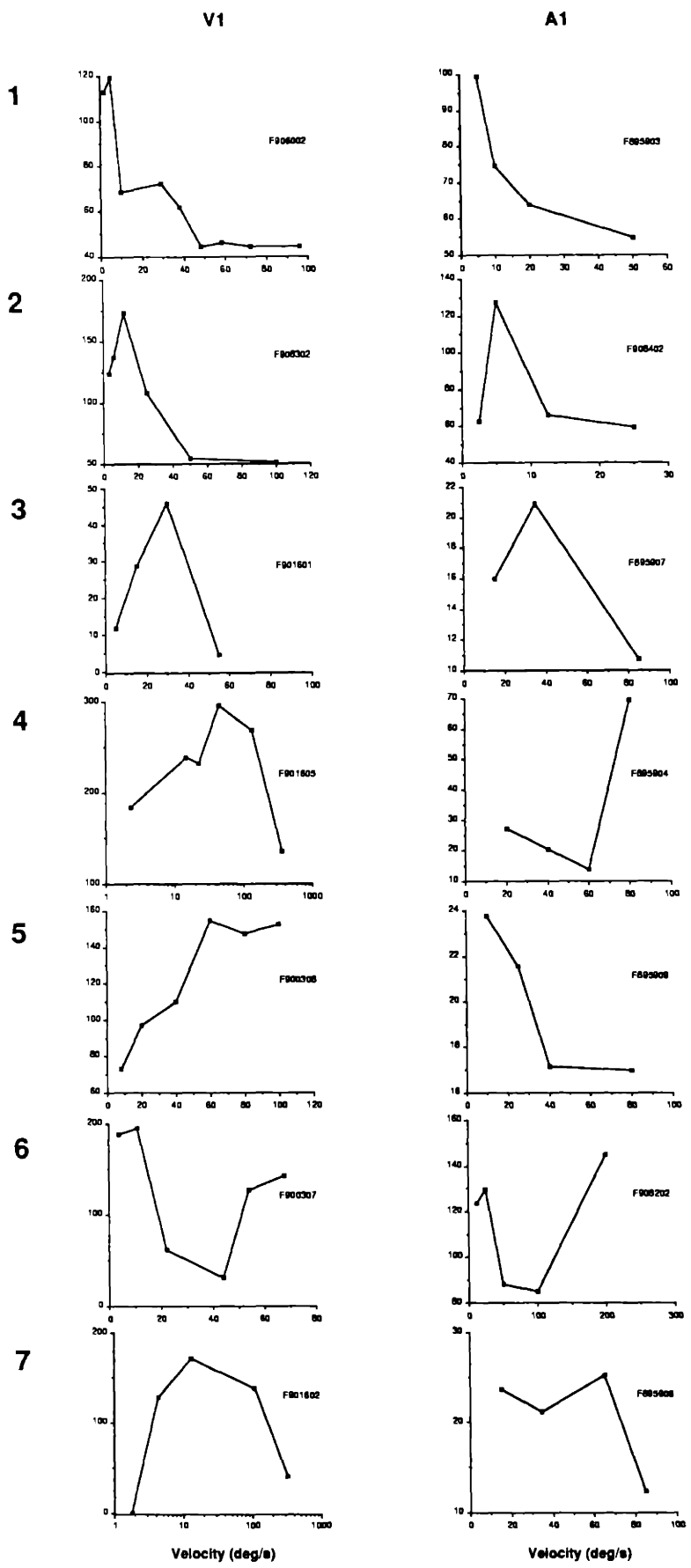

Fig. 11a

Fig. 11b

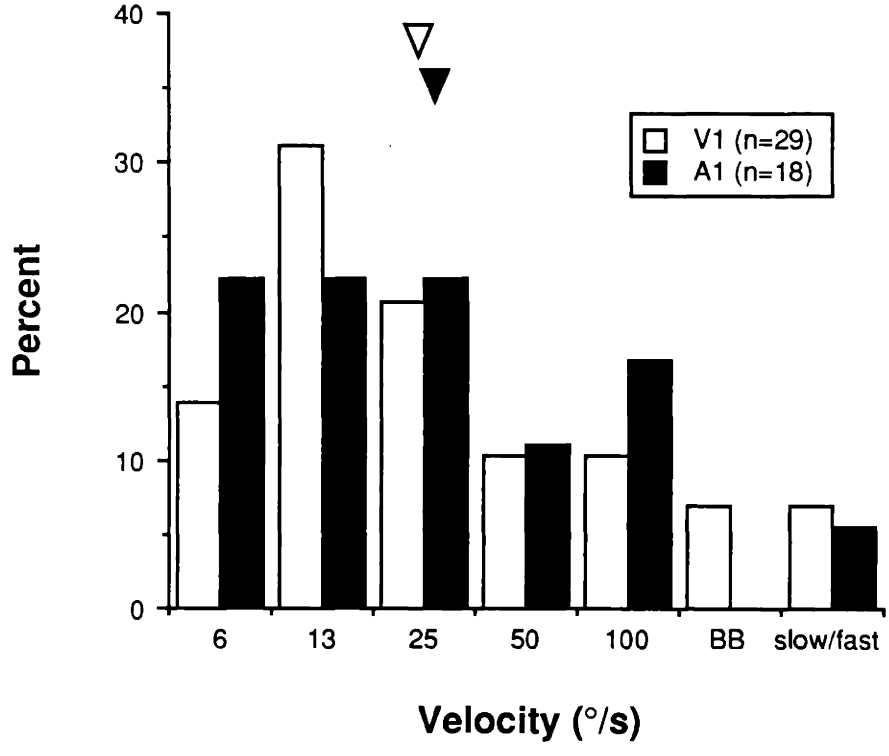
40
30
20
10
0
Percent
V1 (n=29)
A1 (n=18)
6
13
25
50
100
BB
slow/fast
Velocity (°/s)

Fig. 12

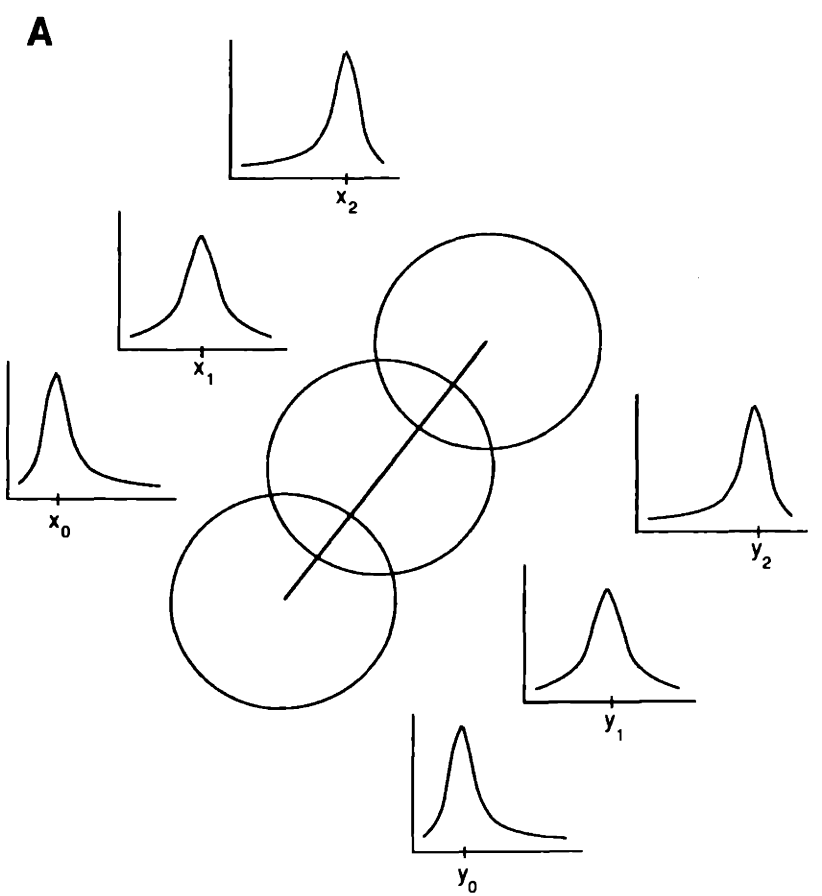

Orientation Selectivity in Visual Space
(or visual cortex)

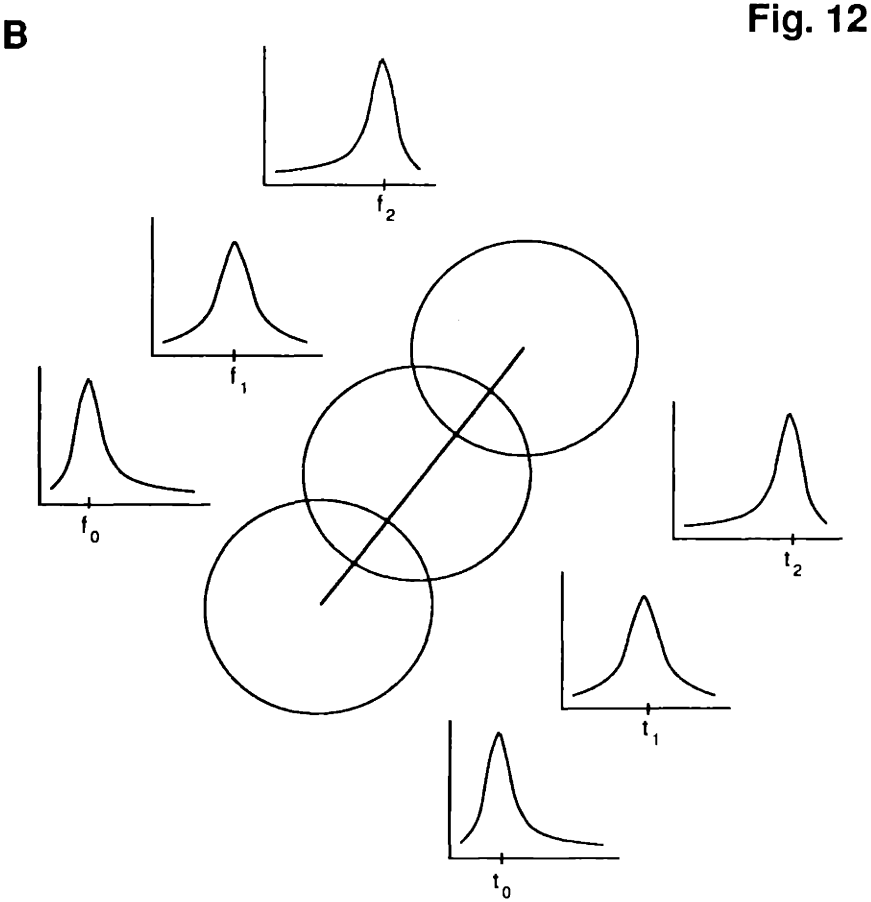

"Orientation Selectivity" in Auditory Space
(or auditory cortex)

SENSORY CORTICES ARE:

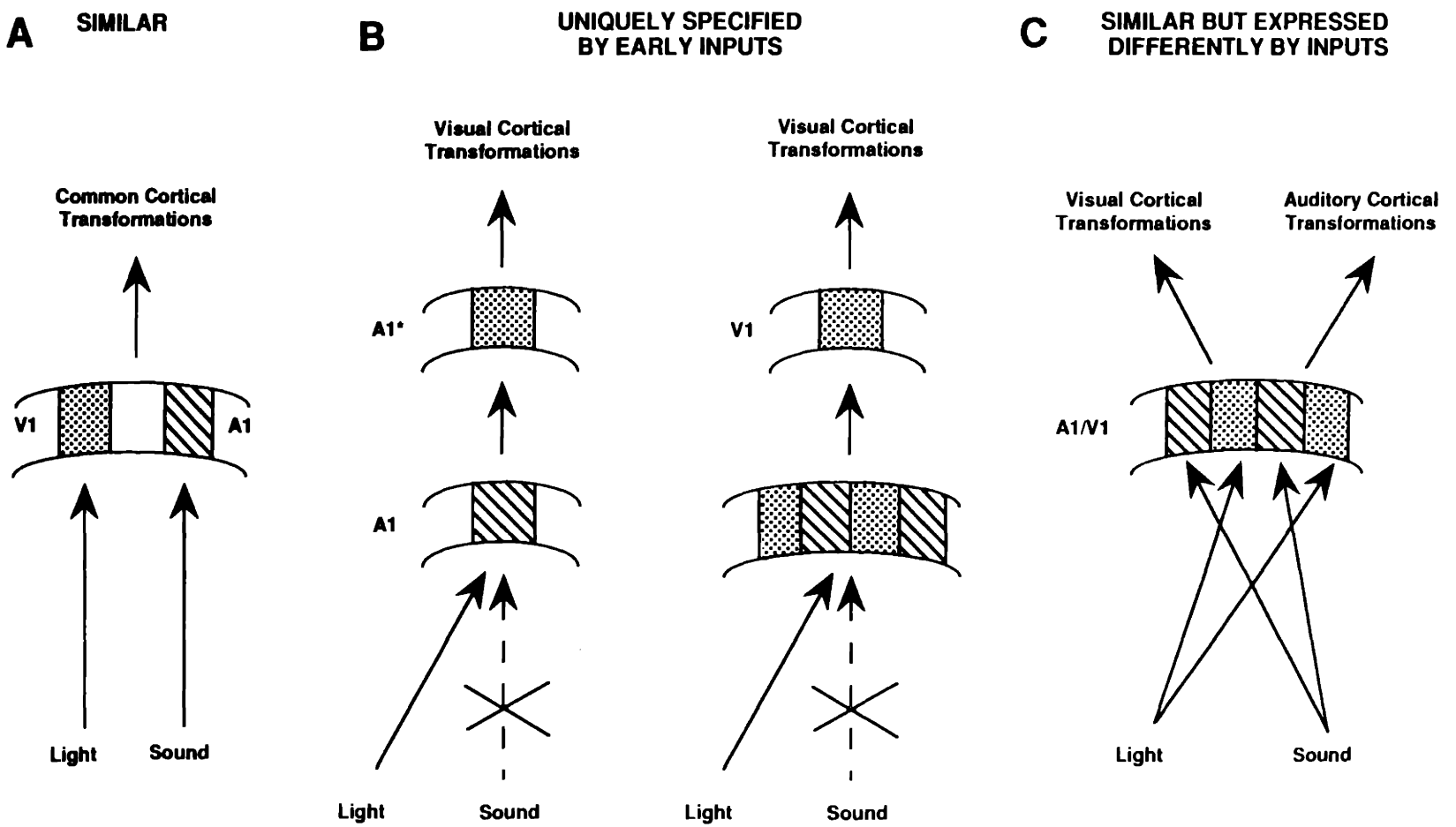

Fig. 13

Summary Discussion

Visual Topography in MGN and A1

Orientation of Map

We have shown that retinal projections to non-visual thalamic targets can be topographically organized. In rewired ferrets, azimuths map onto the variable frequency axis in both auditory thalamus and cortex (see Fig. 1). Elevations map in the orthogonal dimension, within isofrequency lamellae in the MGN and within isofrequency bands in A1. The visual topographies established thus have a predictable relationship to the frequency and isofrequency axes of normal auditory thalamus and cortex. We conclude that the orientation of topographic axes of sensory maps are to a large extent determined by the target structure.

Precision of Map

The precision of topography is dependent on multiple factors: topographic precision of the inputs, convergence/divergence ratios from input to target, and local processing in the target structure. 1) Inputs: relatively large W retinal ganglion cell receptive field sizes may contribute to the crudeness of topography in the visual maps in MGN and A1. 2) Convergence/divergence ratios: Given the very large receptive field sizes of visual cells in the MGN, retino-MGN convergence and divergence ratios are likely to be high. Such ratios are directly related to sizes of single terminal arbors as well as the projection patterns of axons arising from neighboring input cells. Arbors of single retinal W cells in the MGN are narrow and sparse (Pallas et a., 1989). Thus neighboring retinal W cells at single points in the retina may project in a more divergent fashion to the MGN than neighboring X or Y cells in the normal retinogeniculate projection. Convergence/divergence ratios in the MGN-A1 projection are likely to be high, at least along the isofrequency dimension (Pallas et al., 1990; Anderson et al., 1980; Middlebrooks and Zook, 1983). However, it is not known whether single

thalamocortical arbors in the auditory cortex are very large, as in somatosensory cortex, or relatively restricted, as in the visual cortex (in which case adjacent MGN cells would project to widely separate A1 loci). 3) Intracortical mechanisms: Finally, despite highly divergent and convergent projection patterns, topography may be refined via input-dependent modulation of excitation and inhibition in the cortex. Such mechanisms may be responsible for mapping of elevation in the isofrequency dimension of A1 and may similarly be present in normal auditory cortex.

Visual Receptive Field Properties of Cells in MGN and A1

In parallel with the high degree of similarity between X and Y cells in the LGN with their respective retinal X and Y inputs, receptive field properties of visual cells in the MGN reflect the receptive field properties of their retinal W cell inputs. It is hypothesized that the purpose of thalamic transmission as an intermediate processing stage is to allow gating of sensory inputs to the cortex by extraretinal inputs (e.g. Steriade and Llinas, 1988). In this respect, it is possible that the transfer of visual inputs to auditory thalamus and cortex may be influenced by the brainstem, the auditory reticular nucleus, and multiple auditory cortical areas. In these rewired ferrets, the auditory system in the unlesioned hemisphere is intact and maintains its callosal connections with auditory cortex in the lesioned hemisphere (Pallas et al., 1988). This raises the possibility that visual inputs may be gated by auditory centers in the brain, a possiblity which could have intriguing behavioral consequences (Carman, in progress).

The receptive field properties of visual cells recorded in A1 of rewired ferrets are strikingly similar to those recorded in primary visual cortex of normal ferrets. Most notably, visual cells in A1 are tuned for orientation, a feature that normally arises in visual cortex. I view this finding as an expression of commonalities across sensory cortical circuitries. While during development sensory inputs are likely to influence certain details of cortical

microcircuitry (e.g. establishing the extent of a cortical network, changing synaptic weights), I believe that fundamental processing strategies exist in cortices across sensory modalities. Intracortical circuits that produce physiological response selectivities such as that for "orientation" may be as much a defining feature of cortical organization as its laminar structure (cf. Roe, in prep). In this sense, the "orientation" selectivity of visual cells in A1 of rewired ferrets may be the first physiological evidence for a "common cortical circuit"--that is, common across sensory domains, and perhaps even motor and associational domains.

References

Anderson RA, Knight PL, Merzenich MM (1980) The thalamocortical and corticothalamic connections of AI, AII, and the anterior auditory field (AAF) in the cat: evidence for two largely segregated systems of connections. J Comp Neurol 194:663-701.

Kaas J (1991) Plasticity of sensory and motor maps in adult mammals. Ann Rev Neurosci 14:137-168.

Merzenich MM, Recanzone G, Jenkins WM, Allard TT, Nudo RJ (1988) Cortical representational plasticity. In P Rakic and W Singer (eds): Neurobiology of Neocortex. New York: John Wiley and Sons, pp. 41-67.

Middlebrooks JC, Zook JM (1983) Intrinsic organization of the cat's meidal geniculate body identified by projections to binaural response-specific bands in the primary auditory cortex. J Neurosci 3:203-224.

Pallas SL, Hahm JO, Sur M (1989) Retinal axon arbors in a novel target: morphology of ganglion cell axons induced to arborize in the medial geniculate nucleus of ferrets. Soc Neurosci Abstr 15:495.

Pallas SL, Roe AW, Sur M (1990) Visual projections induced into the auditory pathway of ferrets. I. Novel inputs to primary auditory cortex (A1) from the LP/pulvinar complex and the topography of the MGN-A1 projection. J Comp Neurol 298:50-68.

Roe AW (1991) Computational primitives of auditory processing in the central nervous system: a view from a visually innervated auditory pathway in ferrets, *in prep*.

Steriade M, Llinas RR (1988) The functional states of the thalamus and the associated neuronal interplay. Physiol Rev 68:649-742.

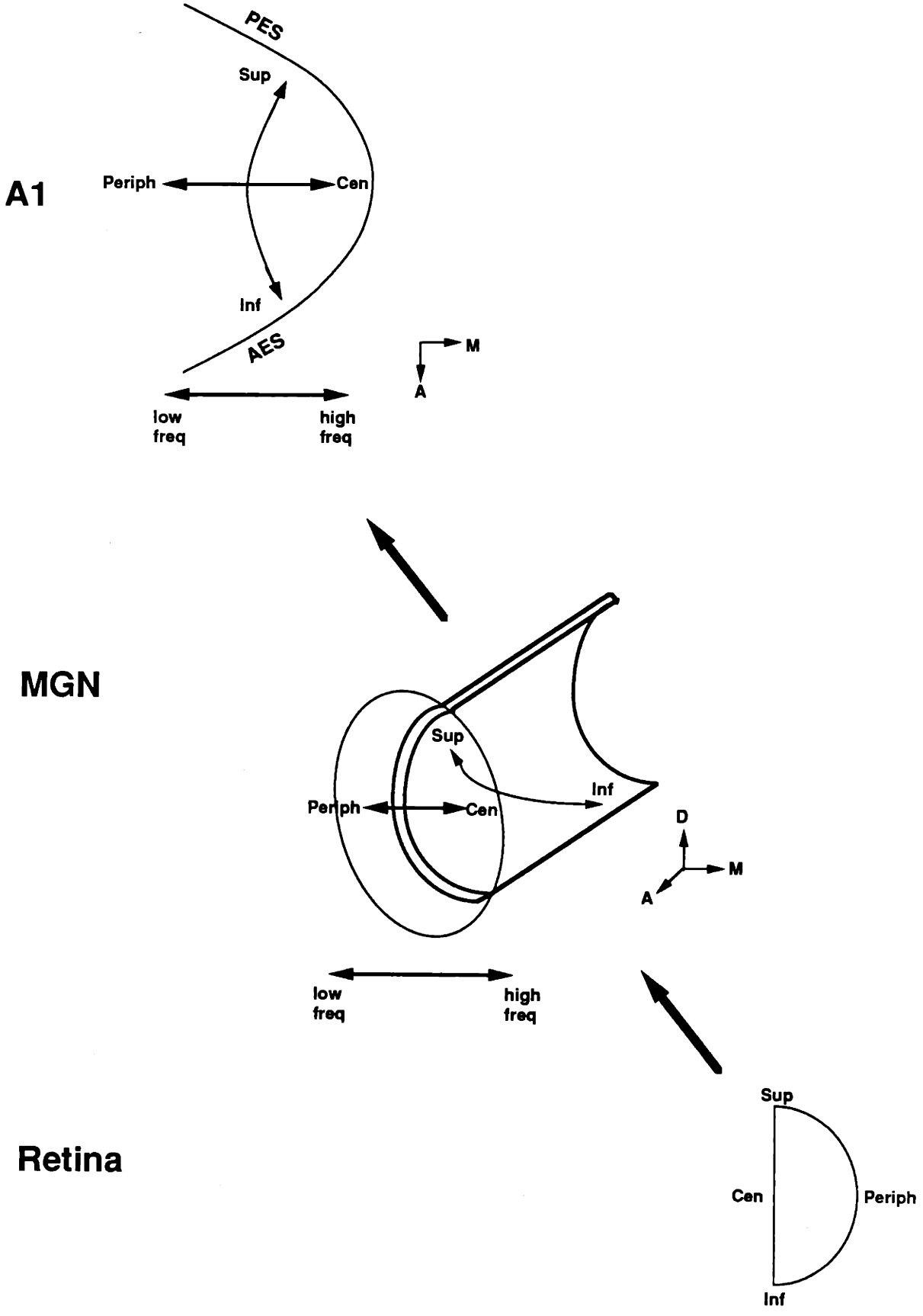
A1
PES
Sup
Periph
Cen
Inf
AES
M
A
low
freq
high
freq
MGN
Sup
Inf
Periph
Cen
D
M
A
low
freq
high
freq
Retina
Sup
Cen
Periph
Inf